Design of a Centrifugal Compressor for Application in Micro Gas Turbines

by
Lodewyk Christoffel Barend de Villiers

Thesis presented in partial fulfilment of the requirements for the degree of Master of Engineering (Mechanical) in the Faculty of Engineering at Stellenbosch University

Supervisor: Dr. S.J. van der Spuy
Co-supervisor: Prof. T.W. von Backström

December 2014

DECLARATION

By submitting this thesis electronically, I declare that the entirety of the work contained therein is my own, original work, that I am sole author thereof (save to the extent explicitly otherwise stated), that reproduction and publication thereof by Stellenbosch University will not infringe any third party rights and that I have not previously in its entirety or in part submitted it for obtaining any qualification.

Date: December 2014

ABSTRACT

Development of a Centrifugal Compressor for Application in Micro Gas Turbines

L. C. B. de Villiers

Department of Mechanical and Mechatronic Engineering, Stellenbosch University, Private Bag X1, Matieland 7602, South Africa.
Thesis: MEng. (Research), (Mechanical)

December 2014

This thesis details the methodology for developing a centrifugal compressor for application in a Micro Gas Turbine (MGT). This research forms part of a larger project, namely project Ballast, initiated by the South African Air Force (SAAF) in conjunction with Armscor. The methodology encompasses the development of a mean-line code that makes use of 1-dimensional theory in order to create an initial centrifugal compressor geometry which includes a rotor as well as radial vaned diffuser. This is followed by a Computational Fluid Dynamics (CFD) simulation process during which the compressor is optimised in order to maximise its performance. Before manufacturing a Finite Element Analysis (FEA) is done in order to ensure that the rotor does not fail during testing. The testing of the compressor is done to compare the numerical results with the experimental results and in so doing confirms the design process.

A previous student had designed a rotor by making use of a mean-line code as well as a CFD optimisation process. The rotor had a measured total-static pressure ratio of roughly 2.8 at 121 kRPM and a total-total isentropic efficiency of 79.1 % at said rotational speed. The inclusion of a vaned diffuser resulted in a higher total-static pressure ratio and accordingly the compressor designed in this report has a CFD determined total-static pressure ratio of 3.0. The efficiency would however drop and as such a total-total isentropic efficiency of 76.5 % was determined theoretically. The theoretical results correlated well with the experimental results and as such it was concluded that the design methodology developed was sound.

UITTREKSEL

Ontwikkeling van ‘n Sentrifugale Kompressor vir Toepassing in Mikro-Gasturbines

(“Development of a Centrifugal Compressor for Application in Micro Gas Turbines”)

L. C. B. de Villiers

Departement van Meganiese en Megatronise Ingenieurswese, Universiteit van Stellenbosch, Privaatsak X1, Matieland 7602, Suid-Afrika.
Tesis: Ming (Navorsing), (Meganies)

Desember 2014

Hierdie tesis bespreek die metodologie vir die ontwikkeling van ‘n sentrifugale kompressor vir toepassing in ‘n Mikro-Gasturbine (MGT). Die tesis vorm deel van ‘n groter projek, genaamd die Ballast projek, wat deur die Suid-Afrikaanse Lugmag (SALM) daargestel is in samewerking met Krygkor. Die metodologie behels die ontwikkeling van ‘n middel-lyn kode wat gebruik maak van 1-dimensionele teorie om die aanvanklike geometrie van die kompressor te skep. Die geometrie bevat beide die rotor asook die gelemde radiale diffusor. Hierdie proses word gevolg deur ‘n Berekeningsvloeidinamika (BVD) simulasie waartydens die kompressor geoptimeer word om sodoende die verrigting ten volle te verbeter. Voordat vervaardiging plaasvind word ‘n Eindige Element Analise (EEA) toegepas om te verseker dat die rotor nie sal faal tydens toetse nie. Die toetse word gedoen sodat die eksperimentele resultate met die numeriese resultate vergelyk kan word. Sodoende word die proses waardeur die kompressor ontwikkel word bevestig.

‘n Vorige student het ‘n rotor ontwerp deur gebruik te maak van ‘n middel-lyn kode asook ‘n BVD optimerings proses. Die rotor het ‘n gemete totaal-statiese drukverhouding van ongeveer 2.8 teen 121 kRPM gelewer en ‘n totaal-totale isentropiese benutingsgraad van 79.1 % teen dieselfde omwentelingspoed. Met die insluiting van ‘n gelemde radiale diffuser word ‘n hoër totaal-statiese druk verhouding verwag en as sulks lewer die nuut-ontwerpte kompressor soos in die tesis bespreek ‘n teoretiese totaal-statiese drukverhouding van 3.0. Die benutingsgraad sal egter daal en daarvolgens het die nuwe kompressor ‘n totaal-totale isentropiese benutingsgraad van 76.5 % gelewer. Die eksperimentele resultate het goed ooreengestem met die teoretiese resultate en as sulks was dit besluit dat die ontwerps-metodologie goed is.

ACKNOWLEDGEMENTS

I would like to thank the following individuals and companies for the help and/or guidance during my MEng studies.

- First of all I would like to thank my Saviour and Heavenly Father for never leaving my side during this journey.
- Dr. van der Spuy and Prof. von Backström for their guidance. It was most helpful and inspiring.
- Thank you David Krige for always being available to answer my questions with regards to CFD and of course with all the help with manufacturing and testing.
- The help and quick response from the Numeca Ingenieurbüro is much appreciated.
- A special thanks goes out to my parents whose love and support helped overcome difficult tasks during my life as well as during my postgraduate studies. Also thank you very much for all the financial support and motivation in helping me proceed with postgraduate studies.
- Thank you Mike Saxor as well as the guys at COMAR for all their patience during the manufacturing of the parts.
- The funding provided by the CSIR as well as the go-ahead to do my MEng by Dr. Glen Snedden is much appreciated.
- A final note of appreciation goes out to all the guys in the Lasraam. Thank you for all the intelligent or otherwise conversations.

DEDICATIONS

To my parents: For all the times that I have made you proud as is the aim with my postgraduate studies; Thank you, but above all else it was a pleasure.

TABLE OF CONTENTS

LIST OF FIGURES

Page

LIST OF TABLES

NOMENCLATURE

Constants

$R = 0.287$	[J/kg·K]
$\gamma = 1.4$	[~]
$\pi = 3.1416$	[~]

Symbols

$A_{1,2,3,4}$	Cross-sectional area at points 1, 2, 3 and 4 respectively	[m^2]
AR	Area ratio	[~]
A, B, C, D	Camber line defining constants	[~]
a/c	Point of maximum camber	[~]
B	Fractional area blockage	[~]
b	Hub-to-shroud passage height	[m]
C	Absolute velocity	[m/s]
c	camber line length	[m]
C_d	Discharge flow coefficient	[~]
C_{pr}	Pressure recovery coefficient	[~]
C_r	Contraction ratio	[~]
c_f	Skin friction coefficient	[~]
d	Diameter	[m]
E	Diffuser effectiveness	[~]
E_i	Imparted energy	[J]
i	Angle of incidence	[º]
$K_{1,2,3,4}$	Vaned diffuser stall parameters	[~]
k	Penalty function coefficient	[~]
L	Mean streamline meridional length, dimensionless diffuser blade loading parameter	[m]
L_B	Vane mean streamline camber length	[m]
l	Leniency	[~]
M	Mach number	[~]
$\dot{m}$	Mass flow rate	[kg/s]
N	Rotational speed	[RPM]
n	Vane thickness coefficient	[~]
P	Penalty function	[~]
p	Pressure	[Pa]
Q	Penalty function value for mass flow rate, pressure or efficiency	[kg/s], [Pa], [~]
r	Radius	[m]

S	Entropy	[J/kg·K]
T	Temperature	[K]
t	Tip/Clearance gap	[m]
$t_{b,bmax,3,4}$	Vane localized thickness, vane maximum thickness, vane thickness at the leading edge and trailing edge respectively	[m]
U	Tangential velocity	[m/s]
V	Velocity	[m/s]
$W_{1,2,3,4}$	Relative velocity at point 1, 2, 3 and 4	[m/s]
W	Weighting value	[~]
x/c	Distance along camber line	[~]
y^+	Dimensionless wall distance	[~]
z	Number of blades or vanes	[~]

Greek symbols

α	Flow angle with respect to tangent	[°]
α_c	Mean stream angle with respect to zenith	[rad]
β	Blade angle with respect to tangent	[°]
Δ	Difference	[~]
δ	Boundary layer thickness	[m]
θ	Camber angle	[°]
μ	Dynamic viscosity coefficient	[kg/s·m]
ρ	Density	[kg/m^3]
Σ	Summation	[~]
σ	Slip factor, point of maximum solidity	[~]
ω	Rotational velocity	[rad/s]
$\bar{\omega}$	Total pressure loss coefficient	[~]

Superscripts

*	Optimum or sonic flow conditions

Subscripts

ave	Average
duct	Circular inlet duct
e	Exit
frictionless	Frictionless/No losses/Ideal
imp	Impeller
inlet	Control volume inlet boundary
mix	Mixing losses

p	Pressure side
r	Radial direction
ref	Penalty function reference value
SF	Skin Friction
s	Suction side
SEP	Separation/Separating flow
sys	System
t	Total conditions, Tangential direction
th	Throat
wake	Wake losses
z	Z/Axial Direction
0	Impeller eye/Ambient/Total conditions
1	Impeller leading edge/Inlet conditions
2	Impeller outlet conditions
3	Diffuser inlet conditions
4	Diffuser outlet conditions

Auxiliary symbols

$\bar{}$	Average of values

Acronyms

ANN	Artificial Neural Network
CAD	Computer Aided Design
CFD	Computational Fluid Dynamics
CFL	Courant-Friedrick-Levy
CPU	Central Processing Unit
CSIR	Council for Scientific and Industrial Research
DMR	Distance along Meridional
EEA	Eindige Element Analise
FEA	Finite Element Analysis
GUI	Graphical User Interface
IGG	Interactive Grid Generator
k-ε	Turbulence model
k-ω	Turbulence model
LE	Leading Edge
LCB	Lodewyk Christoffel Barend (Initials of Author)
MGT	Micro Gas Turbine
BVD	Berekeningsvloeidinamika
RNIG	Random Number Index Generator

ROT	Rotor-Stator Interface
RPM	Revolutions Per Minute
SA	Spalart-Almaras (turbulence model)
SAAF	South African Air Force
SALM	Suid-Afrikaanse Lugmag
THETA	Distance along Tangential
t-t	Total-total
t-s	Total to Static
UAV	Unmanned Aerial Vehicle
ZR	Meridional/Spanwise direction
1-D	One Dimensional
3-D	Three Dimensional

1. INTRODUCTION

1.1. Background

This thesis describes the development of a compressor stage for a Micro Gas Turbine (MGT) for possible use in an Unmanned Aerial Vehicle (UAV). The compact size of a micro gas turbine makes it suitable for use in a UAV (Van der Merwe 2012: 1). Applications of UAVs are various and include aerial combat, national security, crime fighting, disaster management, election monitoring and search-and-rescue operations. Other areas of application include the agriculture and mining industry (Van der Merwe 2012: 1). Figure 1 shows an example of a UAV named the Talarion that has been developed by the SAAB aeronautics group.

Figure 1: Talarion UAV developed by SAAB. (available: http://www.saabgroup.com)

The South African Air Force (SAAF), through ARMSCOR, has made funding available to tertiary institutions in the form of the Ballast project. The aim of Ballast is to increase the extent of knowledge in the field of turbomachinery in South Africa. Work has been undertaken in the development of a centrifugal compressor for a micro turbo jet engine at the University of Stellenbosch for the past three years. The focus of this development is discussed in section 1.3. A centrifugal compressor turbojet engine consists of three main stages, namely the centrifugal compressor, combustion chamber and turbine (Figure 2). The compression stage consists of three main structures, the rotating impeller, radial diffuser and the axial guide vanes or axial diffuser.

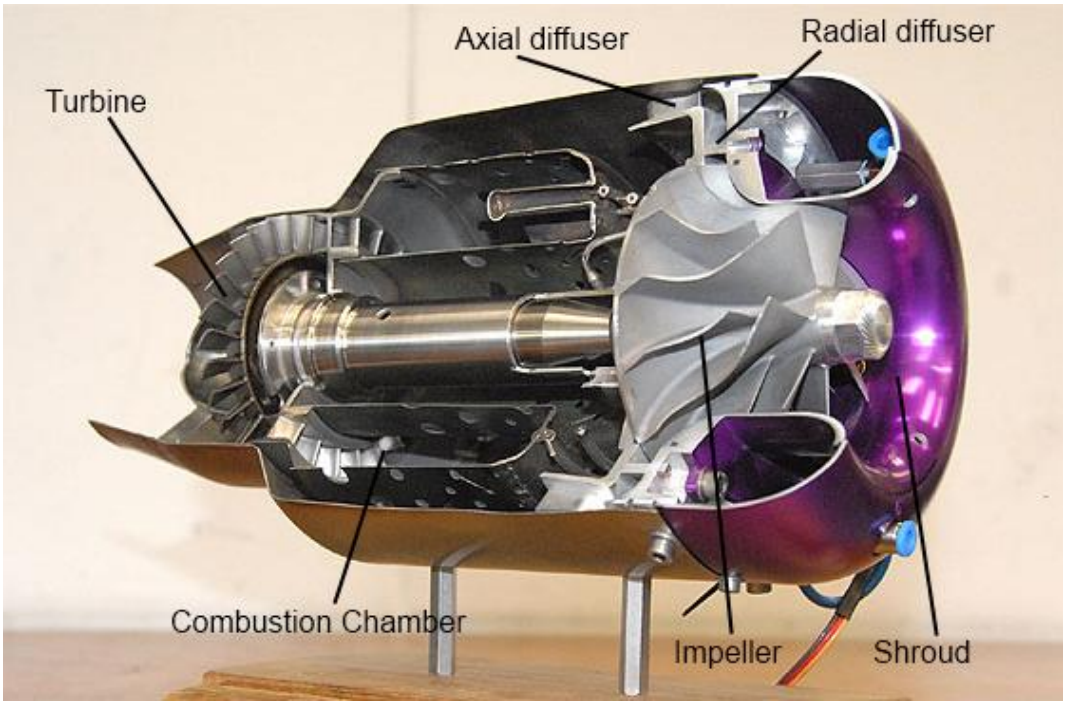

Figure 2: Centrifugal compressor turbo jet engine.

For the purpose of this thesis the development of the impeller and radial diffuser will be considered as well as their interaction. The development of the axial guide vanes will form part of another thesis being undertaken at Stellenbosch University.

1.2. Project motivation

1.2.1. Motivation

Many UAVs make use of positive displacement engines, rotating a propeller that in turn propel the aircraft forward. Gas turbine engines have several advantages over reciprocating internal combustion engines. These advantages include (Langston & Opdyke, 1997: 3);

- A high power-to-weight ratio, hence micro gas turbines can be developed to be more compact which, due to the limited size of UAVs, are better suited for use in UAVs.
- The major components within a gas turbine move rotationally only, and do not reciprocate as in piston engines. Hence gas turbines have longer life spans and lower maintenance costs than piston engines.

- A wide variety of fuels can be used. Natural gas is typically used in land based gas turbines whereas light distillate (kerosene-like) oils are used in gas turbines powering aircraft.
- Since the usual working fluid in the gas turbine is air, the basic power unit requires no coolant.

The research will focus specifically on developing an optimised impeller and diffuser unit for an MGT. The methodology for developing the aforementioned unit is important. Therefore a well-defined methodology will be developed, followed and documented in this thesis for use in future development work.

1.2.2. Market

The United States (US) military UAV market has experienced a large growth over the past decade and is projected to grow at a compound annual growth rate of 12% between 2013 and 2018. This will lead to the US military UAV market generating $86.5 billion in revenues over the period 2013-2018. While the US is the market leader of UAVs it has been found that 556 UAVs are produced worldwide by 195 countries including South Africa. UAVs have also enjoyed a great share in the South African and Asian market for use in border security operations (New Markets for UAVs, 2013: 35) whilst South Africa further employs UAVs for the conservation of the Zebra population (Aerospace Industries Association, 2014: 2).

1.3. Previous Ballast projects at Stellenbosch University

1.3.1. Mean-line code development

De Wet (2011) developed a computer code that made use of 1-dimensional (1-D) turbomachinery theory to analyse a centrifugal compressor impeller. The code was programmed in MATLAB®. The 1-D analysis relied on a combination of fundamental equations and empirical loss models implemented along the machine's mean-line, as presented by Aungier (2000).

The aim of De Wet's thesis was to determine where aerodynamic stall occurred within the compressor of a diesel locomotive turbocharger by making use of 1-D and 3-D analyses. The 1-D analysis was performed using the code described in the previous paragraph and the 3-D analysis was performed by making use of a CFD package, Numeca FINE™/Turbo. De Wet compared the results of the 1-D analysis to that determined using the 3-D analysis and concluded that the results

of the 1-D analysis compared well with that of the 3-D analysis (de Wet, 2011:78).

1.3.2. Impeller & diffuser development

Van der Merwe (2012) designed and tested a centrifugal compressor impeller for a MGT by also making use of 1-D and 3-D analyses. Van der Merwe improved the mean-line code (shown in Appendix A) developed by De Wet and used it to develop an initial impeller geometry. This impeller geometry was then optimised using Numeca FINE™/Design3D. The objectives of Van der Merwe's project was to develop an impeller that had a total-total pressure ratio of 4.72 and a total-total isentropic efficiency of 79.8%, while operating at a mass flow rate of 0.325 kg/s and a rotational speed of 121 kRPM.

The development of a radial diffuser for a MGT was performed by Krige (2013). The objective of Krige's thesis was to investigate, evaluate and redesign the radial diffuser of a BMT 120 KS MGT to obtain a more efficient compressor capable of a higher pressure ratio operating at a higher mass flow rate. Krige made use of the design methodology provided by Aungier (2000) as well as CompAero® combined with Numeca FINE™/Turbo to design the vaned radial diffuser.

1.3.3. Affiliated developments

Other recent MGT theses include a centrifugal compressor test bench developed by Struwig (2013) as well as the development of the turbine stage of a MGT by Basson (2014).

The motivation for Struwig's thesis (Struwig, 2013) was to build a facility which can be used for the development of MGT compressors as well as recording their performance. The facility uses compressed air that flow through and powers the turbine of a turbocharger. The turbine in turn powers the centrifugal compressor of the turbocharger. It is the compressor stage of the turbocharger that serves as the unit used to test the centrifugal compressors.

Basson's (2011: 1) thesis involves the development of the turbine stage of a MGT. The deliverable of Basson's thesis is the documentation of a design methodology for an axial flow turbine stage used in MGTs. Basson proposed making use of the methodology of Aungier combined with CFD software provided by ANSYS® for the design of the turbine stage.

2. LITERATURE STUDY

Centrifugal compressors have a wide range of applications. The automotive and aeronautical industries are but two areas using these compressors. Turbocharger compressors are used to force more air into the cylinders of a piston engine. In doing so the turbocharger increases the theoretical capacity of the engine and increases its power delivery. This has the advantage of developing smaller, lightweight and fuel efficient engines, compared to a normally aspirated, higher capacity unit (Kuiper, 2007: 1).

Jet engines operate in a similar sense in that a compressor forces air into a combustion chamber. The differences being that centrifugal compressors in jet engines do not have a volute like that of a turbocharger, the combustion chamber is not that of a piston engine and the turbine has an axial configuration. The air flowing through the jet engine is accelerated in the exhaust nozzle behind the turbine. This increase in the velocity of the air provides the forward thrust required for an aircraft to fly.

2.1. Centrifugal compressor fundamentals

The compression stage within a MGT consists of three basic components, the impeller (rotor), radial diffuser and axial guide vanes. The air enters the MGT upstream of the impeller leading edge. The total enthalpy rise imparted to the fluid by the impeller is termed the impeller work input. An accurate prediction of the impeller work input is fundamental to all aspects of centrifugal compressor aerodynamic design and analysis.

After exiting the impeller the air enters the radial diffuser stage (Aungier, 2000: 52). The diffuser is used to decelerate the air, converting the kinetic energy into pressure energy i.e. increasing the static pressure of the air. The diffuser can be either a vaneless or vaned diffuser. Thick-vaned diffusers include island or channel diffusers and pipe diffusers. These styles are patterned after classic exhaust diffusers, where the rate of increase in passage area is controlled by increasing the vane thickness with radius (Aungier 2000: 167). Thick vaned diffusers do however require a substantially larger discharge to inlet radius ratio and hence, due to the geometric constraints of the MGT discussed in this report, a radial diffuser will be designed with aerofoil shaped vanes. The design methodology that will be used for the development of this diffuser is provided by Aungier (2000: 167-185).

After leaving the radial diffuser the air is turned from a radial to an axial direction and enters the axial guide vanes. The axial guide vanes ensure that the fluid is

deflected in such a way that stable and favourable flow conditions are provided for the combustion chamber. The design of the axial guide vanes are not discussed in this report. The fundamentals describing the operation of a centrifugal impeller are provided in Appendix B1.

2.2. Impeller-diffuser interaction

Shum *et al* (2000: 777) explains that modelling the interaction between an impeller and vaned diffuser is far more difficult than modelling the interaction between an impeller and vaneless diffuser. Matching a diffuser to an impeller is a non-trivial task, mainly due to complicated flow mechanisms and the absence of quantitative understanding. This means that 2 components that perform well individually may not perform well when combined. Determining the effects that impeller-diffuser interactions have on the performance of compressors is therefore mostly done using empirical equations.

The investigation of impeller-diffuser interaction has largely been focused on the effect of upstream conditions on diffuser performance. Shum *et al* (2000: 777) states that the time-averaged flow alignment of the air meeting the diffuser leading edge after leaving the impeller is the single most important parameter of concern when determining the performance of a diffuser. The diffuser angle of incidence (i) is defined as the difference in angle between the absolute velocity vector (α) and the vane camber line angle at the leading edge of the vane (β) (Aungier, 2000: 110):

$$i = \beta - \alpha \tag{2.1}$$

where both angles (β and α) are measured relative to the tangential direction. Aungier (2000: 177) mentions that the first estimate of the diffuser vane incidence angle should be between -1° and -0.5°.

Shum *et al* (2000: 781) further explains that the ratio of impeller outlet to diffuser inlet radius (r_3/r_2) is another important parameter that a designer must consider. Several compressor experiments have been performed and it has been found that the optimum ratio for this parameter lies between 1.06 and 1.10. Aungier (2000: 178) supports these values with one minor difference in that the upper limit can be as high as 1.12. He continues in stating that for higher impeller tip Mach numbers a larger vaneless space may be required. The reason for this being that the absolute Mach number must be reduced before the air enters the diffuser. The lower limit allows for the distorted impeller outlet flow profiles to smooth out and the blade wakes to decay before the flow enters the diffuser vanes (Aungier, 2000: 178).

It is imperative that the compressor be designed for a pressure ratio as high as possible while maintaining the required efficiency. A higher pressure ratio increases air density, allows for more air to enter the combustion chamber and hence provides better burning (Reitz, 2012: 4). A high pressure ratio centrifugal compressor also allows for better operation of a MGT at higher altitudes as would typically be the case for UAVs (Zheng *et al*, 2010: 1817). Aungier (2000: 178) explains that the loss levels in the radial gap can be high even for a short vaneless space. Consequently a longer than required vaneless space will impose unnecessary losses in efficiency.

2.3. Radial diffuser theory and design

A diffuser is described as an expansion or increase in cross-sectional area of a duct intended to reduce the velocity of a fluid. In so doing the kinetic energy of the fluid is effectively converted into pressure energy in the form of a static pressure rise.

2.3.1. Basic diffuser theory

The basic performance parameter of a diffuser is the pressure-recovery coefficient defined as

$$C_{pr} = \frac{p_e - p_t}{p_{0t} - p_t} \tag{2.2}$$

where e and t denote the exit and throat (or inlet), respectively. If it is assumed that there are no frictional losses, equation 2.2 can be altered by making use of the Bernoulli equation:

$$C_{pr,\,frictionless} = 1 - (V_e/V_{th})^2 \tag{2.3}$$

Steady, one-dimensional, incompressible continuity would require that

$$V_{th}A_{th} = V_eA_e \tag{2.4}$$

Combining equations 2.3 and 2.4 the performance of a diffuser can be written in the form of an area ratio defined as $AR = A_e/A_{th}$. Hence

$$C_{pr,\,frictionless} = 1 - \frac{1}{AR^2} \tag{2.5}$$

It is hence clear that the area ratio brings forth another important parameter that needs to be considered during the design of a diffuser. Japikse (1996: 2-42) further explains that the ratio of cross sectional area of the diffuser outlet to that of the diffuser throat plays a significant role in pressure-recovery. The area ratio is defined as the throat area of the diffuser compared to the exit/outlet area i.e.

$$C_{pr,\,frictionless} = 1 - \left(\frac{A_{th}}{A_e}\right)^2 \qquad (2.6)$$

Hence, the smaller the throat cross-sectional area as compared to the outlet area the higher the pressure recovery in the diffuser will be. Theoretically then if the area ratio is infinitesimally small, the diffuser would bring about a complete recovery of dynamic pressure. This is however not possible since the minimum cross sectional area of the throat is limited by a constraint known as choke which is discussed in section 2.3.4. Therefore, designing a diffuser with a minimum throat area would provide the best possible pressure recovery.

A typical design would have a value of *AR* = 5:1 for which equation 2.5 predicts a C_{pr} value of 0.96 or near complete static pressure recovery. It has been found however that actual values of *AR* are limited to about 0.86 or as low as 0.24. The basic reason for this discrepancy is flow separation. This occurs when the boundary layers on the walls break away and cause an unfavourable reduction in performance (White, 2000: 350). This break-away is also referred to as stall that creates backflow in the diffusing region (Figure 3).

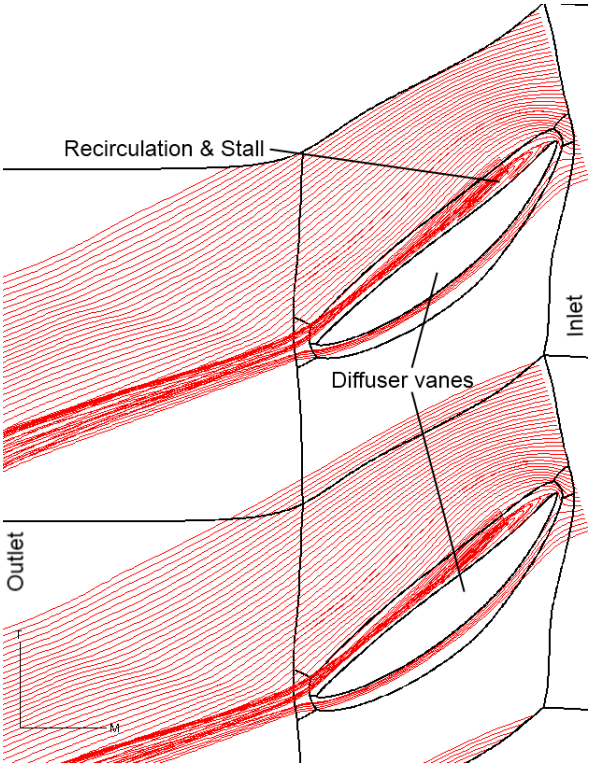

Figure 3: Example of Stall over diffuser vanes.

Stall over diffuser vanes causes deterioration in performance. The diffuser must hence be designed with an angle of incidence and a camber curve that will inhibit stall at the operation point of the compressor.

2.3.2. Vaned diffuser sizing

Aungier (2000: 184) provides a systematic procedure for designing a radial diffuser by making use of the flow chart shown in figure 4.

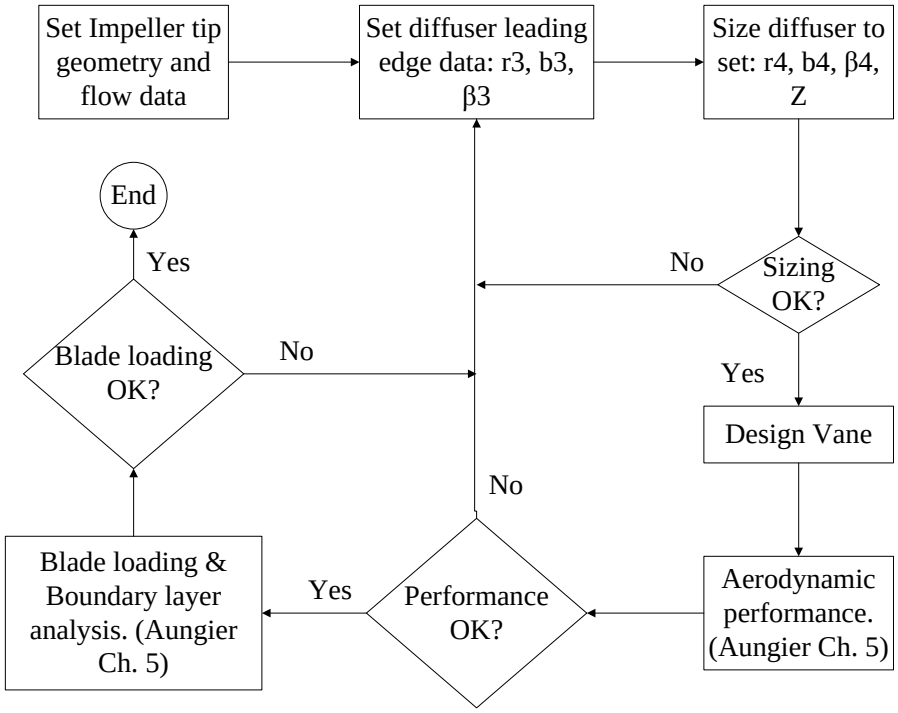

Figure 4: Flow chart of diffuser design procedure according to Aungier (2000: 184).

It is evident from figure 4 that the design procedure is divided into several subtasks. The procedure of Aungier will be used to create a code that will determine the diffuser performance and create the geometry of the diffuser. The "*Blade loading and Boundary layer analysis*" of Aungier requires that the designer program the mesh of the diffuser flow domain as well as CFD theory into the mean-line code. This is a time consuming and unnecessary process given the design tools available, therefor the "*Blade loading and Boundary layer analysis*" will be replaced by using Numeca CFD analyses. The performance curves of the compressor, recirculation and ultimately the design of the entire compressor will also be done using Numeca CFD analyses. The procedure provided by Aungier will therefore be altered.

There are two basic parameters that govern the sizing of a radial diffuser, namely the divergence angle (θ_C) and the blade loading parameter (L). When designing a radial diffuser the designer must adhere to the ranges within which each of these parameters are applicable. These ranges are:

$$10^{\circ} \leq 2\theta_C \leq 11^{\circ} \tag{2.7}$$

for the divergence angle and

$$0.3 \leq L \leq 0.33 \tag{2.8}$$

for the blade loading parameter (Aungier 2000: 178). Aungier also introduces another design parameter, E_d (equation B2.34), which can be used to evaluate the effectiveness of the vaned diffuser design compared to that of a vaneless diffuser design. For incompressible flow it is recommended that this value be between 1.5 and 1.7. Reneau *et al* (1967) recommends an area ratio, *AR* defined as the outlet relative velocity to the inlet relative velocity of between 2.2 to 2.4. During the design of the radial diffuser, the aim is to adhere to the limits of the provided parameters.

2.3.3. Vane design

The flow path of the air through a parallel-walled vaneless radial diffuser is in the shape of a logarithmic spiral. It is therefore assumed that the camber line of the diffuser vane should be defined by a logarithmic function. The vanes would consequently adhere to the flow pattern of the air in the radial space and stall would be avoided. Aungier provides such a function that forms the foundation of the vane design. Defining η as $r/r_{3,}$ the camber line is given by

$$\theta(\eta) = A\ln(\eta) + B(\eta - 1) + C(\eta^2 - 1) + D(\eta^3 - 1) \tag{2.9}$$

where $\theta(\eta)$ and r are defined in the polar coordinate system (Aungier, 1988: 32). To determine the constants A to D in equation 2.9 the user specifies two other constants, K_3 and K_4. K_3 and K_4 can have a value of 1 up to and including 100. These constants will have a direct effect on the shape of the camber line and as such an aerodynamic effect on the blade loading and stall. After K_3 and K_4 have been defined a straightforward procedure ensues in which the constants of equation 2.9 are calculated by making use of the following equations:

$$D = \frac{(\cot\beta_4 - \cot\beta_3)(K_3 + K_4 - 2)}{3(R-1)^3} \tag{2.10}$$

$$C = \frac{(\cot\beta_4 - \cot\beta_3)(K_4 - K_3)}{4(R-1)^2} - \frac{9D(R+1)}{4} \tag{2.11}$$

$$B = \frac{K_3(\cot\beta_4 - \cot\beta_3)}{(R-1)} - 4C - 9D \tag{2.12}$$

$$A = \cot\beta_3 - B - 2C - 3D \tag{2.13}$$

After the constants have been determined it is necessary to impose a vane thickness onto the camber line that would define the final blade shape. The designer must define the maximum blade thickness (t_{bmax}) as well as the leading edge thickness (t_0) that will ensure manufacturability. Aungier provides functions that create the pressure and suction surfaces of the diffuser vanes based on these values. It has been found that an airfoil shaped vane provides for acceptable manufacturing costs, lower stress levels and lower vibration induced forces (Aungier 2000: 181). The governing equations that define the pressure and suction surfaces are hence:

$$t_b/t_{bmax} = t_0 + (1 - t_0)(2x/c)^n \qquad \text{for } x/c \leq 0.5 \tag{2.14}$$

$$t_b/t_{bmax} = t_0 + (1 - t_0)(2 - 2x/c)^n \qquad \text{for } x/c > 0.5 \tag{2.15}$$

where

$$t_0 = [t_{b3} + (t_{b4} - t_{b3})x/c]/t_{bmax} \tag{2.16}$$

Furthermore

$$n = 0.755(0.57 - x/c) \qquad \text{for } x/c \leq 0.539 \tag{2.17}$$

and

$$n = 1.225(x/c - 0.52) \qquad \text{for } x/c > 0.539 \tag{2.18}$$

Once the vane camber line and thickness distributions have been determined the throat area can be calculated. The size of the diffuser throat has a direct effect on the occurrence of choke in the diffuser. As such a definition for choke must be used in order to determine the geometric constraints of the diffuser that would

avoid the occurrence of choke. This definition for choke is described in section 2.3.4 below.

2.3.4. Analysis of the design

Choked flow is defined as the maximum amount of air mass flow rate that can pass through a given area at a specific velocity (F.M. White 1994: 525). Whitfield *et al* (1990: 58) specifies that air will choke in the throat of a radial diffuser as soon as the Mach number at that point (M_{th}) is equal to 1. The dimensionless mass flow rate through the throat is defined as

$$\frac{\dot{m}\sqrt{RT_0/\gamma}}{AP_0} = M_{th}\left(1 + \frac{\gamma - 1}{2}M_{th}^2\right)^{-(\gamma+1)/1(\gamma-1)} \tag{2.19}$$

A graphical presentation of equation 2.19 is shown in figure 5.

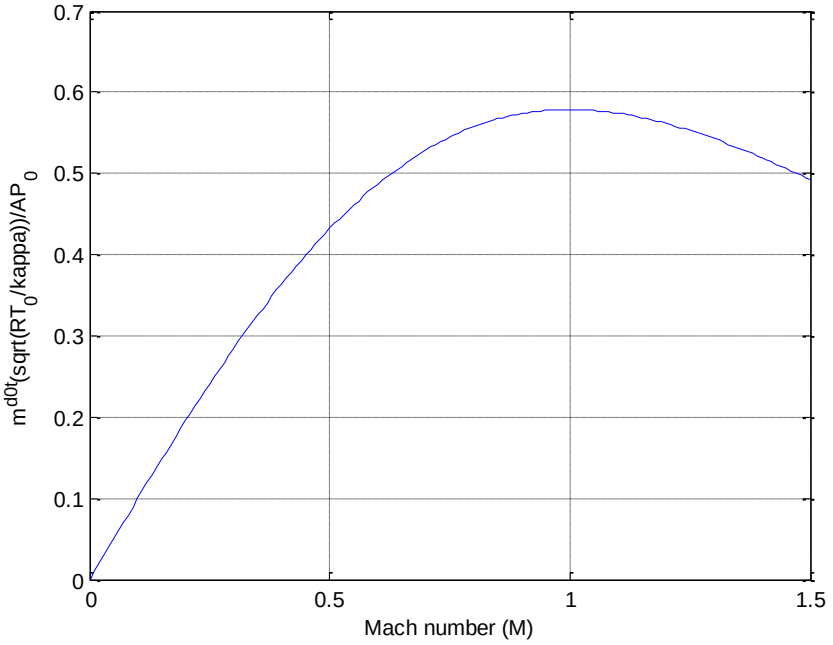

Figure 5: Dimensionless mass flow vs Mach number.

The vane thickness as well as number of vanes will have a direct effect on choke in the diffuser throat. It is therefore important that the designer ensures that the maximum number of vanes of a manufacturable thickness be used for the design, while maintaining a Mach number below but as near as possible to unity. If the Mach number in the diffuser throat exceeds unity, shockwaves will form. These shockwaves can damage and in severe cases destroy components downstream of the radial diffuser.

Another parameter that needs to be considered when analysing vaned diffuser design is blade loading. It is important to ensure that blade loading is not too high at any given point along the impeller blade as well as the diffuser vanes. Japikse (1996: 6-32) limits the blade loading number for the impeller to be between 0.7 and 1.0 as per equation 2.20 below.

$$0.7 < \frac{\Delta W}{\bar{W}} < 1.0 \qquad (2.20)$$

Aungier (2000: 182) states that the blade loading parameter should be less than 0.4 for the diffuser vanes. Using the absolute velocities on the pressure and suction surfaces Aungier states that:

$$\frac{|C_s - C_p|}{C_{ave}} < 0.4 \qquad (2.21)$$

Everitt (2010) investigated stall inception on the radial diffuser of a turbocharger. Everitt's design conforms to the blade loading constraint as specified by Aungier since no spike or excessive fluctuations in the pressure coefficient are present on the diffuser vanes as shown in figure 6.

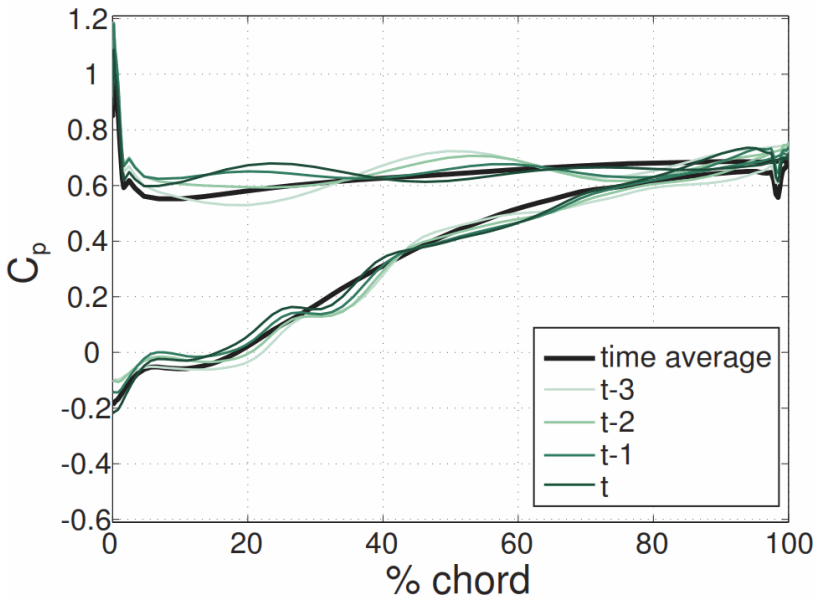

Figure 6: Pressure coefficients as determined using Numeca FINE/Turbo on the pressure and suction surfaces of a radial diffuser vane for 4 snapshots in time (J. Everitt, 2010: 97).

Figure 6 shows C_p values as determined by an unsteady, Numeca FINE^{TM}/Turbo CFD simulation for a turbocharger diffuser at operating conditions. Due to the rotation of the impeller the airflow pattern leaving the impeller blade differs during one diffuser periodic rotation. This is evident from figure 6 in that different profiles for C_p are present at different time steps. Reassuringly though the difference in C_p during the different time steps is minimal. By observing figure 6 Everitt (2010: 96) concluded that the operating point was close to yet not at stall.

2.3.5. Aerodynamic performance of the vane design

In most cases the performance of radial diffusers is determined experimentally. The performance of the radial diffuser as discussed in this report is based on the performance characteristics as described by Aungier (2000: 88-95). The performance analysis starts with a choke analysis as it was decided that this is the most important parameter to adhere to. Choke will be determined using the definition of Whitfield as mentioned in section 2.3.4.

Following the choke analysis, the stall analysis is performed. Stall will be evaluated between the diffuser inlet and the throat by considering the parameters K_3 and K_4, the inlet Mach number (M_3) as well as the inlet blade angle (β_3). By making use of the definition of incidence angle (equation 2.1) and setting it equal to -1, the stall over the diffuser vanes can be controlled initially. The performance analysis then continues to determine the outlet conditions of the diffuser by considering the losses through the diffuser. These losses are categorized in three groups namely surface friction losses, incidence losses and wake mixing losses. The skin friction losses are determined in a similar manner as one would calculate friction losses within a pipeline. The most important parameters are the hydraulic diameter (d_H) and skin friction coefficient (c_f).

Incidence losses occur due to an offset in the inlet incidence angle described in section 2.2. The optimum or minimum incidence loss angle is defined by equation B2.11 which represents a condition where the flow adjustment required to match the blade angle and throat area are approximately balanced. Incidence losses are primarily dependent on the inlet and throat airflow angle, as well as the absolute and meridional velocities at these locations in the diffuser.

The wake mixing model consists of two velocities known as the meridional wake velocity ($C_{m,\ wake}$) and the meridional mix velocity ($C_{m,\ mix}$) (equations B2.24 and B2.25). After the three aforementioned losses have been calculated, the total pressure at the diffuser outlet is altered accordingly. This is done by making use of equation B2.27. The entire process as discussed in this subsection is an iterative

process. As a result, when using a computerized system, the process would have to iterate until convergence of the meridional velocity at the outlet of the diffuser (C_{m4}) has been reached. This iterative process is described in greater detail in Appendix B2.

2.3.6. Blade excitation and vibration avoidance

Several design rules exist to which designers have adhered in an effort to avoid blade excitation within a centrifugal compressor. It may cause cyclic fatigue and compressors may fail, sometimes catastrophically. It is imperative that a designer avoid the occurrence of blade excitation in order to protect the safety of the compressor itself but more so any persons working near such a system.

Vibrations within a centrifugal compressor can occur due to two reasons. The first being the formation of shock waves from the tip of the impeller outlet that collides with the leading edge of the diffuser vanes. This causes a subsequent and severe cyclic loading around the circumference of the vanes in the downstream space. The second reason being that parts within the compressor experience amplified forces inherent during the operation of a centrifugal compressor due to the natural frequency of parts being the same as the frequency of cyclic loads. This leads to vibrations occurring at such amplitudes that structures fail. Kushner (2004: 144) states that the designer should at all times avoid surge as this could also lead to vibration within a compressor.

To overcome blade excitation a prime number is used for the number of impeller blades while using an even number for diffuser vanes (Kushner, 2004: 157). Kushner (2004: 144) also states that the natural frequency of a compressor component can be controlled by varying the blade/vane thickness and even the radius ratio. A more drastic vibration avoidance method is to include damping. The design required by the CSIR does however inhibit the inclusion of damping mechanisms and as such the number of vanes forms the main parameter of blade excitation avoidance.

3. MEAN-LINE CODE DEVELOPMENT AND OPTIMIZATION

3.1. 1-D Code development

The previous theses done by Van der Merwe (2012) and De Wet (2011) have provided a foundation for the continued development of a mean-line code. The code, written in MATLAB®, will be expanded to create the radial diffuser geometry and to calculate the centrifugal compressor performance.

3.1.1. Advantages and disadvantages of using a mean-line code

Since an initial geometry is required for the CFD analysis, a mean-line code can be used to create the geometry of the centrifugal compressor by means of an x,-, y-, z-coordinate system. The 1-D analysis makes use of simple turbomachinery theory that determines the performance of the centrifugal compressor as well as the radial diffuser and hence selects the best geometrical combination of both.

Though the way of obtaining the best geometry is not strictly by means of optimization, the solution does converge after a certain number of steps (Figure 7). Using simple 1-D theory, an initial geometry for the compressor can be created faster than would have been possible with CFD geometry creation modules or manually via a Computer Aided Design (CAD) package.

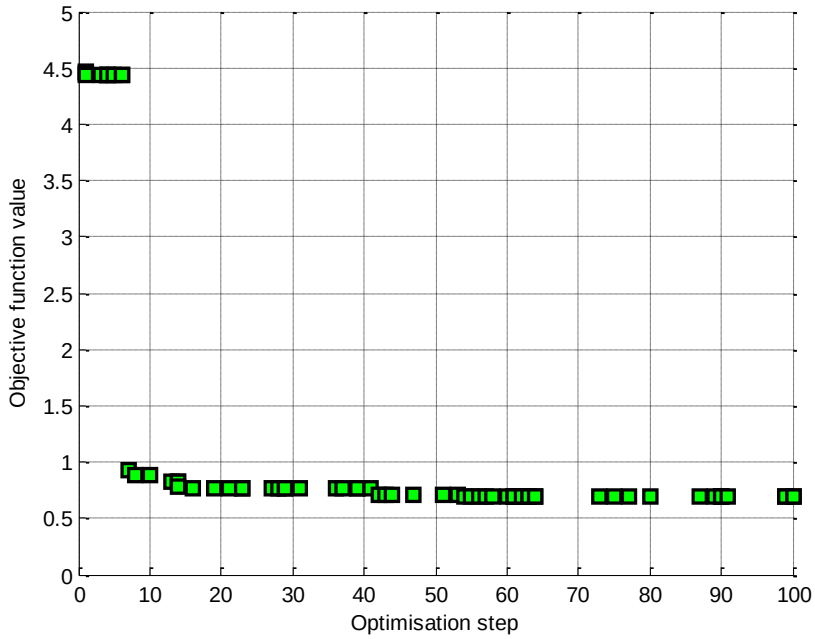

Figure 7: Mean-line code convergence of compressor performance.

The procedure for creating the geometry of the impeller is provided by Aungier (2000: 180-182). Van der Merwe (2012) and De Wet (2011) used this procedure in order to develop the mean-line code that creates the geometry of the impeller. As such the aim was to develop the diffuser geometry by also making use of Aungier's procedure. In doing so continuity of the design methodology is ensured.

Aungier (2000) provides a theoretical framework in which the designer can create his/her own CFD computation. This is required in order to determine aerodynamic performance parameters such as blade loading and boundary layer growth. This is however very tedious and could most probably not be as accurate as using existing CFD packages. Van der Merwe (2012) and De Wet (2011) used Aungier's procedure but excludes the CFD process by rather using Numeca FINE^{TM}/Turbo for the CFD computation. In order to ensure continuity within the ballast project, the author thus aimed to follow this basic methodology and as such the mean-line code provides only an initial means of creating a centrifugal compressor geometry, which includes the diffuser geometry, and determining its performance.

3.1.2. Execution and flow of the mean-line code

The existing flow diagram of the mean-line code can be seen in Appendix A1 (Figure 48) and the main function '*optimise.m*' is shown in Appendix A2. The means by which the main function operates is that the main geometric and operating properties of the compressor are provided. The user can then specify which of these parameters should be altered/variable when running the program. Variable parameters are given a range within square brackets ([]). The main function then calculates the number of parameters that need to be altered i.e. within square brackets.

It is common practice for the user/designer to increase the number of iterations should the number of variable parameters also increase. From here the program selects, at random, a value within the range of the variable parameters as well as the required constant parameters and feeds it into the other functions. The program then calculates the performance of the impeller as well as diffuser. After the performance has been calculated the geometry of the compressor design that has delivered the best performance is saved until another better performing geometry has been realized.

It is important to design the compressor by considering the interaction between the compressor's impeller and radial diffuser. Therefore it was decided that the best means of creating the diffuser geometry was to capture the thermodynamic

conditions at the trailing edge of the impeller and to feed this data into the radial diffuser functions that would create the diffuser geometry and determine its performance.

3.2. Implementation of radial diffuser theory into mean-line code

Since the code had to create the diffuser as detailed in the procedure of Aungier (Figure 4) certain changes had to be made. The reason for this, as discussed in section 3.1.1 above, is because some aerodynamic properties had to be determined using CFD. Since the geometry had to be created iteratively, the processes as seen in figure 4 had iterations within themselves. The major alterations to Aungier's process can be seen in figure 8.

As mentioned in section 2.3.2 two parameters are of importance when designing a radial diffuser, the divergence angle ($2\theta_c$) and the blade loading parameter (L). Due to the radial dimensional constraints as set for the MGT by the CSIR (a diameter of roughly 75 mm) it was found difficult to adhere to the L constraint since the diffuser vanes had to fit within the given radial distance. It was however possible to adhere to the constraints of $2\theta_c$ while maintaining a near choked flow through the diffuser throat.

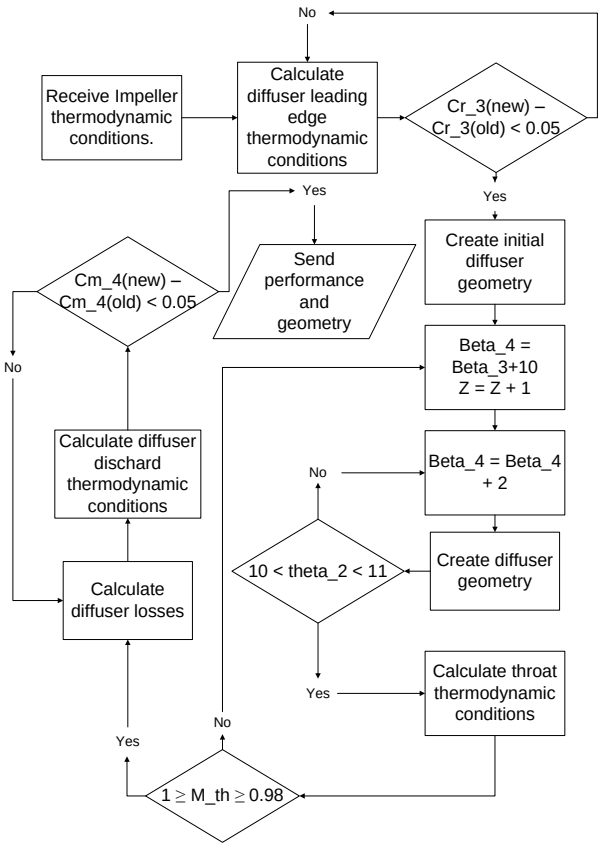

Figure 8: Diffuser design flow diagram.

Figure 8 shows that an iterative process takes place in which the diffuser vane outlet angle (β_4 denoted as Beta_4) is altered until the diffuser adheres to the required limits of $2\theta_c$. After this iterative process the throat aerodynamic conditions are calculated. Should the throat not be close to choke, another vane would be added. Since $2\theta_c$ is dependent on the number of vanes (equation B2.14) the entire iterative process has to be repeated to ensure that $2\theta_c$ falls within the accepted limits. In so doing the diffuser design code ensures that the diffuser adheres to the constraints of $2\theta_c$ as well as maintaining near choked flow in the throat as this provides better diffusive properties (section 2.3.1).

After the throat thermodynamic conditions have been calculated the diffuser discharge thermodynamic conditions need to be calculated. As described in detail in Appendix B2, this is an iterative process until convergence of C_{m4} has been reached. After C_{m4} has been calculated the performance as well as the required geometrical parameters of the diffuser are sent back to the function *getPerf()* (Figure 49).

The requirements of the impeller designed by Van der Merwe (2012) were to obtain a high as possible total pressure while maintaining a certain degree of

isentropic efficiency. With the development of the new compressor that incorporates the design of a new impeller and diffuser, new requirements had to be created. In contrast to a total-total pressure ratio it was decided that a total-static pressure ratio will best suit the requirements of the new compressor as first of all, the static pressure will be measured more easily during testing and secondly, the ultimate goal of a diffuser is to convert the kinetic energy of the gas into a static pressure rise.

3.3. Geometry obtained from mean-line code

In section 2.3.3 it was mentioned that the diffuser vane camber line is defined by a logarithmic function consisting of several constants that in turn consist of two parameters, K_3 and K_4. These constants are user defined and as mentioned influence the blade loading and stall on to the blade. Since the author had decided that the diffuser vane camber line had to be altered during CFD optimization the values for K_3 and K_4 were kept constant at 1. The camber line profile created by defining K_3 and K_4 is shown in figure 9.

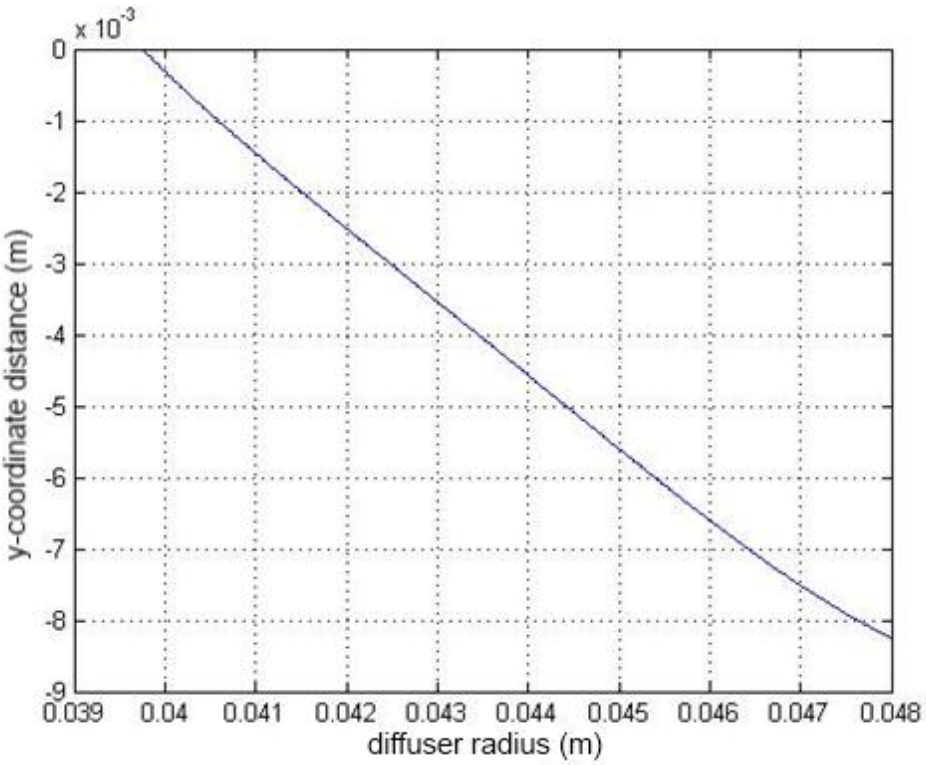

Figure 9: Diffuser camber line.

This has no effect on the performance of the diffuser as calculated by Aungier's theory since the diffuser performance depends on the outlet angle of the vanes (β_4)

and outlet area. The resulting vane shape created when introducing the governing equations that define the pressure and suction surfaces are shown in figure 10. Figure 10 shows the sharp leading edge of the diffuser vane as it is believed to perform better than a blunt or rounded leading edge. It was also assumed that defining the trailing edge thickness of the vane as zero would provide a better area ratio and reduce the risk of recirculating air in front of the axial guide vanes. This could in turn reduce the risk of having non-favourable conditions for combustion.

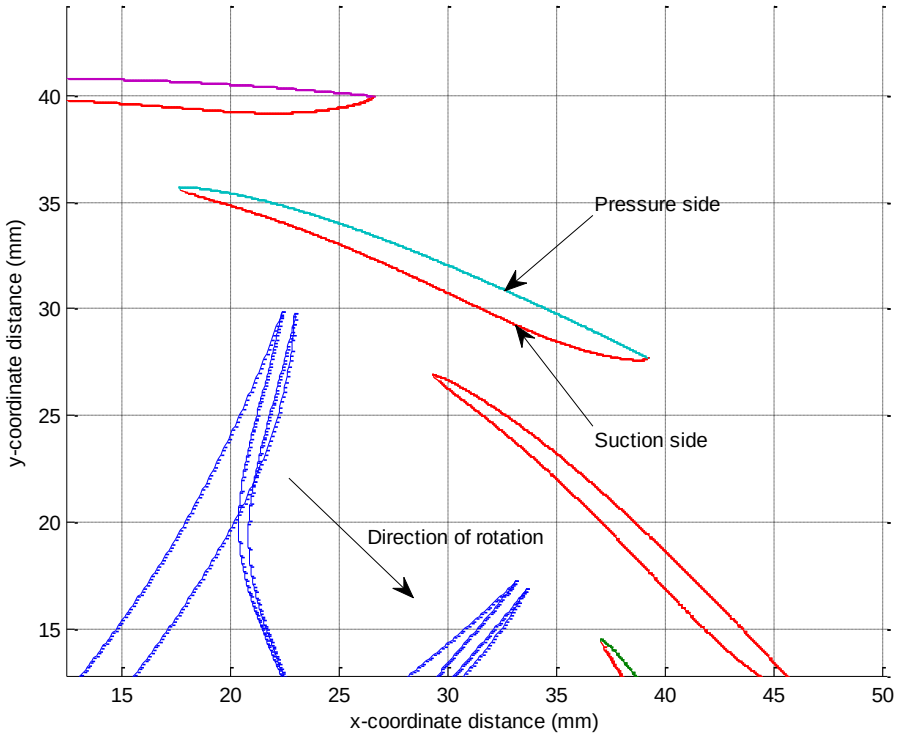

Figure 10: Diffuser vane shape for K_3 & K_4 equal to 1.

In section 2.2 it was discussed how the radial gap or the radius ratio (r_3/r_2) has a significant effect on the interaction between the impeller and diffuser and how it can affect the efficiency and pressure ratio of the diffuser. The size of the radial gap must also be selected carefully depending on the impeller trailing edge Mach number i.e. for higher Mach numbers a longer radial gap or larger r_3/r_2 value is required. Since the mean-line code determines the Mach number at the diffuser throat the author has decided not to allow for alteration of the diffuser inlet radius during the mean-line performance evaluation but rather set the inlet radius to a constant lower value i.e. $r_3/r_2 = 1.06$. The reason being that this lower limit allows for a larger vaned radial diffuser space since the outer radius is severely constrained. Furthermore it also decreases the losses found in the vaneless gap. In

so doing it is believed that a larger vaned radius will allow for greater static pressure recovery.

When defining the inlet radius of the diffuser vanes to be variable, i.e. r_3/r_2 = 1.06 to 1.12, the mean-line code suggests that r_3/r_2 be closer to 1.12. As such the diffuser throat is further from the outlet of the impeller as would have been in the case where r_3/r_2 = 1.06. Without diffuser vanes then, the Mach number would be lower at $r_3 = r_2 1.12$ than at $r_3 = r_2 1.06$. Accordingly, to ensure a Mach number near unity at the diffuser throat for $r_3 = r_2 1.12$ more diffuser vanes would have to be used in order to decrease the throat cross-sectional area. This is evident when comparing figure 11 to figure 12.

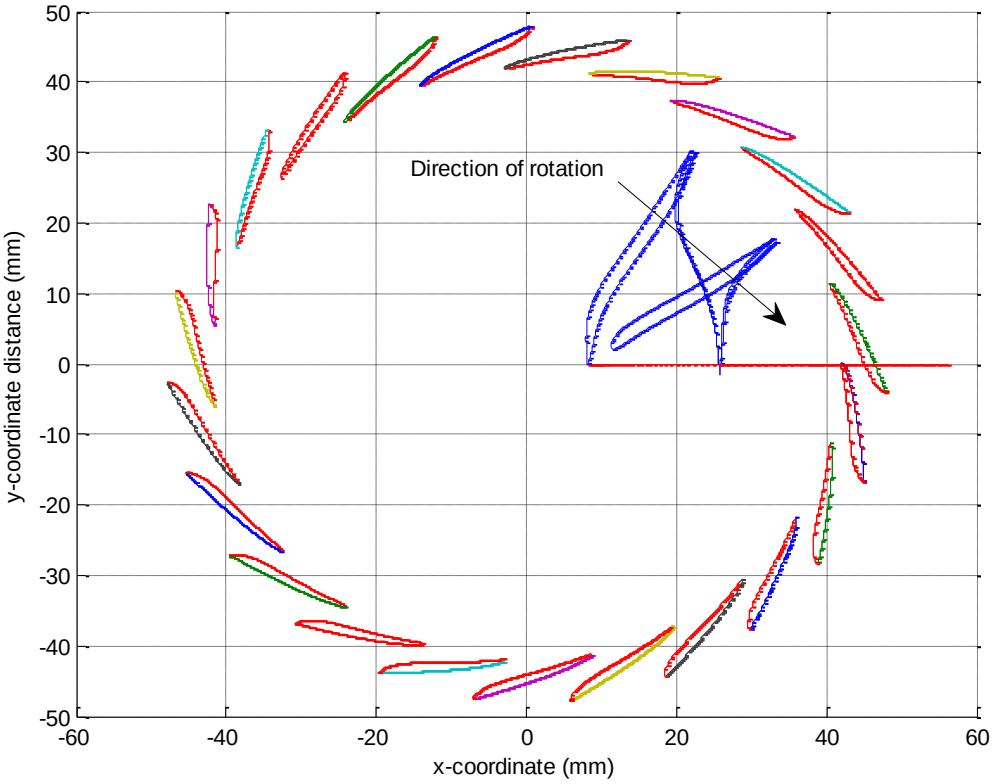

Figure 11: Diffuser geometry for $r_3 = r_2 1.06$ to 1.12.

Though the mean-line code theory suggests that a longer vaneless gap might be more appropriate one should remember that the mean-line code is based on 1-D theory. It is believed that a larger vaned radial distance would allow for greater pressure recovery. As such r_3 was kept constant at $r_2 1.06$ and the resulting diffuser geometry is shown in figure 12. Figure 12 shows a longer vaned space

since the diffuser inlet is closer to the impeller trailing edge as well as having fewer vanes (17 vanes compared to 23 as in figure 11).

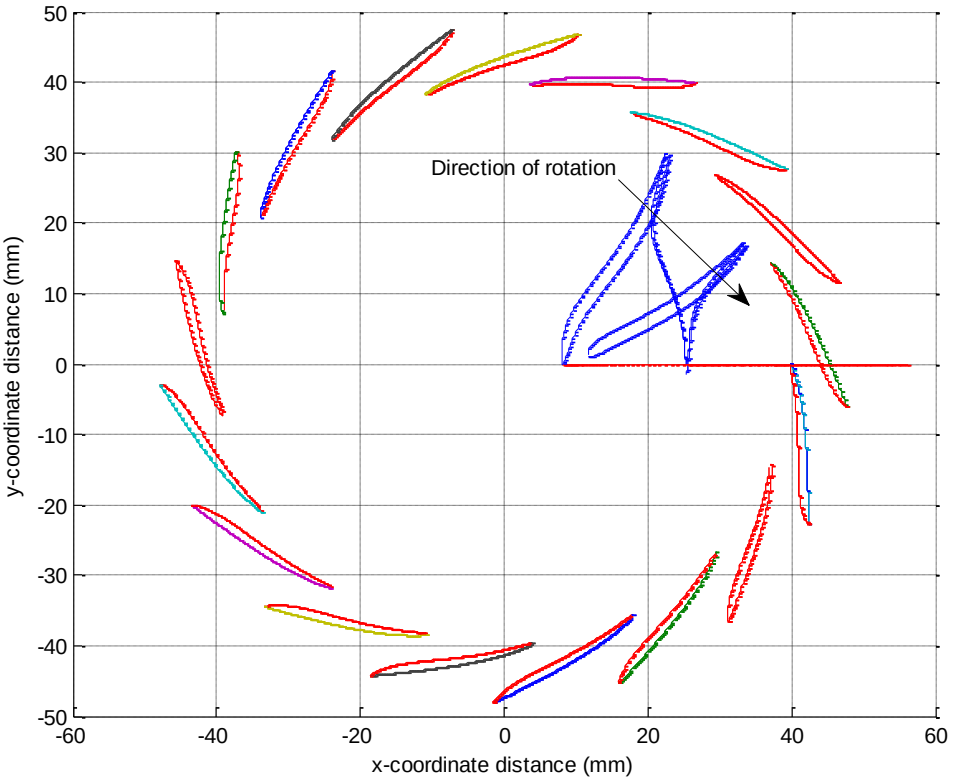

Figure 12: Diffuser geometry for $r_3 = 1.06r_2$ (MATLAB® figure)

The author aims to allow for alteration of the diffuser inlet radius during CFD optimization which will more accurately incorporate the effects of losses and pressure rise.

To create the geometry of the centrifugal compressor in a CFD program the coordinates of the geometry had to be written to a text file in a *.geomTurbo* format. In order to make sure that this geometry creates the required curves and surfaces it was decided to first of all create a simple geometric plot using the plot function within MATLAB®. The hub and shroud curves/surfaces of both the impeller and diffuser are shown in figure 13 (an isometric plot of this geometry is depicted in figure 51).

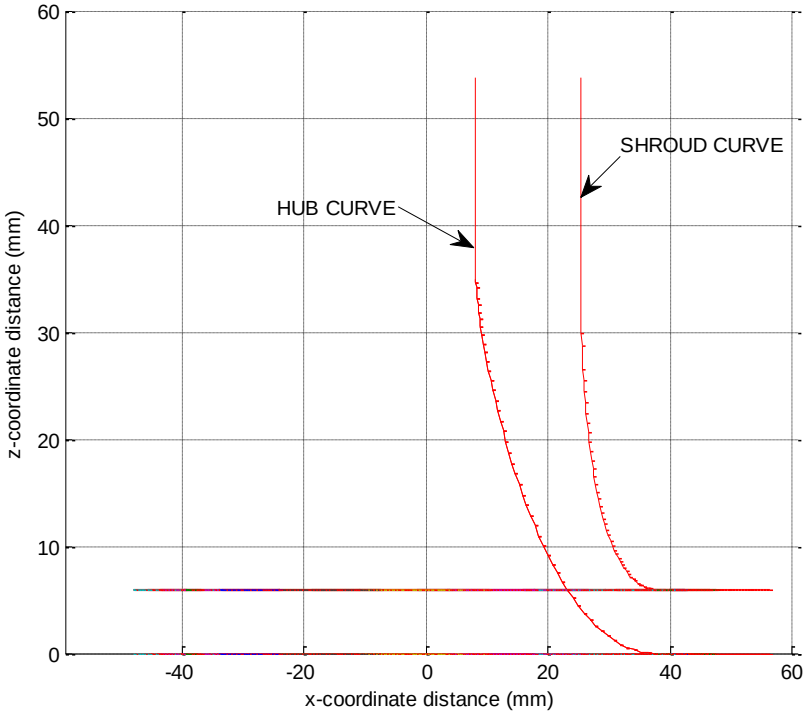

Figure 13: Hub and shroud curves of the impeller and diffuser.

Figure 13 and 51 show that the hub and shroud curves extend upstream from the impeller inlet and downstream from the impeller outlet. This was done in order to incorporate a well-defined inlet and outlet that had to be created during the meshing operation discussed later on. A further alteration to the outlet had to be done and is discussed in section 4.1.2

4. VALIDATION AND CFD SETUP

Although 1-D turbomachinery theory exists that can be used to design turbomachines it is important to realize that certain flow patterns and phenomena cannot be determined by making use of this theory. These flow patterns include recirculation, boundary layer growth and blade loading. Therefore it has been decided that CFD simulations be implemented for the design of the centrifugal compressor discussed in this report.

4.1.Meshing, CFD setup and validation

Before any design can make use of CFD, validation of the simulation setup has to be performed in order to make sure that said simulation has, in fact, been set up correctly.

4.1.1. Mesh setup

Mentioned in section 3.1.1 the geometry created by the mean-line code is in the form of points within a Cartesian coordinate system. These points are written to a text file with a *.geomturbo* format. Numeca provides two mesh generator modules namely Autogrid 5® and Interactive Grid Generator (IGG). Autogrid 5® has several advantages compared to IGG. First of all the geometry can be imported by making use of the *.geomturbo* file. Secondly the topology of the machine can be set up more easily. Autogrid 5® also provides functions that can be used to create a favourable and high quality mesh.

After the geometry has been imported the user continues in setting up the topology of the model. This involves defining the sort of machine that will be simulated and optimised. Appendix D1 shows the Graphical User Interface (GUI) of Autogrid 5® (Figure 52). The specific format of the *.geomturbo* file allows Autogrid 5® to create the hub and shroud curves, the shape of the main blades and also whether a splitter blade is present, of which the geometry is also defined. Figure 14 shows the leading edge (LE) of a blade and how all curves imported into Autogrid 5® are defined. The main and splitter blades hub and shroud curves as well as the hub and shroud curve itself are hence of a jagged shape. There are therefore certain locations were the blade surfaces do not intersect the hub and shroud surfaces.

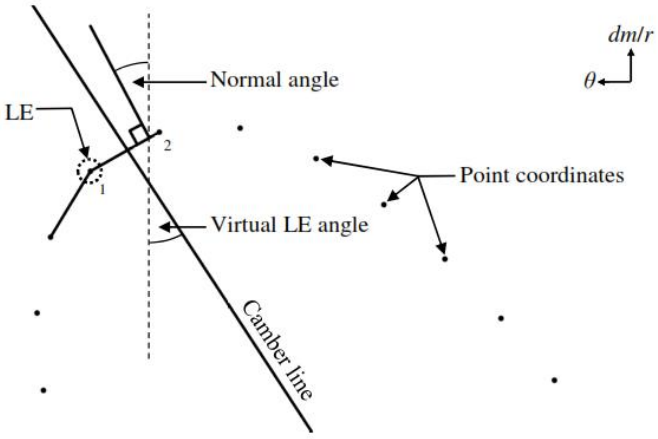

Figure 14: Point coordinates used to define a blade section (Van der Merwe, 2012: 23).

Autogrid 5® cannot mesh a domain with this error present and therefore the user must expand the main and splitter blades hub and shroud curves. An expansion of 0.015 mm was used and was sufficient in allowing the blades to pass through the hub and shroud surfaces.

After the user has defined what type of machine needs to be modelled the number of blades are defined. Following this procedure is the setup of the cell width on the walls. When the length scale is set to millimetres (mm) Autogrid 5® selects a default cell width size of 0.01 mm at the walls. This can be altered later should the $y+$ values not coincide with the turbulence model used.

After this process the user defines whether or not a tip gap exists between the impeller and shroud. Since the impeller is not a shrouded design a tip gap was defined. Van der Merwe (2012: 46) defined the tip gap as 4% of the value of the impeller trailing edge blade height. Hence

$$t = 0.04b_2 \tag{4.1}$$

Since b_2 is 6 mm the tip gap was calculated to be 0.24 mm. The author did however decide to make the tip gap 0.2 mm. The reason being that the height of the cells spanning from the shroud wall to the blade edges will have a value of nearly 0.01mm and increase in height further from the shroud wall due to a bias. Since 0.2 is a smaller multiple of 0.01 it was believed that the mesh in the tip gap remain better structured, resulting in a better mesh quality. A smaller tip gap also lessens the flow of air over blade shroud edges and as such the airflow through a rotor channel can be maintained better. Autogrid 5® also allows the user to define a blade fillet at the hub surface.

Several samples for optimization (see section 5.2.1) had to be created and simulations run for each of the samples. Therefore a coarse as possible mesh of high quality had to be created in order to reduce computational time. In excluding the blade-hub fillets the mesh, which is of body fitted structured type, retains a good quality since the cells are stacked more orderly at the hub surface. It was argued that the loss in accuracy is negligible when excluding the blade-hub fillets and considering the time saved during simulations.

A surface at a 50% span between hub and shroud is created first and the user can then make use of several built in Autogrid 5® functions in order to create a good quality mesh. These functions include a mesh quality check, an optimizer (Figures 53 and 54) and a manual mesh altering tool (Figures 15 and 16). The manual mesh altering tool allows the user to insert the number of nodes on each edge of the blocks surrounding the blade. The number of nodes on the block edges surrounding the main blade is shown in figure 15.

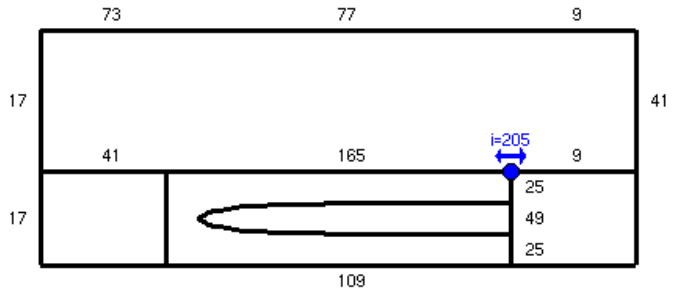

Figure 15: Grid definition for main blade.

The same procedure is followed for the splitter blade with minor differences on the locations of the nodes. Figure 16 shows the number of nodes that make up the splitter blade flow domain.

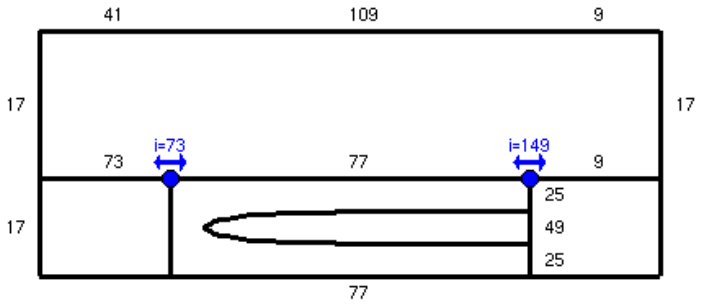

Figure 16: Grid definition for splitter blade.

A good quality mesh is ensured when 3 factors adhere to constraints. These factors are orthogonality, expansion ratio and aspect ratio. These factors must fall within the limits as shown in table 1 (De Wet, 2010: 34). Table 1 shows the mesh quality of the impeller as designed by Van der Merwe (2012).

Table 1: List of mesh constraints, values obtained and error.

Constraint	Adherence	Value obtained	Error
Aspect ratio	< 2100	337.65	0.0%
Expansion ratio	< 3.0	3.0369	1.22%
Orthogonality	> 24°	34.335	0.0%

4.1.2. CFD setup

Following the mesh setup is the simulation setup. FINE™/Turbo is the module used to simulate the impeller. The performance of the impeller is of concern at the design point. The blades and hub, which form part of a moving boundary, were defined to rotate about the impellers axis at a rotational speed of 121 kRPM. Figure 55 shows the GUI of FINE™/Turbo where the user defines the boundary conditions. The FINE™/Turbo module detects the hub, shroud and blades making it easy for the user to define the speed at which the moving part rotates. The hub surface is seen, within FINE™/Turbo, as a surface greater than the hub surface of the actual compressor. As such the hub cannot be defined as a constant rotating body but rather as an area defined rotating body. The boundary conditions are set up as follows:

- The inlet boundary is defined by making use of total conditions and an extrapolated absolute velocity (see table 2).

Table 2: Total quantities imposed on inlet boundary (V extrapolated).

Quantities	Definition	Value	Units
$V_r/\|V\|$	Constant	0	~
$V_t/\|V\|$	Constant	0	~
$V_z/\|V\|$	Constant	-1	~
Absolute Total Pressure	Constant	101325	Pa
Absolute total temperature	Constant	293	K
Turbulent viscosity	Constant	0.0001	m^2/s

The user can define the quantities as being either constant or user defined. User defined quantities allow the designer to import a profile for said quantity. It was assumed that the velocity profile at the inlet boundary is completely uniform and in a purely axial direction (-z direction) hence the total pressure and temperature will be uniform. The no-slip condition would allow for minimal flow development from the inlet boundary to the inlet of the impeller blades but the effects are assumed to be negligible.

- The outlet boundary was defined with an imposed static pressure of 260000 Pa.

It was also realised during initial simulations that convergence was difficult to achieve in that the simulations blew up/diverged. The reason being that backflow occurred at the outlet boundary, resulting in the calculation of negative densities. To overcome this common problem FINE^{TM}/Turbo has a function called "*backflow control*" which was employed for the outlet boundary. Another means of overcoming this problem is to pinch the outlet. The Numeca support department suggested the means by which the outlet should be handled (Figure 17).

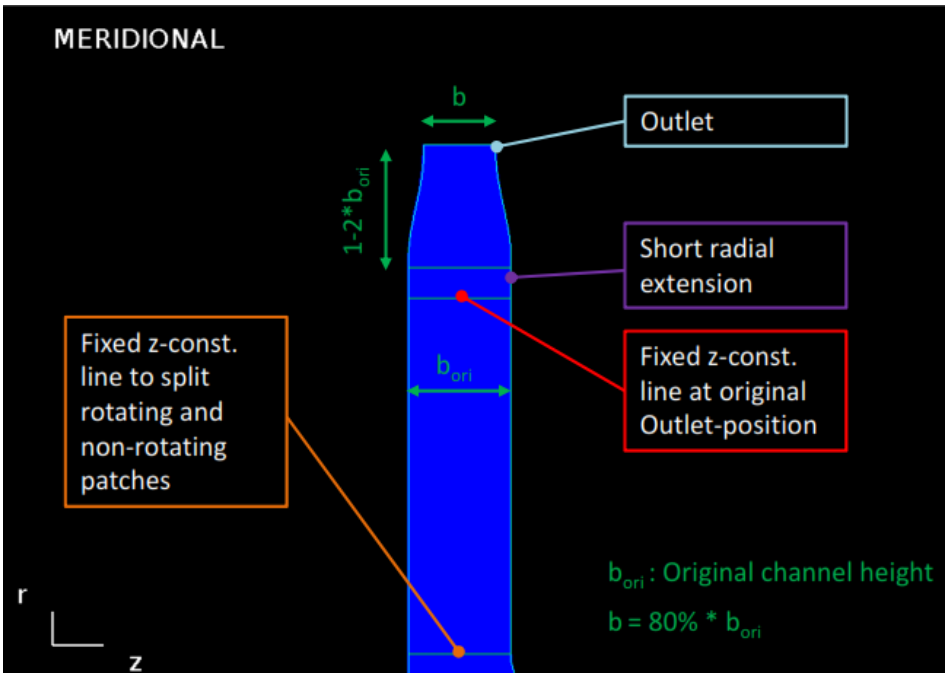

Figure 17: Use of pinch to overcome outlet boundary backflow (Courtesy of Numeca International: April 14, 2013)

By making use of figure 17, the MATLAB® function that writes the *.geomturbo* text file could be altered such that a well-defined pinch exists at the outlet.

The boundaries that encompass the flow volume of a CFD simulation consist of several types. These boundaries are the inlet, outlet and wall boundaries. The wall boundaries can be stationary, moving or symmetric. The inlet and outlet conditions can be defined as a mass flow rate, velocity or other thermodynamic conditions (either static or total). It is common practice to define an inlet boundary with the total pressure found at that point during testing or operation of the design, as done by Everitt (2010: 58) whereas the outlet boundary may be defined as a static pressure that is expected at that point (Versteeg & Malalasekera, 2007: 268), also during operation. The operation of a centrifugal compressor requires the rotation of the impeller blades and the hub whereas the shroud is to remain stationary. The boundaries that make up the blades, hub and shroud were therefore defined accordingly.

The no slip condition is appropriate for the velocity components adjacent to the walls as this conforms to basic fluid mechanics theory (Versteeg & Malalasekera, 2000: 273).

FINE™/Turbo detects, due initially to the format of the *.geomturbo* file, the hub, shroud and blade surfaces. In order to create a well-defined inlet and outlet of the flow domain the hub and shroud surfaces extend further upstream and downstream from the impeller than found on the actual machine. Therefore the rotating hub surface had to be limited within the ZR (meridional) coordinate system such that only the required rotating surfaces are encompassed. This is done by defining the upper and lower bounds of both the radius (r) and height (z).

Table 3: Dimensional constraints of impeller hub.

Dimensional constraint	Value (m)
Lower radius limit	0.008138
Upper radius limit	0.038000
Lower axial limit	0.000000
Upper axial limit	0.040000

In contrast the actual upper radius limit is 0.0375 m and the actual upper axial limit is 0.035 m. It was decided however to incorporate higher limits because first of all the effects are negligible and secondly, the upper ranges during optimization may well be as high as the upper values seen in table 3. The fluid selected was air as a perfect gas. FINE™/Turbo provides several common fluids used in industry.

Air can be used as being either real or perfect. It was argued that the difference in results when simulating air as a perfect gas would be negligible compared to simulating air as a real gas.

Turbulence models that are available in the field of CFD are:

- k-epsilon (k-ε) model
- Wilcox k-omega (k-ω) model
- Menter SST k-ω model
- Spalart-Allmaras (SA) model
- Reynolds stress equation model
- Prandtl's mixing length model

It has been found that the SA model is best suited for modelling aerofoils and as such is often used for turbomachinery simulations (Versteeg & Malalasekera, 2007: 90). Bradshaw (1996: 620) also states that, if modelling separating flow (stall) is of importance, the favourite turbulence model is the k-ε model with growing interest in the Wilcox k-ω and SA models. The rate of convergence for CFD simulations is important for any designer. It has been found that if turbulent quantities need to be simulated accurately and a good convergence rate is required the SA model is preferred (FINE^{TM}/Turbo v8.9, 2011: 4-9).The SA turbulence model was chosen to determine turbulent quantities of all the CFD simulations.

The geometry of the compressor flow domain that must be modelled determines the rotor-stator interface (ROT) that must be employed. The "*Conservative Coupling by Pitchwise Rows*" function was employed since first of all the spanwise patch length on either side of the ROT for both the rotor and diffuser flow domains are the same. Secondly the ROT for both these flow domains is a circular arc (FINE^{TM}/Turbo v8.9, 2011: 8-40).

The stability of the simulation as well as the quality of the mesh must be confirmed. As such the simulation is run for three mesh levels. These mesh levels are denoted 222 (coarse), 111 (medium) and 000 (fine). Since the setup defined in FINE^{TM}/Turbo is used during the optimization process it was imperative to make sure that the simulation converges as quickly as possible. Hence the numerical model was set up as follows:

- Courant-Friedrich-Levy (CFL) number set to 600. The CFL number globally scales the time-step sizes used for the time marching scheme of the flow solver. A high CFL number allows for quicker convergence but

should it be too high the simulation will be unstable and diverge (FINE/Turbo user manual, 2011: 6-2).

- Central Processing Unit (CPU) booster employed.
- Number of simulation steps for the 222 and 111 grid levels set to 25.
- Convergence level for the 222 and 111 grid levels set to -3.0 (log scale).

The simulation starts with the 222 grid level, continuing on to the 111 grid level and finally the 000 grid level. In doing so the stability of the setup and mesh quality is not only checked but the simulation process quickened. The reason being that the simulation is quicker in coarser grid levels and when convergence is reached in a coarser grid level, the thermodynamic conditions and other quantities are passed on to the finer grid level as initial conditions. In doing so the finer grid level obtains a more accurate initial solution from which to start computing, allowing for faster simulation.

- Initial conditions are provided by estimations from the user. Table 4 show the initial conditions from which the 222 grid level starts computing.

Table 4: Initial conditions provided by the user.

Condition	Value	Unit
Static Pressure	220000	Pa
Static Temperature	340	K
V_r	90	m/s
V_t	-60	m/s
V_z	-40	m/s

The entire computational domain assumes thermodynamic conditions as defined in table 4. From here FINE^{TM}/Turbo calculates the flow conditions accurately.

4.1.3. Validation of impeller under operating conditions

First of all a basis must be chosen by which the author's simulations will be compared. Since Van der Merwe (2012) has already made use of the same CFD package (Numeca) and the results of his design had been validated, it was agreed that his results be used as the basis of comparison. Though this thesis involves the design of an impeller as well as a radial diffuser validation could only be done by first simulating an impeller only as this was the design done by Van Der Merwe (2012).

The optimised impeller geometry of Van Der Merwe was obtained, meshed as discussed above and simulated in FINE^{TM}/Turbo. The design point operating conditions as set forth by the CSIR for the design of Van der Merwe's impeller was that of pressure ratio and isentropic efficiency at a given mass flow rate (see section 1.3.2). The author decided that the pressure ratios as determined by Van der Merwe would suffice for comparison purposes.

Figure 18 shows the pressure ratio (t-t) performance curves as determined by FINE^{TM}/Turbo. It is clear that although there are certain discrepancies the basic shape and values of the curves resemble that of Van der Merwe's results. There can be several reasons for the discrepancies. The main reason is believed to be that the inlet total pressure as set up by the author is not the same as that set up by Van Der Merwe. The author used 100 kPa for the inlet total pressure as it was assumed to be near the same pressure present during testing at Stellenbosch. The inlet total temperature was set to 293 K. It is believed that Van Der Merwe used 98 kPa. It is thus believed that at a lower inlet total pressure the compressor will choke at a higher mass flow rate and should the author have made use of a lower inlet total pressure the curves would have correlated better. It is clear that at the design point mass flow rate of 0.325 kg/s (1 on the x-axis) and a rotational speed of 121 kRPM the curves would coincide at almost the exact same value.

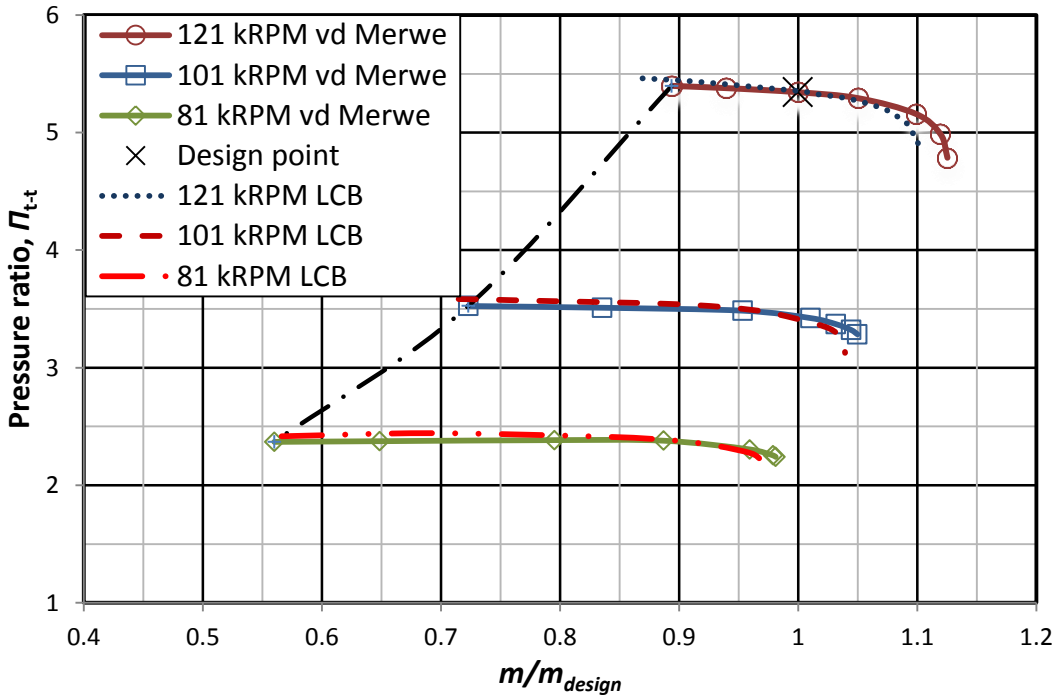

Figure 18: Validation of CFD setup to that of Van der Merwe's CFD results.

Another very important factor to consider is the y^+ values used for the simulation. The y^+ values when using the SA turbulence model are required to be less than 10 (FINE^{TM}/Turbo v8.9, 2011: 4-12). Figure 19 shows the y^+ values on the hub as well as main and splitter blade surfaces.

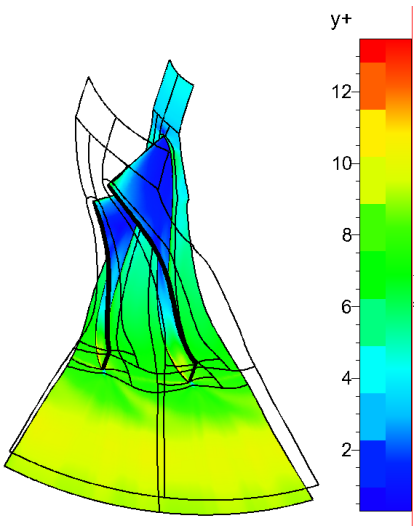

Figure 19: y+ values on the hub, main and splitter blades for Van der Merwe's impeller.

Although the shroud surface is not visible within figure 19 it is safe to assume that the y^+ values on the shroud surface is also within the required range as the y^+ values only approach a value of 10 further downstream of the rotor. The results resemble the results of Van der Merwe acceptably and the y^+ values are within the required range. It was therefore concluded that the setup used in FINE^{TM}/Turbo would be acceptable when designing or optimising the compressor.

When observing initial CFD simulation results of the mean-line code rotor it was discovered that severe recirculation occurred at the shroud immediately downstream of the impeller (Figure 20).

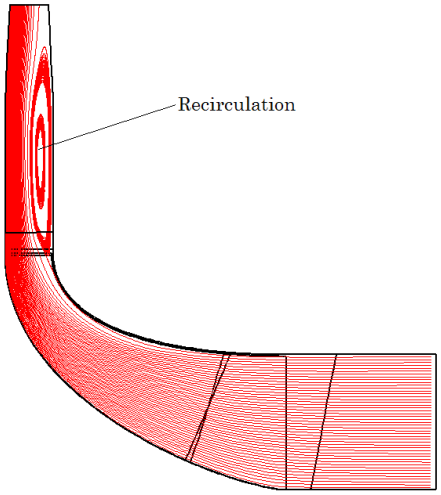

Figure 20: Flow lines showing Recirculation at shroud curve downstream of mean-line rotor.

This was assumed to be problematic as the diffuser vanes would not be able to effectively capture the airflow and therefore the air would not be subjected to an increase in static pressure. This was proven to be a correct assumption, as discussed in section 5.2.3. Therefore when the design/optimization process is implemented it is important to allow for alteration of the hub and/or shroud curves such that this recirculation can be reduced or eliminated.

4.1.4. Impeller and radial diffuser mesh setup and simulation

The processes of creating the mesh for the impeller and the diffuser are the same. The process had to therefore be repeated twice, once for the impeller and once for the diffuser. The main considerations for the diffuser mesh setup are as follows:

- The diffuser had to be defined as a radial diffuser and not any other row type. This might seem obvious yet it is worth mentioning as this is a required user input for Autogrid5®.
- The diffuser has 17 blades as per the *.geomturbo* file as opposed to 7 for the impeller.
- The diffuser is a stator row and not rotating as the impeller.
- There exists no gap in between the diffuser vanes and the shroud.
- The diffuser section would ultimately have fewer elements than the impeller section.

The mean-line code creates a hub and shroud curve for the impeller as well as diffuser, yet when defining another row in Autogrid5® and importing the

geometry of the diffuser the shroud and hub curves of the diffuser are ignored. Autogrid5® scans the *.geomturbo* file for the x-, y-, z-coordinates of the diffuser vane and imports only the vane geometry. It is therefore important when importing the geometries that the diffuser vane lies within the hub and shroud curves of the impeller. It was also required to expand the hub and shroud edges of the diffuser vanes as the rotor-stator interface (ROT) and outlet would not be created by Autogrid5® and the meshing could not continue. The final mesh quality of the impeller and diffuser is summarized in table 5.

Table 5: Impeller and Diffuser mesh quality (*imp* indicates mesh quality for impeller only).

Constraint	Adherence	Value obtained	Error
Aspect ratio^{imp}	< 2100	297.14	0.0%
Expansion ratio^{imp}	< 3.0	3.0369	1.21%
Orthogonality^{imp}	> 24°	34.337	0.0%
Aspect ratio	< 2100	65.916	0.0%
Expansion ratio	< 3.0	2.5079	0.0%
Orthogonality	> 24°	25.072	0.0%

The error of mesh quality for the Expansion ratio of the impeller was assumed to be acceptable. As was mentioned, the profile of the diffuser mesh allows for a better structured mesh and ultimately a better mesh quality. This is evident from table 5 as the diffuser maximum expansion ratio is less than that of the impeller.

5. COMPRESSOR DESIGN

The initial requirements of the CSIR were that a centrifugal compressor be designed and tested. The design had to fit within given geometrical constraints whilst the compressor performance adhered to a required isentropic efficiency, pressure ratio and mass flow rate (see section 1.3.2).

5.1.Compressor design methodology

Proceeding the validation of the FINE™/Turbo setup is the final and most important steps in setting up the design of the compressor. As mentioned the compressor design has to encompass a well designed impeller, diffuser as well as the interaction between these 2 rows.

5.1.1. Foundation of the design procedure

Numeca makes use of several modules that can be used for the successful design of a turbomachine. These modules are:

- Autogrid 5® and IGG for mesh generation.
- FINE™/Turbo for the simulation and performance calculation of the turbomachine in question.
- CFView® is the post processor where the user collects the results of the FINE™/Turbo simulation. CFView® can be used to find the pressure ratios, efficiencies and view flow phenomena such as recirculation, pressure coefficients and more.
- Autoblade® is used to define the parameters of the turbomachine. This process is described in section 5.1.2
- FINE™/Design3D is the final module that the designer uses to set up a design database and optimise the compressor.

Designing and optimizing a single stage turbomachine would require using all of the above mentioned modules in a procedure explained in the Numeca user manuals whereas designing and optimizing a turbomachine with 2 or more stages become much more complex. A script is used to couple the 2 rows to one another in a single, meshed flow domain. The project file is required to have a specific layout and the user must make manual alterations to this project file in order for the database generation and optimization to run as required. Appendix E1 (Figure 58) shows the layout of the project file used for successful database generation and optimization.

The process starts off with a base run during which the mesh as well as simulation of the initial geometry is done. The base run requires the user to create and run a simulation for the design point of the compressor. After this has been done the user creates a stall point as well as choke point. The entire computational setup for these stall and choke points are the same as for the operating point, apart from the outlet pressure. In the case of the compressor design point the outlet static pressure was set to 280 kPa. The choke point pressure was set at 270 kPa and the stall point pressure at 283 kPa. The design point has a user defined initial solution. The solution of the converged design point simulation is used as the initial solution for the choke and stall point simulations. In doing so the computation time for the choke and stall points is reduced.

The user then duplicates the base run file and names it DB02. The user then makes use of the DB02.iec file to create a database generation module. This creates a different .iec file. The .iec file is a text file that contains all details of the entire project. The user alters the line marked "IGG_AUTOGRID_FLAGS" within the .iec file by providing the grid generation module as well as the version of said grid generation module, and also the directory in which the script file is located (Appendix E2).

The next step is to set up the parameter files for the 2 rows (discussed in detail in the following section). The user alteration is to insert the 2nd row parameters into the 1st row parameter list manually and in a specific format (Appendix E2 discusses this procedure)

The user must also make manual alterations within the script file. The names of the 2nd row free parameters are defined differently in the 1st row parameter list and as a result must be inserted into the script file Appendix E2.

5.1.2. Parameter definitions using Autoblade

The Autoblade module has been developed in order to provide the designer with a complete and very efficient environment in which to design turbomachinery geometry. Autoblade consists of two functions: "*Modeller*" and "*Fitting*". The blade modeller is an advanced geometric modeller for 3-dimensional turbomachinery blades. It initiates the parameter creation process by allowing the user to define the type of turbomachine. The fitting module allows the designer to import an existing geometry by making use of the *.geomturbo* file and determining parameter values that best fit the imported (target) geometry. The Autoblade GUI can be seen in Appendix D3 (Figure 56).

The parameter values define a given set of default curves within Autoblade. These curves have to be selected by the designer such that the curves best suit the geometry of the compressor. An example would be that the impeller blade camber lines are best defined by a Bezier curve whereas the diffuser vanes camber curves best suit a B-Spline curve. The designer would also define the number of points from which these curves would be created. These points will then make up the parameters that are later used to alter the compressor geometry for database generation and optimization. Care must be taken however that the curves have sufficient points in order to best resemble the target geometry, while at the same time not generate too many parameters that would lengthen the optimization process. Figure 21 shows how the B-spline is defined and similarly the Bezier curve. It is clear from figure 21 that the leading edge point is fixed and that the points, that will make up the camber curve free parameters, are equi-spaced downstream of the leading edge.

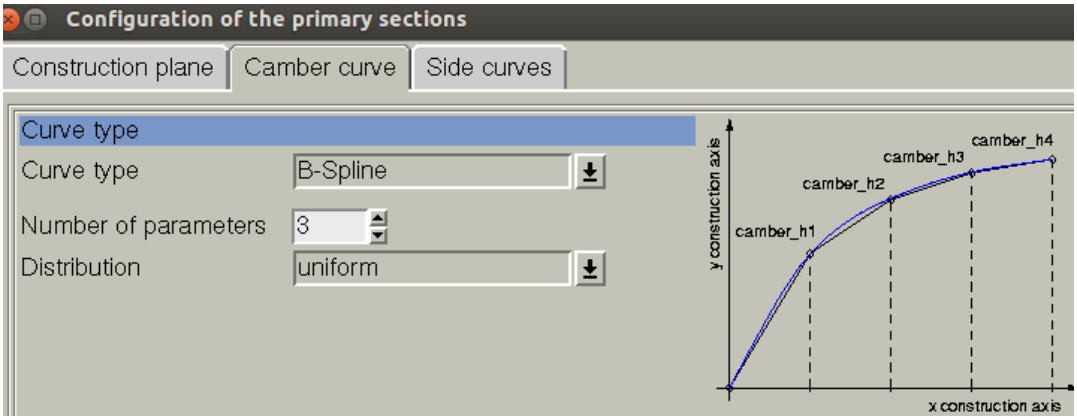

Figure 21: B-Spline definition for camber curve.

The impeller geometry was fitted as follows:

- The hub and shroud curves were defined as B-splines with 7 points. Enough points were specified to ensure that the optimization process would be able to alter the hub and shroud curve in order to eliminate the recirculation problem (Figure 20) and improve the compressor performance.

- The camber curve was defined with a Bezier curve with 8 points. This gave the advantage of not having to alter the inlet blade angle since, when the camber curve is altered a different inlet angle would be created.

- The leading edge height at the shroud and hub was given freedom to vary between 35 and 40 mm. This meant that the leading edge would remain straight albeit at a different angle with regards to the radial plane.

- The lean angle at the impeller trailing edge was allowed to vary between -5 and 5 degrees.

The hub and shroud curves of the diffuser had to be defined such that modelling and fitting within Autoblade could be done successfully. The diffuser vane shape was of importance as the free parameters must be imported into the impeller optional parameter list. Hence, the hub and shroud curves of the entire compressor would be altered during optimization as was defined by the impeller row only. The diffuser vanes existed within these curves and as such the vane shape only had to be defined such that the optimization process could provide the best performing diffuser possible. Initially the author defined the camber curve of the diffuser as a B-Spline with 7 points (free parameters). After the initial optimization process it was found that the diffuser vane had an abnormal shape.

It was important to ensure that the diffuser vane is not of an abnormal shape but rather a smooth, airfoil shape. To overcome this problem, the author reduced the number of points of which the B-spline, that defines the diffuser vane camber curve, consisted.

The leading edge of the vane camber curve does not contain a B-spline point and hence does not have freedom to be altered. Therefore only 3 points, uniformly spaced downstream of the leading edge were specified to make up the B-spline. In so doing, it was ensured that the camber curve cannot take up a B-spline curve shape with a period of more than one. If the B-spline consisted of more points, the camber curve shape could have a period of more than one that would result in an unwanted wave shape.

5.2.Database generation and optimization

The second to last phase of the compressor design involves the generation of a database preceded by the final optimization phase. The FINE^{TM}/Design3D GUI can be viewed in Appendix D4 (Figure 57). FINE^{TM}/Design3D allows for three steps that the designer uses in order to ultimately create the best possible compressor design. The first step is known as *Autoblade Screening* but is not used during the design as discussed in this report. The second step is the database generation which, depending on the amount of samples requested by the designer, is the most time consuming procedure.

5.2.1. Database generation

The database generation process involves gathering all the setups as was done previously into one module (FINE™/Design3D) and according to each setup run individual processes that will ultimately lead to the final compressor design. Said setups include that of the mesh in Autogrid5® (.trb file), CFD simulation as in FINE™/Turbo (.iec file) as well as the different row parameters as in Autoblade® (.par file).

As was mentioned, a design point, choke point as well as stall point were created during the base run setup. This was done in order to make use of multipoint optimization. Multipoint optimization is done in order to ensure that the compressor best adheres to the 3 requirements namely pressure ratio, efficiency and mass flow rate. This is done especially in the case of designing more than one row. When starting the database generation the designer must ensure that all computations present under "*Computation control*" as in figure 22 below are selected.

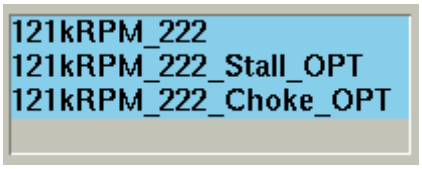

Figure 22: Computation Control box under Computation Management (Design3D).

Therefore the setup of the 3 base run points will be taken into account during the database generation. The reason for creating three base run points will be discussed in the following section.

The "*Continues*" solution was used as it is best understood and is the simplest form of database generation. A random number index generator (RNIG) of 7 was used. Making use of 7 for the RNIG has no specific implication other than the fact that should a RNIG of 7 be used for a second database, the samples would be exactly the same. When the database is being created, FINE™/Design3D randomly selects a value within the range of all free parameters and creates a corresponding compressor geometry. These geometries can be very obscure but will not determine the final compressor design.

In the "*Computation Management*" interface the designer can select four processes that can be carried out by FINE™/Design3D. These include:

- Parametric Blade Modeller: The process by which all the parameters, either free or frozen/constant, are selected and used to create a compressor geometry.
- Mesh Generator: The created geometry is meshed as defined by the designer in Autogrid5®. This process therefore requires that a reference .trb (mesh setup) file be provided.
- Flow Solver: As per the FINE™/Turbo simulation process set up by the designer (in this case the FINE™/Turbo setup of the base run), a simulation is run by which the performance of the compressor created in the aforementioned steps is determined. The conditions that are of importance for evaluation are defined later on and will be used during the optimization procedure.
- Post Processing: The performance of the compressor is then documented automatically by FINE™/Design3D in the _dbs directory.

The following process of setting up the objective function is critical. The CSIR requires that a compressor be designed of which the total-total isentropic efficiency is 79.8 % and the total-total pressure ratio be 4.75 while operating at a mass flow rate of 0.325 kg/s. With the inclusion of a vaned diffuser it was discussed that these conditions be altered. The reasons being that the diffuser converts kinetic energy into a static pressure rise and as such a total-static pressure ratio is of interest rather than a total-total pressure ratio. It was argued that the loss in total conditions still served as a good reference as to how efficiently a compressor operates and therefore a total-total isentropic efficiency was still of concern. The vaned diffuser would however result in a compressor with a lower efficiency as the vanes cause more losses.

The base run setup defined the outlet static pressures as being fixed and hence a total-total pressure ratio was selected as the pressure quantity that will be optimised later on. Furthermore the total-total isentropic efficiency and mass flow rate were also selected as derived quantities.

For a sample to be valid two processes have to be executed without error, the mesh setup and the simulation. If the mesh contains negative cells it is automatically rejected during the FINE™/Design3D process and should the simulation diverge no post processing would be done. During conversation with Numeca support it was discovered that a centrifugal impeller will allow for roughly 85% of the requested samples to be valid. This 85% can be considered a leniency (l_{imp}) of the impeller geometry. This leniency does however diminish

with the inclusion of another stage/row as the possibility of a poor mesh or diverging solution increases.

The designer must then use his/her own discretion in selecting the number of samples that must be created. For thoroughness 60 samples were requested. From the 60 samples 51 were valid that could be used for the optimization process. Assuming that the impeller geometry will allow for an 85% leniency when creating the database one can deduce that

$$51 = 60*0.85*l_d \qquad (5.1)$$

were l_d is the leniency of the diffuser geometry. Hence l_d = 1. Given that the geometry of the diffuser vanes is less complex and as such the possibility of negative cells being present within the diffuser flow domain would be much less, the author concluded that the setup required for database generation process was successful.

The designer should examine the geometry of the samples that are created. This can be done by importing the parameter file (.par file) of any valid sample from the _dbs directory into Autoblade. This .par file is available in the _flow*sample#* file of a valid sample and the _flow*sample#* file is available in the _dbs file. During this examination the designer can see whether or not any abnormal geometries are created for either the impeller or diffuser. Figure 23 shows a diffuser vane shape that is believed to provide good diffuser performance.

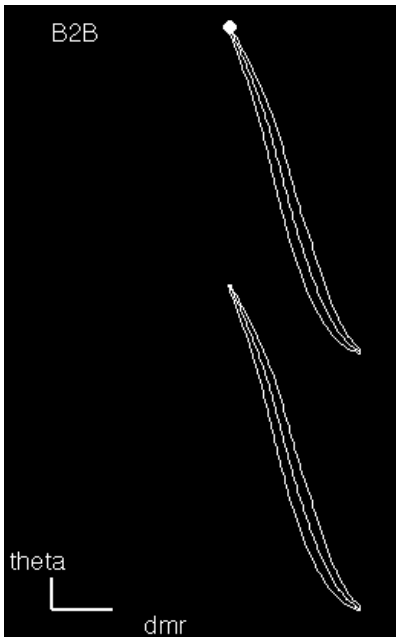

Figure 23: Altered, airfoil shape diffuser vane on a Blade to Blade (B2B) view.

The database generation process can then be left to run until the requested number of samples has been generated.

5.2.2. Optimization

The optimization process is less complicated than the data generation process. During the design of the compressor the simplest form of optimization was used. The GUI of the optimizing module is much the same as that of the database generating module with a few differences. Within the "*Settings*" tree the designer enables the type of optimization process that needs to be carried out including the number of design iterations. The objective function is also created here.

The objective function must incorporate the 3 base run points discussed in section 5.2.1 in order to carry out multipoint optimization. From a performance perspective it is important to design a compressor with a good total-static pressure ratio while adhering to a mass flow rate of 0.325 kg/s and an total-total isentropic efficiency of near 0.798.

The number of iterations that are required is determined by the convergence of the optimizer and design history. Should the design history not have converged within a given number of steps the designer can simply alter the requested number of required optimization steps (iterations) and the optimization process can continue until convergence has been achieved. The simplest form of optimization was chosen i.e. the "*Genetic Algorithm*" method and the designer can decide whether a coarse, medium or fine optimization process needs to be done. It was found that a negligible difference of the objective function convergence existed between the fine and medium optimization processes. A larger difference in the convergence history existed between the coarse and medium optimization in that the objective function of the medium optimizer converged much better. Hence only the medium optimizer was employed in order to save on computational space and time.

From a performance point of view it was believed that the total-static pressure ratio was most important to increase as much as possible, while adhering to a mass flow rate of 0.325 kg/s and a total-total isentropic efficiency of near 0.798. Therefore the derived quantities of total-total pressure ratio, mass flow rate and total-total isentropic efficiency were coupled to the base run design point, choke point and stall point respectively. It is believed that although the base run design point simulation setup defines the outlet static pressure as fixed, the increase in the outlet total pressure might actually increase the outlet static pressure as well. The reason being that the initial outlet static pressure of 280 kPa was, during the base run simulation, well within the range that will allow the simulation to converge. The optimization process then increases this range such that the 280kPa

still lies within, yet on the lower limit, of this stable operating range. This implies that the actual design point static pressure has increased. After the optimization process the designer can then create a performance curve of the optimised design that will reveal the actual performance and design point of the compressor.

In doing so the designer ensured that the design point achieves a total-static pressure ratio of as high as possible. Since the total-total isentropic efficiency was coupled to the stall point the author also ensured that a stall margin was still present and in doing so also provides for a compressor with an efficiency that is as high as possible. By coupling the mass flow rate quantity to the choke point it is assumed that the requirement for the mass flow rate is also met. When employing multipoint optimization, the performance curve of the compressor has to have a well-defined choke and stall margin while achieving a pressure ratio of as high as possible.

Accordingly the objective function consists of a penalty function for each of these 3 parameters. The penalty function is defined as

$$P = W\left(\frac{Q_{imp}-Q}{Q_{ref}}\right)^{k} \tag{5.2}$$

where Q_{imp} is the imposed value, Q_{ref} is a reference value and Q is the actual value of the 3 performance parameters. The imposed values for the pressure ratio, mass flow rate and isentropic efficiency were 3.5, 0.325 and 0.75 respectively. W is the weighting value and k the exponential value. An initial optimization proved that W cannot be set equal for each of the requirements. The reason being that the mass flow rate converged to a value higher than 0.325 and it was feared that this might cause the turbine (or any other stage downstream of the compressor) to choke. Hence a weighting value had to be defined for the mass flow rate that is higher than that of the efficiency. It was also found that the pressure ratio did not increase as much as required and hence the weighting value of the pressure ratio was also increased. Table 6 shows the values for the different weighting functions as well as the penalty value range.

Table 6: Penalty function setup for the required performance parameters.

Objective Function Value	Pressure Ratio (t-t)	Isentropic Efficiency (t-t)	Mass Flow Rate (kg/s)
Penalty type	Minimum	Minimum	Equality
Penalty Weight	45	20	25
Penalty Value Range	0.273 -> 1.230	0.169 -> 1.222	0.007 -> 6.097
Exponent	2	2	2
Reference/Imposed value	3.5	0.75	0.325

Preceding the setup of the objective function and optimization process the designer can continue in running/starting the process. A well-executed optimization will show that the design history of the objective function has converged as can be seen below.

An Artificial Neural Network (ANN) is used in order to construct an approximate model of the compressor geometry and estimate what the performance would be. The constructed model consists of layers that start with an input layer, has several layers in between that are joined together with connections of varying intensity and ends with an output layer (FINE^{TM}/Design3D User Manual, 2011: 3-21). This forms the basis of creating an optimised geometry. This process starts off rough as the CFD determined performance is not the same as that of the ANN estimate. Figure 24 shows that after a certain number of iterations though the ANN estimated performance and CFD determined performance start becoming similar denoting that the ANN has refined the compressor geometry.

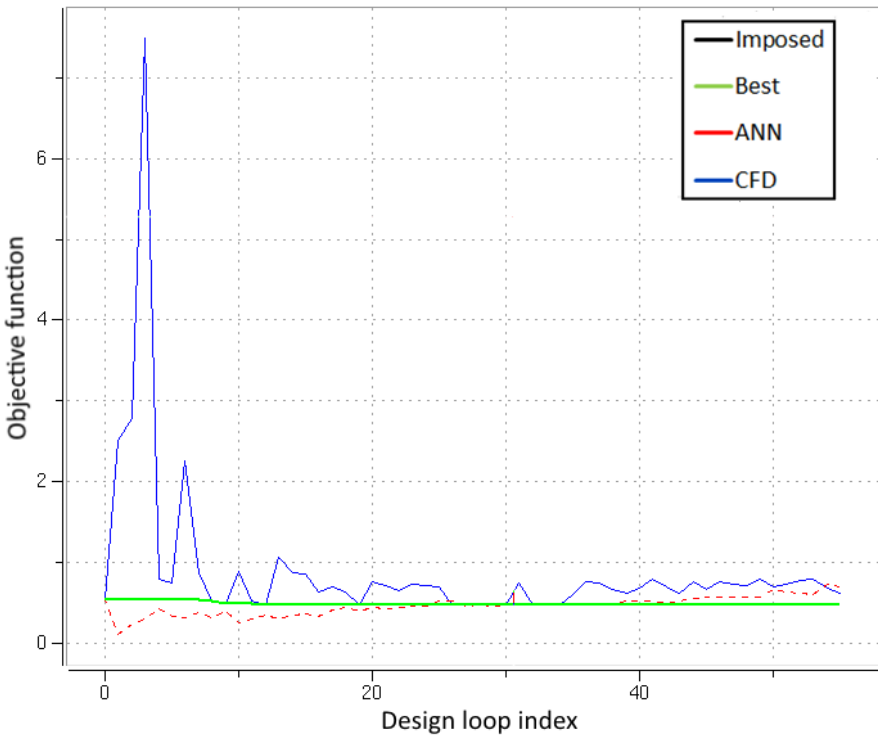

Figure 24: Convergence of Objective function.

It can be seen that at around 25 iterations the objective function was at a best value. However, as was mentioned, it was feared that a higher than required mass flow rate could cause downstream rows/stages of the MGT to choke. Hence the weighting function was altered to ultimately consist of the values as in table 6 and the optimization started again. The objective function struggled to converge closer to the "*Best*" value but the convergence of the individual parameters was found to be better. Figure 25 shows the convergence for the mass flow rate.

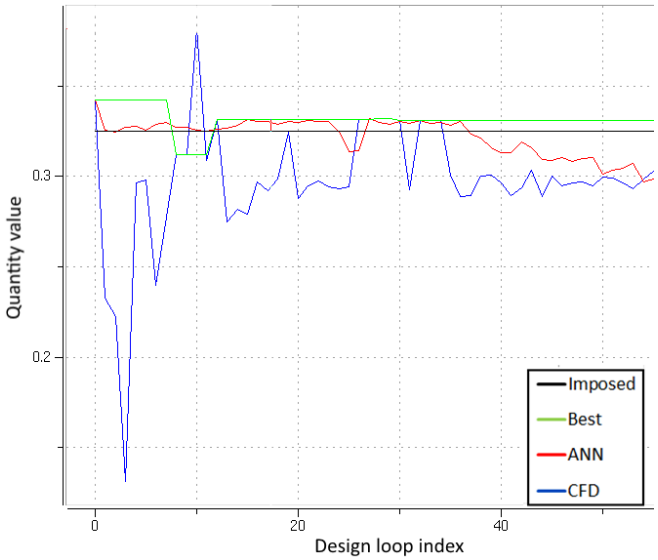

Figure 25: Convergence of the mass flow rate.

At around 25 iterations one can see that the mass flow rate of the compressor is higher than required. After the alterations to the penalty function the mass flow rate drops off to around 0.3 kg/s, which is safe in that it was realized that no choking would occur downstream of the compressor. It was also realized from the assumption of the outlet static pressure being within, yet on the lower range of the stable operating range, that the mass flow rate as converged in figure 25 might be within the choke margin. The convergence of the pressure ratio can be seen in figure 26.

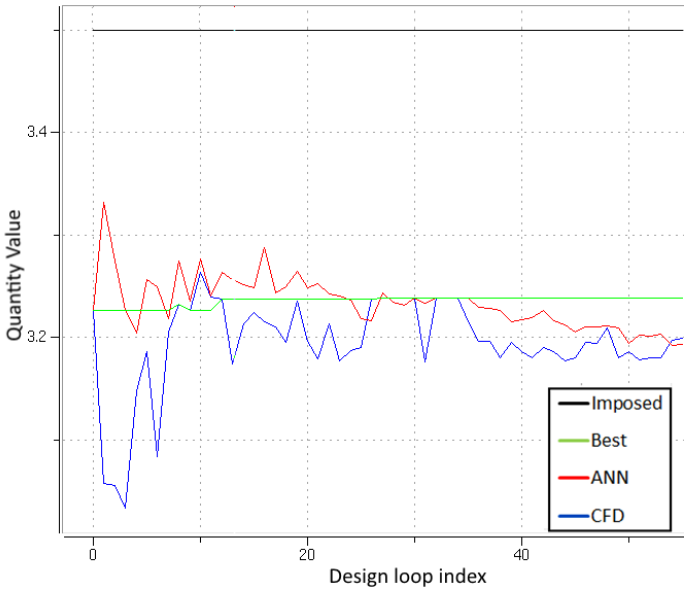

Figure 26: Total-total Pressure ratio convergence.

Although a best value for the pressure ratio is obtained around 30 iterations, the assumptions made for the mass flow rate as previously discussed were considered. It should also be taken into account that the decrease in pressure ratio is negligible considering the scale of the y-axis i.e. the pressure ratio drops from ~3.24 at 30 iterations to 3.2 at 55 iterations. The final convergence history of interest is that of total-total isentropic efficiency.

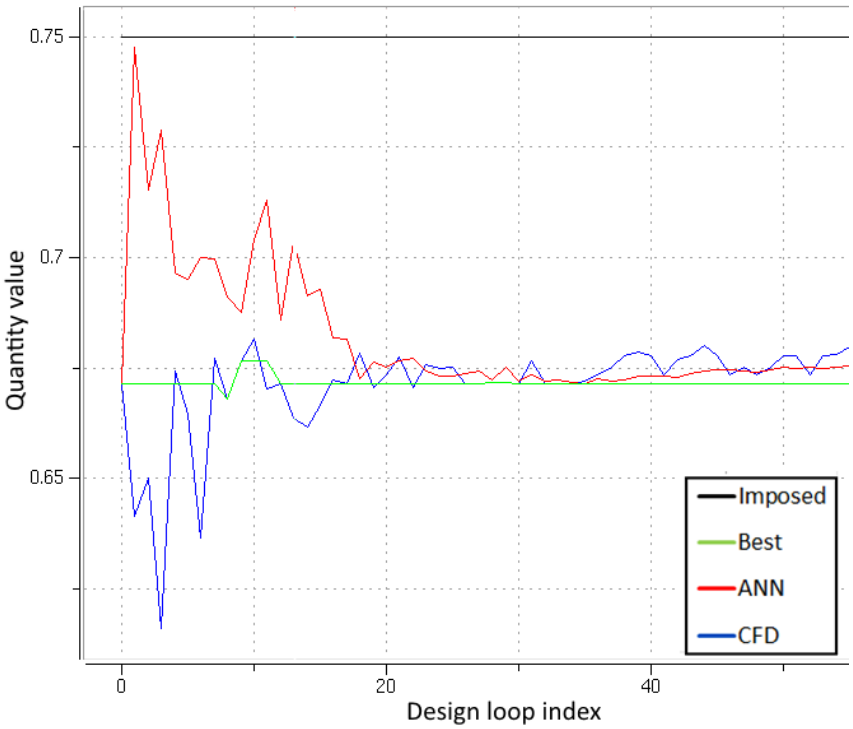

Figure 27: Convergence for Total-total Isentropic efficiency.

The decrease in mass flow rate from 30 to 55 iterations caused a slight increase in efficiency. After consideration it was decided that the more acceptable mass flow rate, the negligible decrease in pressure ratio and slight increase in efficiency better suites the requirements as set forth by the CSIR. Another factor worth considering is that the convergence of the parameters as discussed above is as per the FINE^{TM}/Turbo setup. It is still unclear what the total-static performance of the compressor would be as well as what the performance curves would look like. Also, the performance as determined by the optimization process as in figures 25 to 27 are determined over the entire flow domain and not from the inlet of the impeller to the immediate outlet of the vaned diffuser.

It is also clear that the geometry of the impeller blades as well as diffuser vanes have changed. Figure 28 and 29 shows the change of the impeller blades.

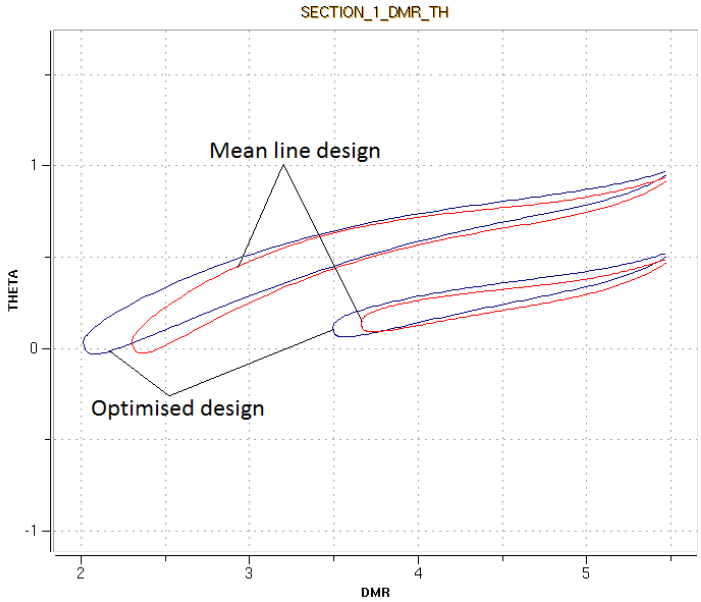

Figure 28: Alteration of impeller blade geometry at the hub depicted along tangential (THETA) and distance along meridional (DMR) plane.

The blue line in figure 28 above represents the final optimised geometry of the impeller blade at the hub. It is clear that the blades have increased in height and that a more backswept trailing edge had been created during the optimization process. Figure 29 below shows similar changes to the impeller blades at the shroud.

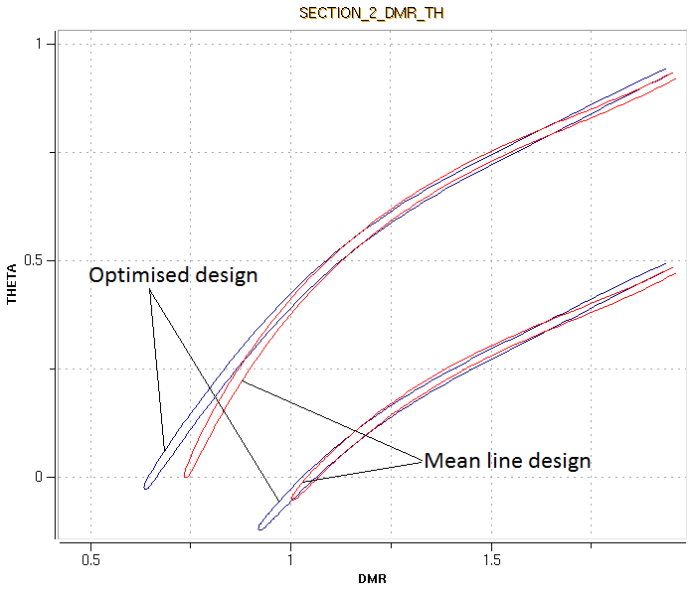

Figure 29: Alteration of impeller blade geometry at the shroud depicted along tangential (THETA) and distance along meridional (DMR) plane.

Again it is clear that the impeller blades have increased in height with a more backswept effect. The increased backsweep was expected with the inclusion of a vaned diffuser. The changes to the diffuser vanes are shown in figure 30 and 31.

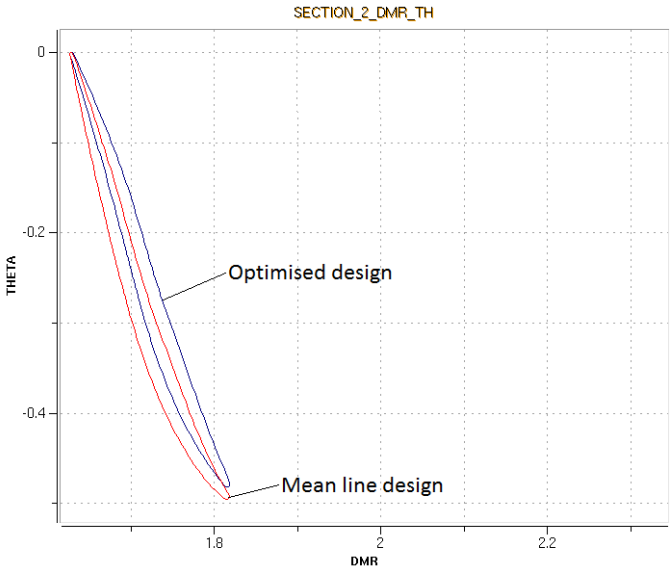

Figure 30: Alteration of diffuser vane geometry at the hub depicted along tangential (THETA) and distance along meridional (DMR) plane.

The inlet and outlet radius of the diffuser vane at the hub have not changed and as such the optimization process suggests that a radius ratio of r_3/r_2 = 1.06 is more suitable for this compressor design. Yet it is clear that the optimised vane does not have the same camber line curve as that of the initial (mean-line) vane. The camber curve of the optimised vane is more radial and this is believed to cause better pressure recovery.

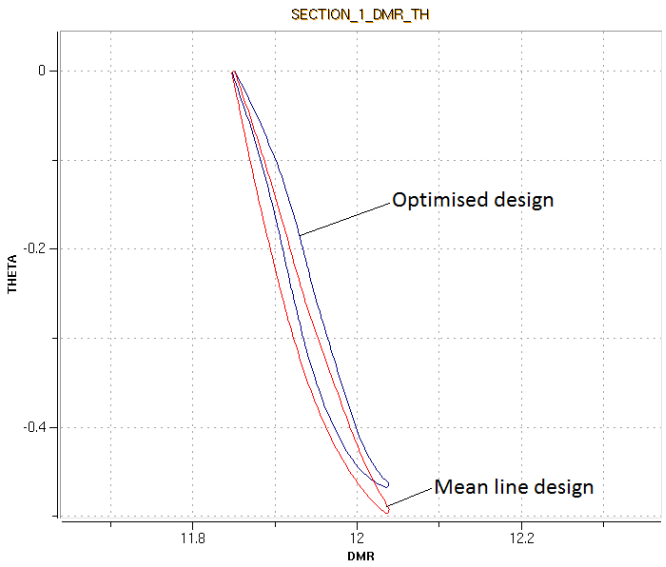

Figure 31: Alteration of diffuser vane geometry at the shroud depicted along tangential (THETA) and distance along meridional (DMR) plane.

Again it is clear that the inlet and outlet radius of the diffuser vane does not change. This is believed to be due to the fact that the number of diffuser vanes cannot change during the optimization process. As such the diffuser throat area is severely limited and the Mach number at the diffuser throat is mainly dependent on the number of blades and the distance of the throat from the trailing edge of the impeller. It is believed that the optimizer tried to keep the Mach number at the diffuser throat near unity and as such the leading edge radius (r_3) of the diffuser is equal to $1.06r_2$.

The most observable difference of the optimised diffuser vane is the curvature of the camber curve which is more radial than that of the mean-line vane camber curve. Considering the difference of the vane shape at the shroud and hub it is clear that a lean angle is present at the trailing edge (Figure 63). This curvature into the radial direction increases pressure recovery.

5.2.3. Performance evaluation of the optimised design

For each of the optimization iterations a design file is created. The final design file within the _opt directory contains the geometry of the best performing compressor. The 1st and 2nd row *.geomturbo* files can be found within the final design file and were used to create a mesh of the compressor. This mesh generation process of the final design is the same as discussed in section 4.1.1.

A FINE^{TM}/Turbo simulation was started where the setup is similar to that as discussed in section 4.1.2 above. A performance curve was created in order to determine the operating point. It is believed that, although the static pressure at the outlet of the compressor flow domain was fixed during the optimization process, the static pressure of the operating point for the final design rises and allows the fixed outlet pressure to remain within the stable simulation range. It was assumed that the pressure ratio of the compressor is the main performance parameter whereas the efficiency and mass flow rate are requirements and/or restrictions that need to be fulfilled. Accordingly it is important that the total-static pressure ratio be better than that previously achieved. The performance curves of the pressure ratio of the compressor as designed by this process, compared to that designed by Van der Merwe (2012) is shown in figure 32.

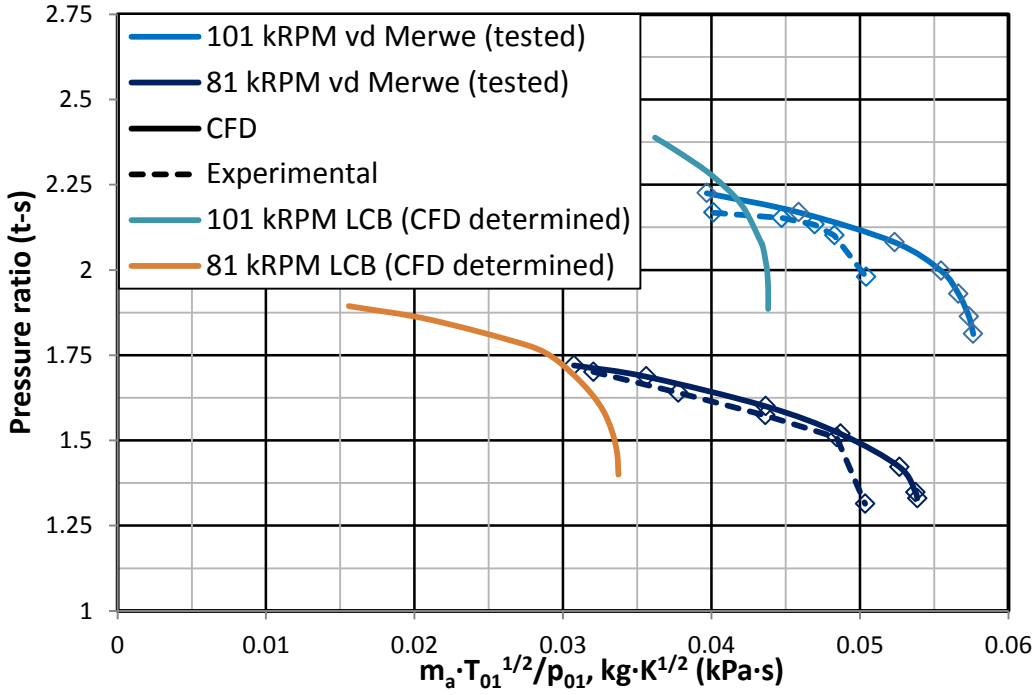

Figure 32: Pressure ratio comparison for De Villiers and Van der Merwe.

Van der Merwe only shows results up to 101 kRPM. The efficiency of the newly designed compressor is expected to decrease due to the inclusion of a vaned diffuser but the efficiency of the impeller only is expected to be higher due to the back swept blades. Van der Merwe designed for a high as possible total-total pressure ratio whereas this design requires a high as possible total-static pressure ratio. The theoretical efficiency obtained by Van der Merwe (2012: 77) at 121 kRPM for the entire compressor including the vaneless diffuser was 79.1 %.

Figure 33 shows the final efficiency of the newly design compressor from inlet to the outlet of the vaned diffuser.

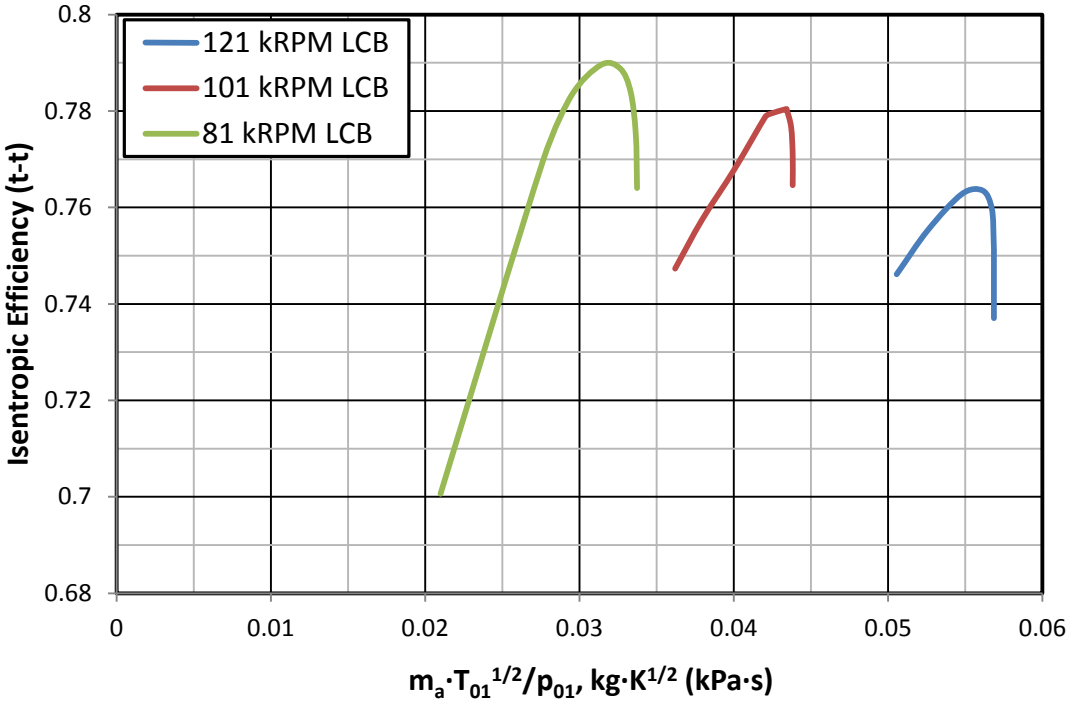

Figure 33: Isentropic efficiency (t-t) of newly designed compressor.

An inlet total pressure of 98 kPa, inlet total temperature of 298 K and a non-dimensional mass flow rate of 0.055 translates into a mass flow rate of 0.312 kg/s. At this point it is clear that the efficiency of the entire compressor with the inclusion of the vaned diffuser is roughly 76.5 %. This is lower than the efficiency obtained by Van der Merwe but as mentioned the inclusion of a vaned diffuser will decrease the efficiency.

Figure 32 reveals that the increase in pressure ratio for the newly designed compressor compared to that of Van der Merwe's compressor at 101 kRPM is higher than the increase in pressure ratio at 81 kRPM. It is believed that the increase in pressure ratio of the newly designed compressor compared to that of Van der Merwe's compressor may be even higher at the design speed of 121 kRPM. Figure 34 below shows the pressure ratios of the newly designed compressor at 81, 101 and 121 kRPM.

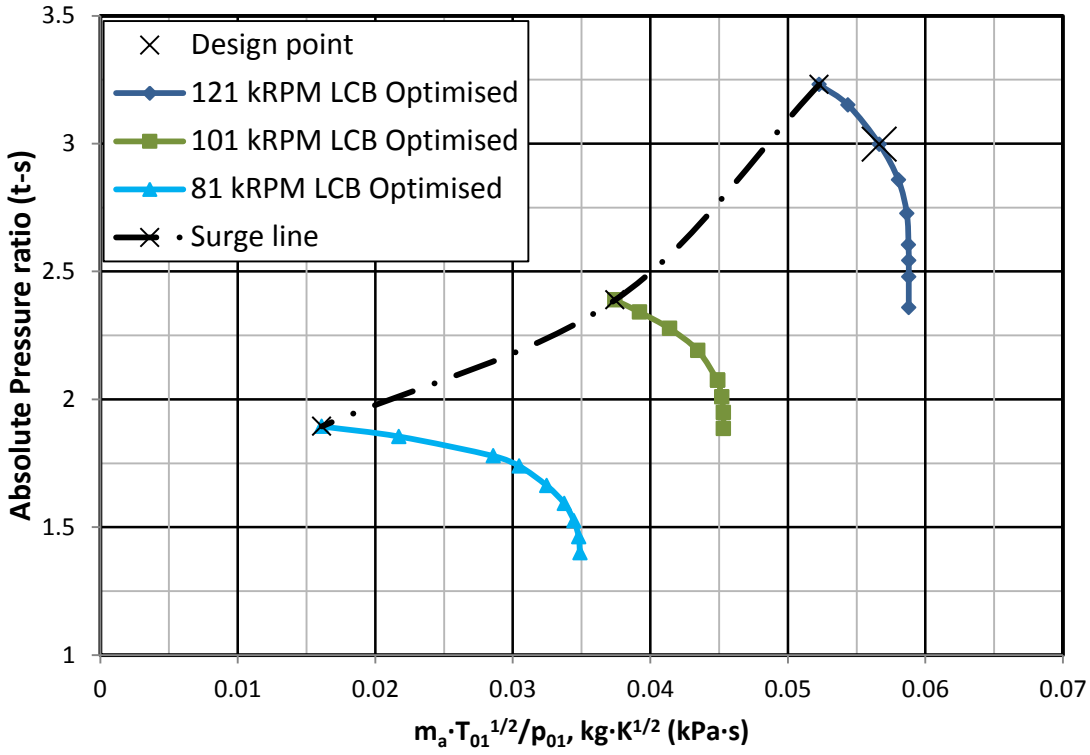

Figure 34: Pressure ratio (t-s) of newly designed compressor.

Figure 34 above reveals that the newly designed compressor provides a significant increase in static pressure ratio as the total-static pressure ratio at the design speed of 121 kRPM is 3.0 compared to 2.8 for Van der Merwe's design. Examining figure 34 further reveals that the mass flow rate achieved through the new compressor is closer to 0.325 kg/s than previously. This is believed to be due to the vaned diffuser that constricts the mass flow rate through the compressor.

This further illustrates that the assumptions made as well as methodology used during the development of the mean-line code were acceptable in that the number of vanes in the diffuser determined the mass flow rate and static pressure recovery very well. The proximity of choking can be illustrated by observing the relative Mach number through the whole compressor (Figure 35).

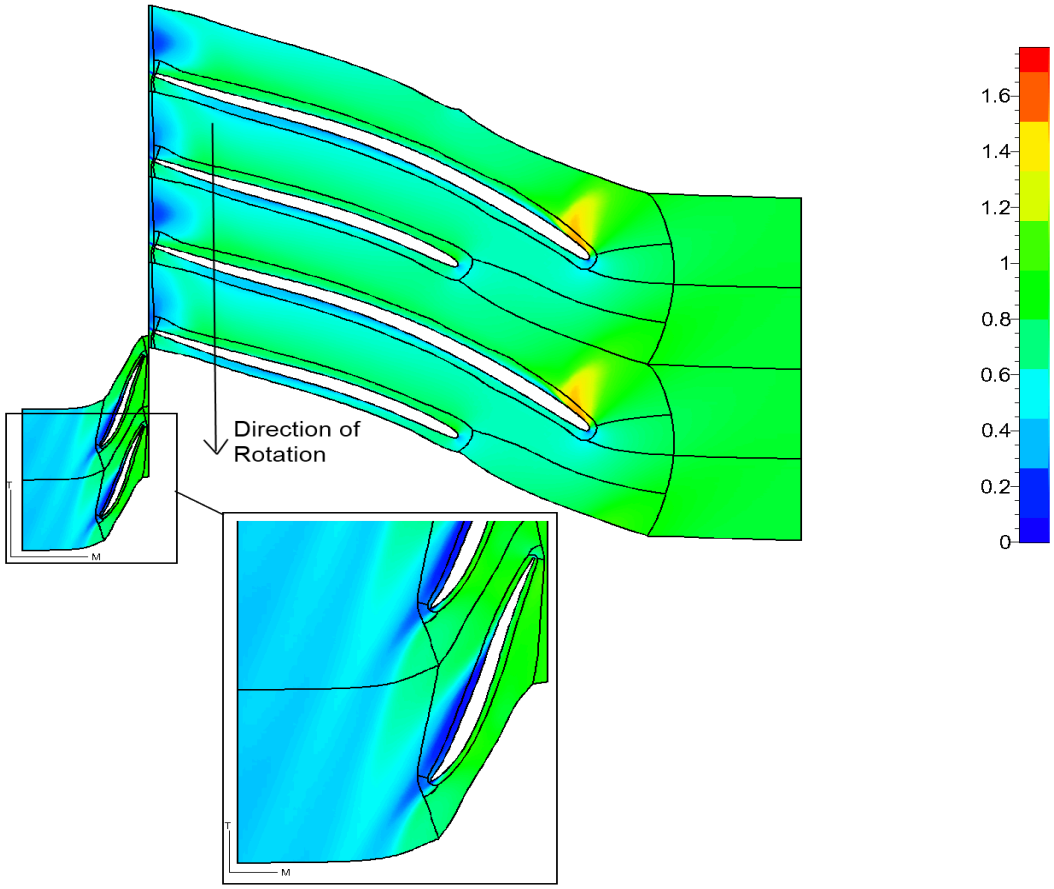

Figure 35: Relative Mach number within the entire compressor.

Figure 35 shows that a higher than unity Mach number exists at the leading edge of the impeller. This Mach number does not however encompass the entire inlet area and as such will not cause choking at the rotor inlet. It is clear that a near unity Mach number exists within the diffuser throat. If the diffuser causes choking the MGT can be throttled in order to move the operating point up and into the stall margin, closer to the surge line of the performance curve. In doing so an even higher pressure ratio will exist while excluding choke and the formation of shock waves.

As was previously mentioned the initial geometry of the compressor exhibited unwanted recirculation at the shroud curve immediately downstream of the rotor. This unwanted recirculation is a phenomenon that had to be removed or at the very least reduced in the new compressor design. Figure 36 reveals that the recirculation in the vicinity of the diffuser has been removed.

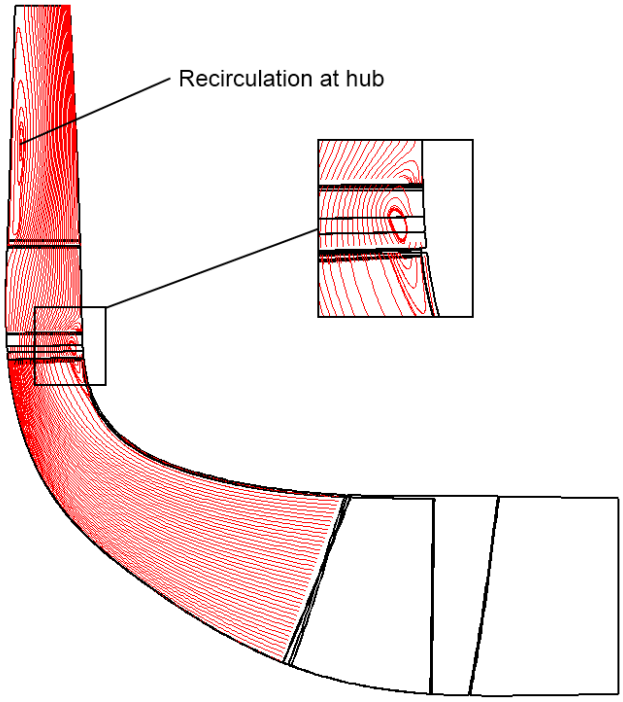

Figure 36: Flow lines for optimised compressor design (recirculation removed).

Recirculation does still exist at the trailing edge of the rotor (enlarged inset) yet it is assumed that the decrease in performance due to this recirculation is negligible. What is of concern is the recirculation around the hub at the outlet of the diffuser. It should be noted however that the hub curve of the actual MGT turns into the axial direction immediately after the diffuser outlet. Hence the flow profile downstream of the diffuser is treated as an unknown.

As mentioned in section 2.3.4 Aungier (2000: 182) noted that the blade loading should not exceed that as defined in equation 2.21. Numeca FINE^{TM}/Turbo does not have the definition of Aungier available in order to determine stall over the diffuser vanes. Numeca makes use of different definitions which the user can use to view the pressure coefficient value over the diffuser vane. The definition selected is:

$$C_{p2} = \frac{2(p - p_{inlet})}{\rho_{inlet} w_{inlet}^2} \qquad (5.3)$$

Figure 37 shows the pressure coefficient distribution as per equation 5.3 over the diffuser vanes for 3 different spans.

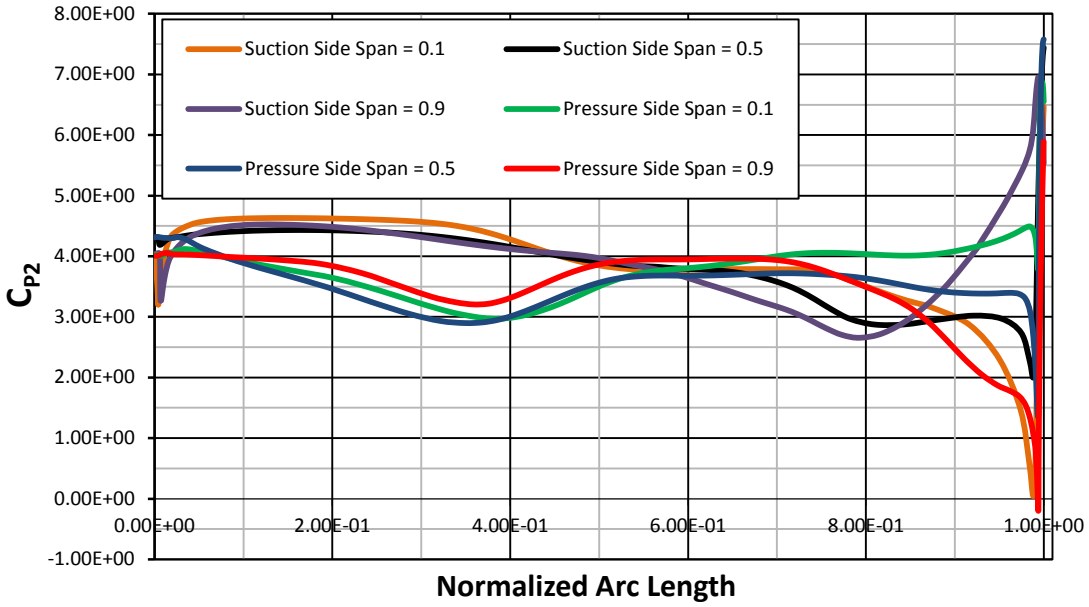

Figure 37: Pressure coefficient distribution over diffuser vane at varying spans (0 = trailing edge and 1 = leading edge of diffuser for Normalized Arc Length).

In all span cases it is clear that no spike or excessive variation occur that would indicate the existence of stall over the diffuser vanes. Figure 38 provides a visual interpretation of the air flow over the diffuser vanes at a span of 50% which can also be used to determine whether or not stall exists on the diffuser vane.

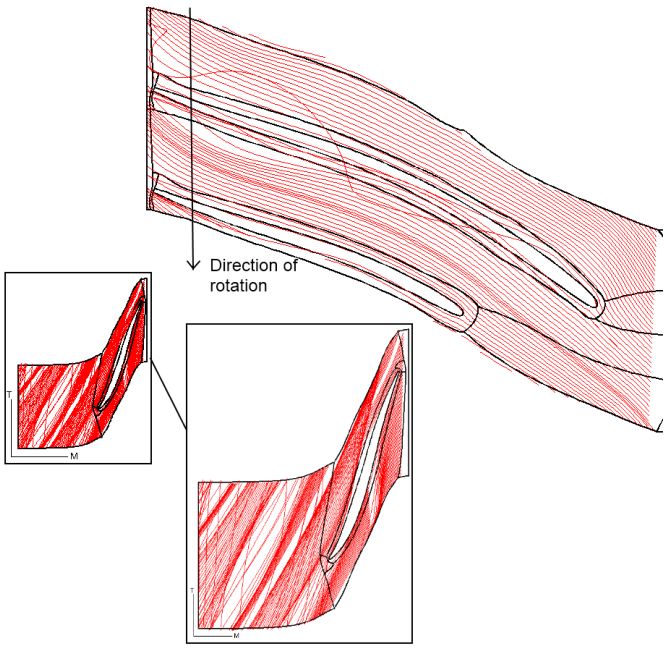

Figure 38: Stream lines over diffuser vanes @ 50% span.

From figure 38 it is clear that some swirl takes place immediately downstream of the diffuser vane however, examining the stream lines immediately adjacent to the vane on both the pressure and suction side reveals that no stall occurs. Figure 60 shows similar flow lines at a span of 11.25% and 90% for the diffuser.

5.2.4. Rotor Structural analysis

Due to the high rotational speed at which the rotor will operate it is critical to employ a Finite Element Analysis (FEA) in order to determine how much the rotor will displace and the amount of stress the rotor will experience. The material used to manufacture the rotor is Aluminium T6082 (Al_T6). The properties of Al_T6 is given in table 7 below.

Table 7: Material properties of Aluminium T6082.

Property	Value
Modulus of Elasticity/Young's Modulus (GPa)	69
Sheer Modulus (GPa)	26
Density (kg/m^3)	2700
Poisson Ratio (~)	0.33
Tensile Yield Strength (MPa)	276

As mentioned in section 4.1.1 a shroud gap of 0.2 mm was defined. As such it was important that the impeller does not exceed a radial displacement of more than 0.2 mm especially around the leading edges of the blades. It is acceptable if the displacement of the impeller is more than 0.2 mm at the trailing edge as here the shroud is in an axial direction from the impeller blades. At the same time it is important that the maximum stresses experienced by the rotor do not exceed 276 MPa. The maximum stresses are expected to be around the blade hub interface as the small radiuses of the fillets around these areas are typical areas of stress concentration.

Due to the backswept blades of the newly designed impeller it was difficult to obtain symmetric boundaries and second of all to constrain these boundaries as required within SimXpert®. It was therefore decided that for the purposes of determining stress and displacement the built-in FEA function within SolidWorks® could be used. There are certain advantages of using SolidWorks® instead of SimXpert®. The complication of having to create symmetric boundaries does not exist. A phenomenon that is of concern is that of hoop displacement. In order to accurately model this phenomenon it is required to only constrain the

impeller on the upper most surfaces. This lessens the complication of applying symmetric boundary constraints. The user needs to only select the material from an extensive materials list in SolidWorks® instead of defining the material properties manually. Ultimately setting up a simple FEA (as is of interest for the design as discussed in this report) in SolidWorks® is much simpler and time saving than using SimXpert®. Figure 39 below illustrates how the impeller was constrained and the forces defined.

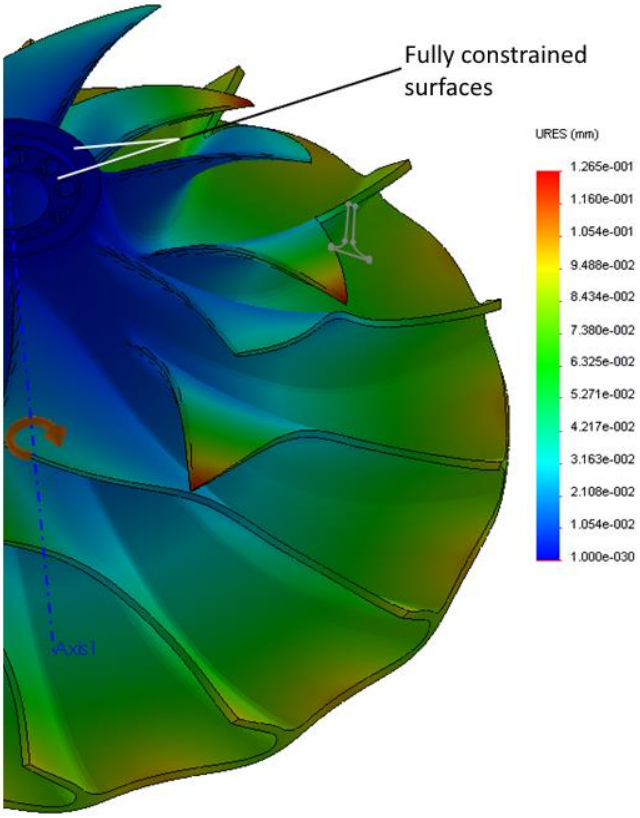

Figure 39: Constrained definition and absolute displacement of impeller @ 121 kRPM.

Visible in figure 39 are the surfaces that the user constrained. Both of the surfaces at the rotor inlet were constrained fully in that no local displacement or rotation in any axis (x, y or z) could occur. Also visible is the direction of rotation as shown around “Axis 1” in the figure. The rotational speed was set to 121 kRPM, which would contribute to the main centrifugal forces experienced by the impeller.

As expected the largest displacement occurs at the leading edge of the splitter blade. This is due to the fact that the leading edge is not fully radial but higher at the shroud than at the hub. The centrifugal force would hence force the splitter blade downward and forward, assuming that the aerodynamic forces exerted on

the blades are negligible. Also clear in figure 39 is how the displacement increases at higher radiuses on the impeller. This is due to the fact that centrifugal force is directly proportional to the radius of the moving body.

Since the maximum displacement of the impeller is 0.127 mm, which is not only in the radial direction, it can be concluded that the impeller will not come into contact with the shroud during operation. Another important factor is the stresses experienced by the impeller during operation. Figure 40 below shows the Von Mises stresses experienced by the impeller.

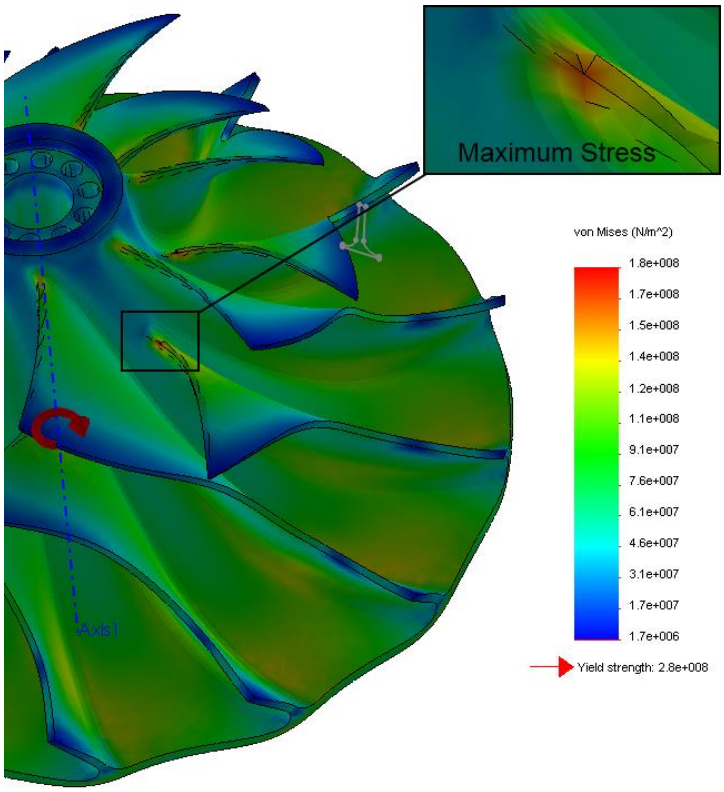

Figure 40: Von Mises stresses experienced by impeller @ 121 kRPM.

As shown in table 7 the Yield strength of Aluminium T6061 is 275 MPa (~280 MPa) and since no stress experienced by the impeller exceeds this value it can be concluded with certainty that the impeller will not fail during operation. Also shown is the location of maximum stresses. The small radii of the fillets around the blade-hub interfaces are typical areas of stress concentration. The maximum stress is found to be on the leading edge of the splitter blade at the hub (enlarged inset) of 180 MPa. Once it had been concluded that the new compressor design will perform well and safely it was manufactured. Appendix F2 and F3 (Figures 61 to 66) shows images and details of the final manufactured parts.

6. BASELINE TEST RUNS AND TEST SETUP

6.1.Test setup

The next step in the development process is to manufacture the newly designed compressor and testing the performance of said compressor. A comparative test had to be run first in order to create a baseline against which the new compressor will be evaluated. The existing BMT 120 KS MGT served as the baseline performance comparison. Figure 41 shows the layout of the test bench used to determine the performance of the MGT as well as the newly designed compressor.

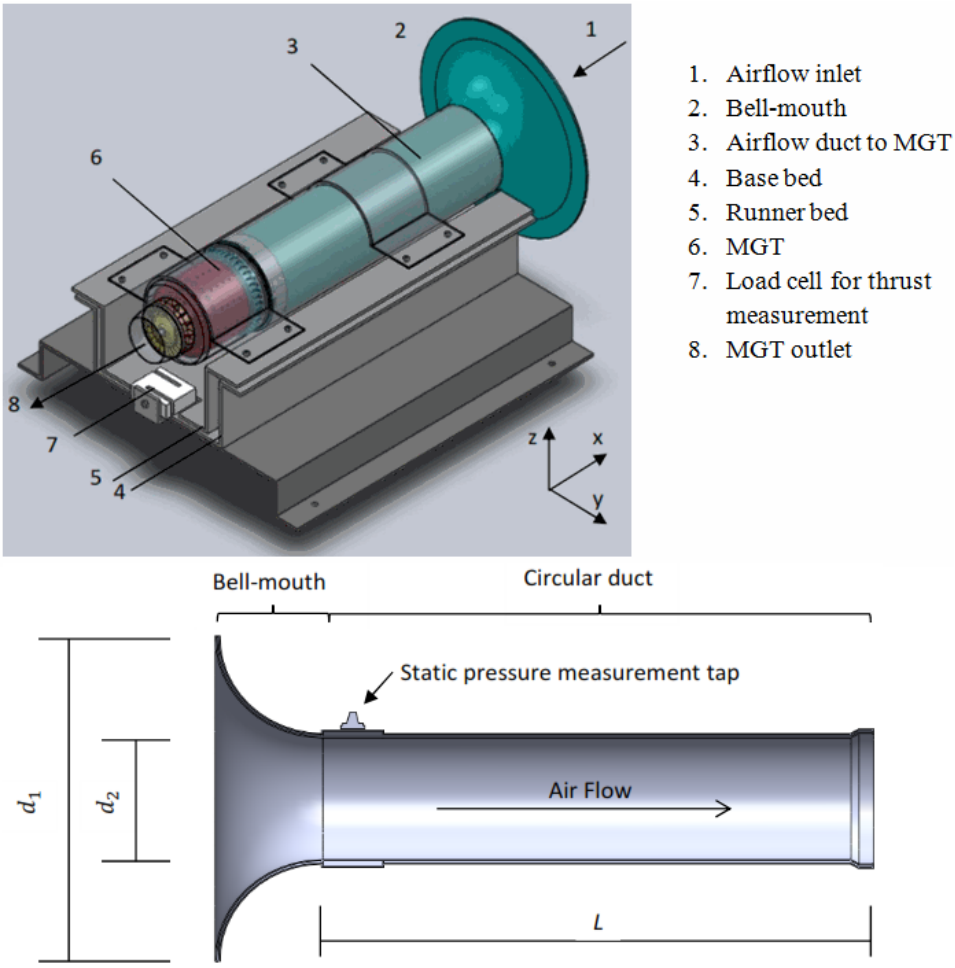

Figure 41: Test bench of MGT (Krige, 2013: 41).

The instrumentation used during testing would be a collection of static pressure taps and thermocouples. Figure 42 shows the location of these pressure taps and thermocouples within the test setup.

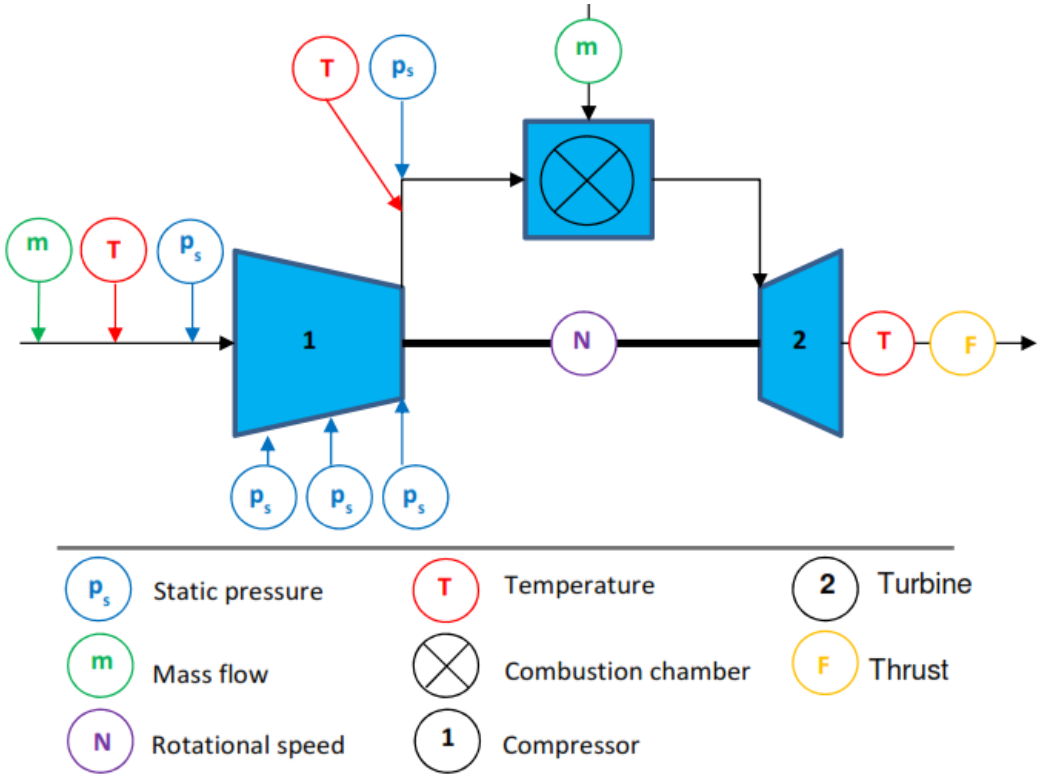

Figure 42: Pressure and temperature sensors within test setup (Krige, 2013: 42).

The atmospheric pressure measured within the test cell was done using a mercury barometer and the atmospheric temperature read using a simple, tubular alcohol thermometer. The atmospheric pressure and temperature during the baseline test were 100.960 kPa and 295 K respectively. The static pressure tap within the airflow duct was used in order to determine the pressure drop relative to the atmosphere in order to calculate the air mass flow rate by:

$$\dot{m} = \rho_{duct} C_d A_{duct} \left(\frac{2\Delta p / p_{duct}}{1 - \beta^4} \right)^{1/2} \tag{6.1}$$

The density in the duct was calculated within Excel® by making use of the static pressure measured within the duct and the perfect gas equation:

$$\rho = \frac{p}{RT} \tag{6.2}$$

where the static temperature was assumed to be the atmospheric temperature as it was assumed that no losses occur from the bell-mouth inlet to the impeller leading edge. The discharge flow coefficient (C_d) was selected as 0.988 as it is the same value that Krige (2013: 99) used on the same test bench. The variable β is defined

as d_2/d_1 where d_1 = 280 mm and d_2 = 102 mm (Krige, 2013: 41) and is hence equal to 0.364. The mass flow rate of the fuel is measured by a load cell. The load cell measures the weight of the fuel reservoir in increments of 0.02 seconds during testing. Hence the final mass flow rate can be calculated. The front cover of the compressor was designed such that pressure taps can measure the static pressure at the diffuser inlet and outlet. In so doing the total to static pressure ratio over the compressor can be measured. A thermocouple allows for measurement of the static temperature at the diffuser outlet whilst the inlet total temperature will be taken as the atmospheric temperature since it is assumed that negligible losses occur from the bell-mouth inlet to the rotor leading edge.

6.2.Baseline test results

Figure 43 shows the total-static pressure ratio of the BMT 120 KS MGT that served as the baseline comparison.

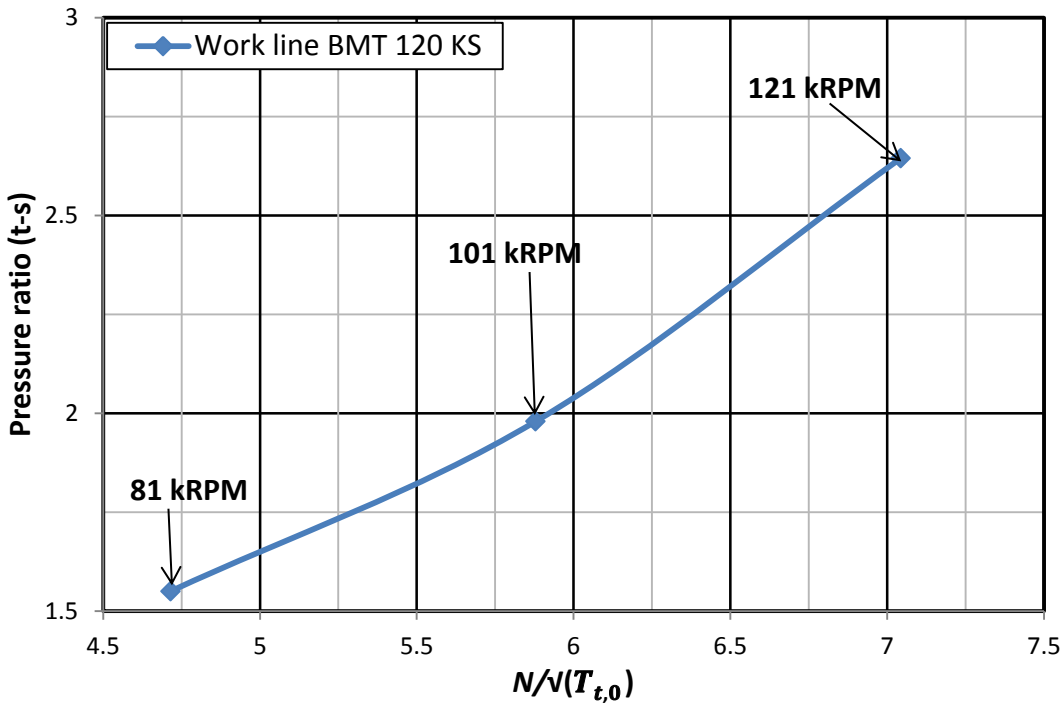

Figure 43: Total-Static pressure ratio work line of BMT 120 KS MGT.

It is expected that the newly designed compressor will provide a higher total-static pressure ratio than that of the BMT 120 KS MGT. However, the alterations to the design in order for the MGT to be assemblable might alter and in the worst cases reduce the compressor performance. Another factor of importance is the thrust of the. Figure 44 shows the work line of the thrust provided by the BMT 120 KS MGT.

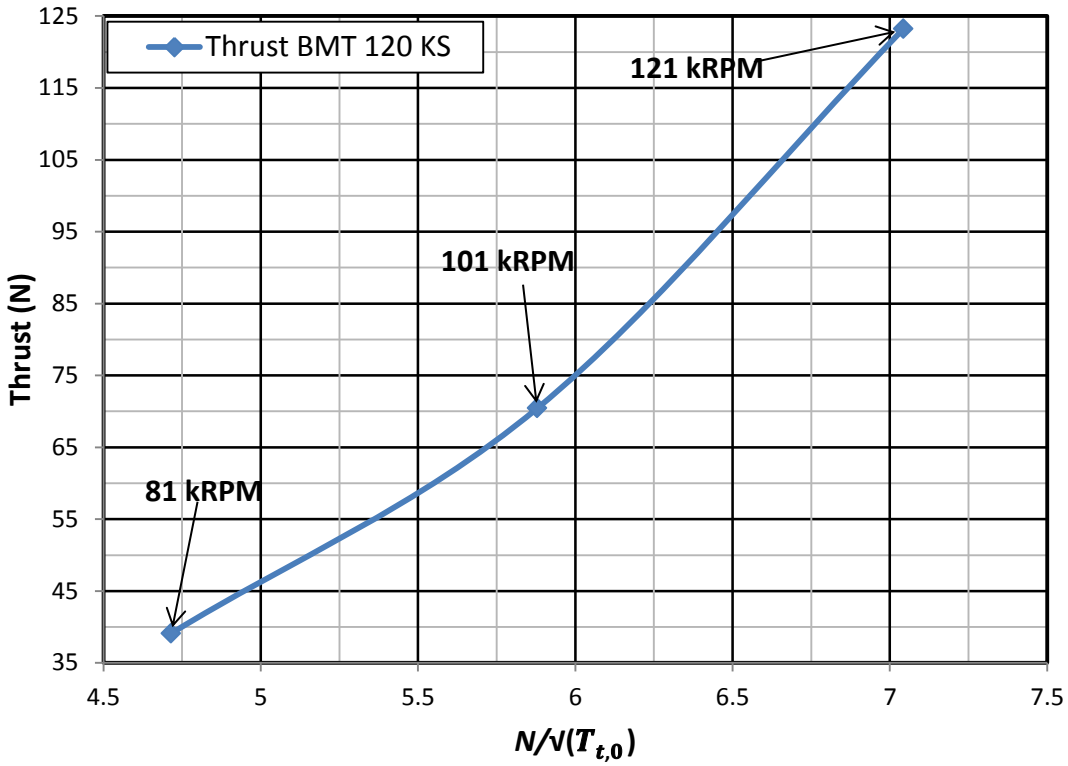

Figure 44: Thrust work line of BMT 120 KS MGT.

Figure 44 shows that a maximum thrust of nearly 125 Newton (N) is provided by the BMT 120 KS MGT. Even though the newly designed compressor performs better than the existing compressor it is not to say that the thrust provided by the entire MGT would be higher. The thrust provided is dependent on several other factors inherent in the combustion process, turbine stage and outlet nozzle of the MGT.

7. RESULTS OBTAINED

A design parameter that had an effect on the performance of the MGT was that of compressor-turbine matching. This implies that the compressor be designed such that the turbine is able to provide sufficient power to the compressor in order for the compressor to rotate at 121 kRPM. For this design however compressor turbine matching was not considered since the redesign of the turbine forms part of another research project. As such the compressor had a maximum rotational speed of 109 kRPM. The total-static pressure ratio work line of the newly designed compressor compared to that of the existing BMT 120 KS MGT compressor is seen in figure 45.

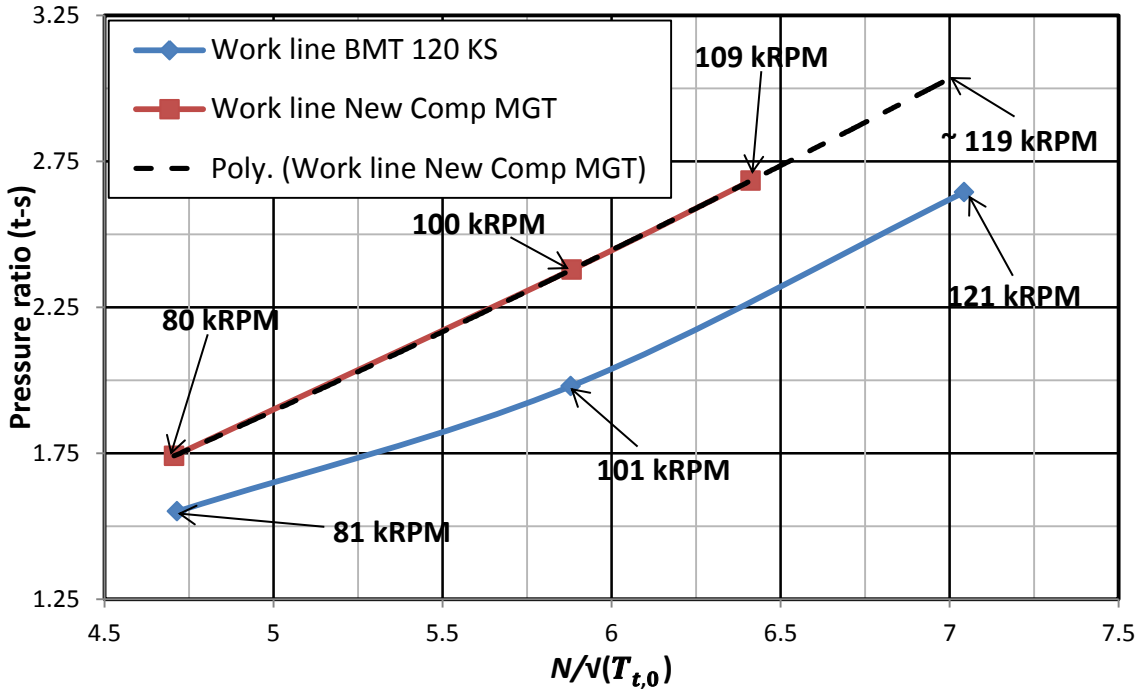

Figure 45: Total-static pressure ratio work line of BMT 120 KS compressor vs newly designed compressor.

As an estimate a 2nd order polynomial trend line was fitted to the measured work line of the newly designed compressor. Due to the difference in atmospheric temperature between the baseline and final test runs the corresponding maximum rotational speed during final testing was 119 kRPM. Figure 45 shows that an estimated total-static pressure ratio of little more than 3.0 will be delivered by the newly designed compressor, which is higher than the 2.64 that the original compressor of the BMT 120 KS delivers. This compares well with the CFD simulated performance shown in figure 46.

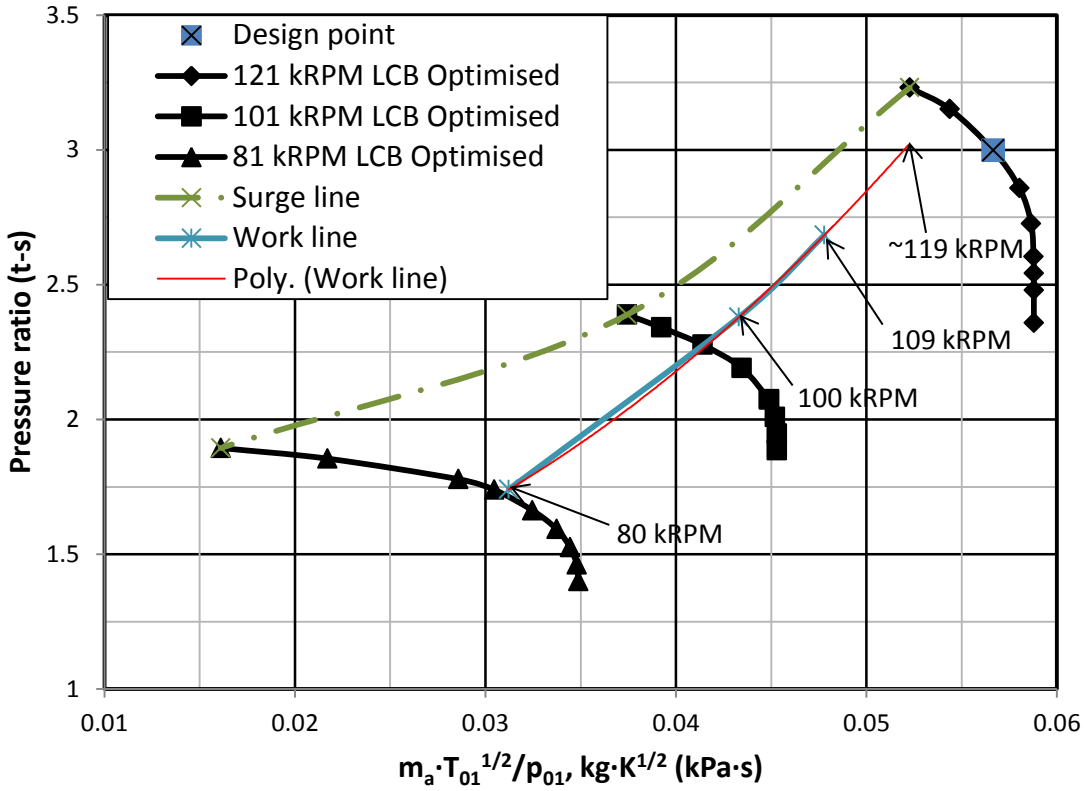

Figure 46: CFD and experimental result comparison for new compressor design.

Figure 46 shows that the design point of the CFD simulation is somewhat different at 121 kRPM than the estimated operating point deduced from testing. The suggested stall margin during testing is also much smaller. In order to assemble the MGT, 6 diffuser vanes had to be altered and as such the diffuser channels are not all the same (see Appendix 6). This will result in varying flow through the diffuser channels. The pressure was measured in a single diffuser channel at a single point. These geometrical alterations will have a significant effect on the measured test results.

The mass flow rate that was measured is that of the entire MGT and not only one channel of the compressor. Therefore, the pressure measured and mass flow measured do not actually represent the same point of the machine, and consequently the CFD determined mass flow rate and measured mass flow rate differ. If a MGT engine is used in an aircraft, it would be possible to throttle the engine by means of a variable geometry outlet nozzle in order to prevent the engine from stalling or choking. The thrust delivered by the new MGT is shown in figure 47.

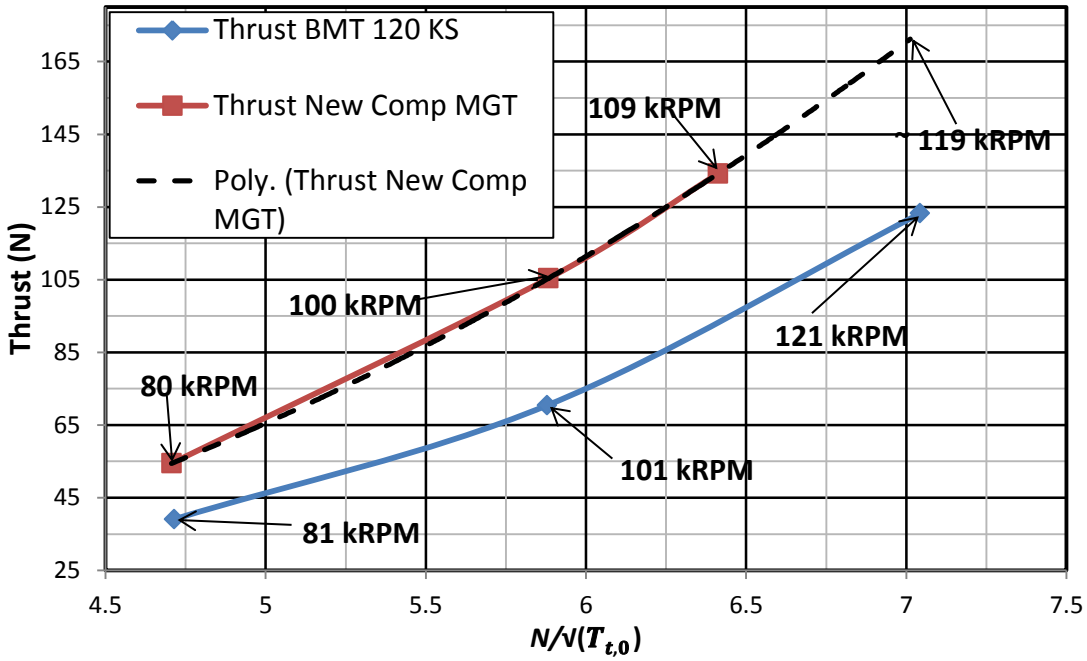

Figure 47: Thrust work line of the BMT 120 KS MGT compared to the new MGT design.

With the inclusion of the new compressor design the thrust of the MGT also increased. Again a 2nd order polynomial trend line was fitted to the measured work line to estimate the thrust at 119 kRPM, as this agreed with the correct dimensionalized rotational speed correlating with the baseline test run at 121 kRPM. The fitted work line seen in figure 47 suggests that the thrust provided by the new MGT at 119 kRPM is roughly 170 N compared to the 125 N of the BMT 120 KS. This results in a 30 % increase in thrust.

It is also clear that the increase in thrust provided by the new MGT over the BMT 120 KS becomes less at lower RPMs. It is believed that the thrust provided by the new MGT at much lower RPMs may even be less than the thrust of the BMT 120 KS. It is therefore believed that the new compressor is not well matched to the combustion chamber or turbine of the original BMT 120 KS. It is concluded that the new compressor exhibits an increase in overall performance.

8. CONCLUSIONS AND RECOMMENDATIONS

This report discusses the development of a centrifugal compressor for application in micro gas turbines (MGTs) as the development of well performing turbomachines and the stages inherent have enjoyed great interest in the field of engineering. The development of a design methodology, as well as the performance improvement of the compressor was an important deliverable to the CSIR. Although the CSIR specified a total-total pressure ratio it was decided that, with the inclusion of a vaned diffuser a total-static pressure ratio would serve as the basis of the compressor's performance while adhering to an acceptable total-total isentropic efficiency and mass flow rate.

The design process starts with the further development of a mean-line code that makes use of 1-D turbomachinery theory in order to create an initial compressor geometry. This geometry was then developed further using the CFD packages FINE^{TM}/Turbo and FINE^{TM}/Design3D in order to increase the performance of the compressor. It was found that assumptions made during the development of the mean-line code were correct when flow phenomena like the Mach number and stall were studied during the CFD post processing stage.

The performance of the new compressor was compared to that of the BMT 120 KS MGT and it was found that the new compressor performed significantly better in that an acceptable mass flow rate and total-total isentropic efficiency was obtained with an increase in static pressure rise. Not only did the newly designed compressor perform better, the performance as determined using CFD compared well with that measured during testing. It can therefore be concluded that the methodology used to design a good performing compressor is sound.

It is recommended that the mean-line code be developed further in order to design an initial geometry for the entire MGT. The interaction between rows within stages is as important as the interaction between stages within the entire MGT and as such the development of a good performing compressor is an iterative process between stages. The author also recommends that the assemblability of the compressor be altered in order to better accommodate the diffuser vane shape.

9. REFERENCES

Aungier, R. H. (1988). A Systematic Procedure for the Aerodynamic Design of Vaned Diffusers. *Flows in Non-Rotating Turbomachinery Components*, 27-34.

Aungier, R. H. (2000). *Centrifugal Compressors, A Strategy for Aerodynamic Design and Analysis.* Three Park Avenue, New York: The American Society of Mechanical Engineers.

AuthorNotAvailable. (2014, May 28). Retrieved May 28, 2014, from Aerospace Industries Association: http://www.aia-aerospace.org/assets/AIA_UAS_Report_small.pdf

Basson, J. G. (2011, July 29). Design Methodology for a Small Jet Engine Turbine. Stellenbosch, South Africa: Department of Mechanical and Mechatronical Engineering Stellenbosch University.

Bradshaw, P. (1996). Turbulence Modeling with Application to Turbomachinery. *Prog. Aerospace Sci. Vol. 32*, 575-624.

De Wet, A. L. (2011). *[MSc, Mech. Eng.], Performance Investigation of a Turbocharger Compressor.* Stellenbosch, South Africa: Department of Mechanical and Mechatronical Engineering Stellenbosch.

Dixon, S. L. (1998). *Fluid Mechanics, Thermodynamics of Turbomachines.* 225 Wildwood Avenue, Woburn, MA: Butterworth-Heinemann.

Everitt, J. (2010). *[MSc, Mech. Eng.], Investigation of Stall Inception in Centrifugal Compressors Using Isolated Diffuser Simulations.* Cambridge, MA, United States: Department of Aeronautics and Astronautics, Massechusetts Institute of Technology.

International, N. (2011, April). User Manual, FINE/Turbo v8.9. *Flow Integrated Environment*. Brussels, Belgium: Chaussée de la Hulpe.

Japikse, D. (1996). *Centrifugal Compressor Design and Performance*. Wilder, Vermont, USA: Thomson-Shore, Inc.

Japikse, D., & Baines, N. C. (1998). *Diffuser Design Technology.* White River Junction, Vermont, USA: Edwards Brothers Incorporated.

Kuiper, D. (2007). Turbocharger Design and Performance Analysis. *Globe Turbocharger Specialties Incorporated (GTSI)*, 1-8.

Kushner, F. (2004). Rotating Component Modal Analysis and Resonance Avoidance Recommendations. *Proceedings of the Thirty-Third Turbomachinery Symposium*, 143-162.

Langston, L. S., & Opdyke, G. J. (1997). Introduction to Gas Turbines for Non-Engineers. *Published in the Global Gas Turbine News, Volume 37: No. 2*, 3.

Mackenzie, C. (2013). *UAV Market Research.* Retrieved March 2014, from RUSI Defence Systems: https://www.rusi.org/downloads/assets/RDS_2013_Mackenzie.pdf

Reitz, R. D. (2012). Reciprocating Internal Combustion Engines. *Summer Program on Combustion* (pp. 1-33). 2012 Princeton-CEFRC: Copyright by Reitz, R.D.

Reneau, L., Johnstaon, J. P., & Kline, S. J. (1967). Performance and Design of Straight, 2-Dimensional Diffusers. *Journal of Basic Engineering*, 141-150.

SaabPressCentre. (2011, September 22). *Saab Receives Order on Avionics Equipment for the Talarion UAV*. Retrieved April 7, 2012, from www.saabgroup.com: http://www.saabgroup.com/en/about-saab/newsroom/press-releases--news/2011---9/saab-receives-order-on-avionics-equipment-for-the-talarion-uav/#.U3n3wMzzfEc

Shum, Y. K., Tan, C. S., & Cumpsty, N. A. (2000). Impeller-Diffuser Interaction in a Centrifugal Compressor. *Journal of Turbomachinery*, 777-786.

Struwig, D. J. (2013). *[MEng (Research), Mech. Eng.], The Development and Verification of a Centrifugal Compressor Test Bench.* Stellenbosch, South Africa: Department of Mechanical and Mechatronical Engineering, Stellenbosch University.

Van der Merwe, B. B. (2012). *[MEng (Research), Mech. Eng.], Performance Evalaution of a Micro Gas Turbine's Centrifugal Compressor Diffuser.* Stellenbosch, South Africa: Department of Mechanical and Mechatronical Engineering, Stellenbosch University.

Versteeg, H., & Malalasekera, W. (2007). *An Introduction to Computational Fluid Dynamics, The Finite Volume Method.* Essex, England: Pearson Education Limited.

White, F. M. (1994). *Fluid Mechanics.* TA367.W48: McGraw-Hill, Inc.

Whitfield, A., & Baines, N. (1990). *Design of Radial Turbomachines.* Essex, England: Longman Scientific & Technical.

XinQian, Z., YangJun, Z., & MingYanh, Y. (2009). Research and Development of Transonic Compressor of High Pressure Ratio Turbocharger for Vehicle Internal Combustion Engines. *State Key Laboratory of Automotive Safety and Energy*, 1817-1823.

APPENDIX A: MEAN-LINE CODE DEVELOPMENT

A1: Previous & altered mean-line code flow diagram

Figure 48 provides the original flow chart of the mean-line code as developed by Van der Merwe (2012). The program can be run from the MATLAB® interface by simply typing in *"optimise"*. The code of the main function *"optimise.m"* is given in Appendix A2. As was mentioned the parameters that define the geometry of the compressor, the design point as well as operating thermodynamic conditions can be either constant or variable within a range defined by two values within square brackets.

A global variable *".imp"*was created such that any of the other functions can collect the parameters defined in the main function and hence calculate the performance and geometry of the compressor. The user should also define the amount of iterations required for acceptable convergence of the compressor performance. Apart from the constant parameters defined, the main function selects a random value within the given range for the altering variables and feed it into the other functions including the *"getPerf"* function. The objective function consists of the Total-total pressure ratio and the isentropic efficiency. The values of these parameters are then calculated in the *"getPerf"* function and then sent back to the main function.

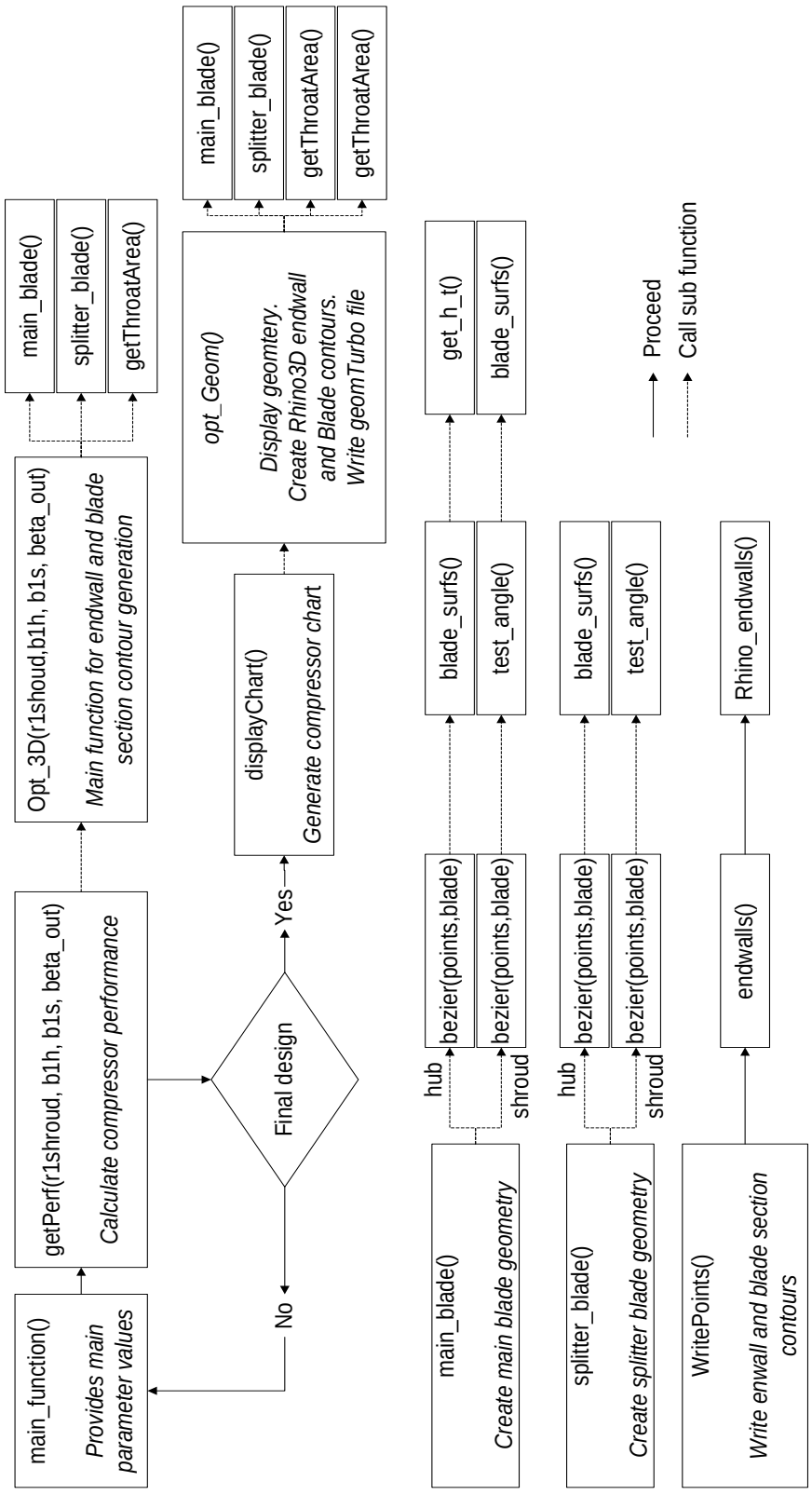

Figure 48: Original mean-line code flow diagram.

If a value of the objective function has been calculated to be better than a previously calculated value the geometry of the compressor is saved and the iterative process continues until the amount of optimization steps have been reached or a better objective function value has been calculated.

The altered mean-line code (figure 49) works in a near similar sense apart from a few key differences. The main function has added parameters that are used to define the geometry of the radial diffuser. These parameters can be either constant or variable as is the case for the parameters for the impeller. The initial solution starts by calculating the performance of the impeller in the *"getPerf"* function after which the thermodynamic conditions are sent to the *"diffuser2"* function. Here the performance of the compressor (excluding the axial guide vanes) is calculated. The performance results are then sent back to the *"getPerf"* function and in turn sent back to the main function.

Another difference between the altered mean line code and the original code developed by Van der Merwe (2012), is that the objective function in the new code consists of the total to static pressure ratio as opposed to a Total-total pressure ratio. The isentropic efficiency remains Total-total.

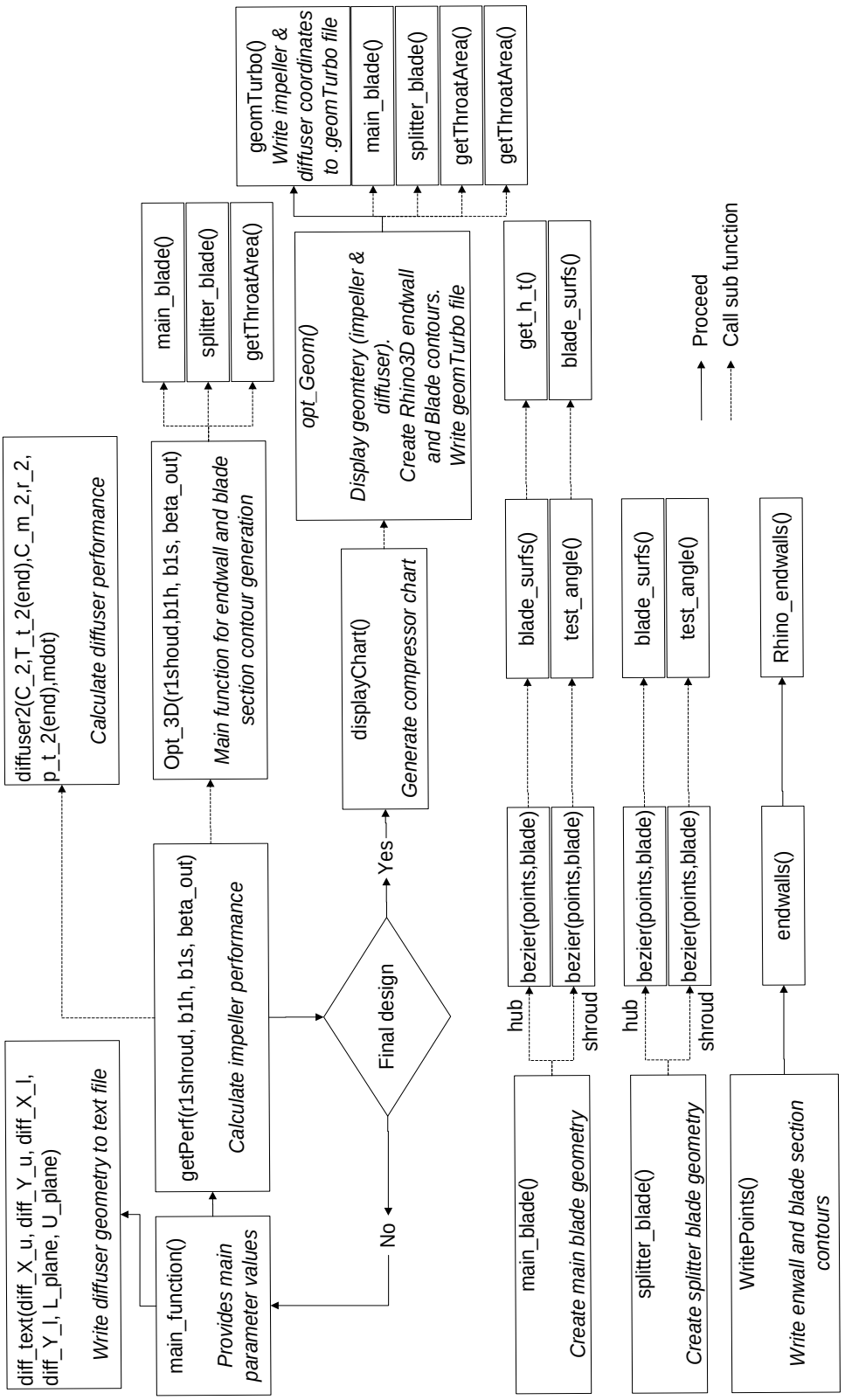

Figure 49: Altered mean-line code flow diagram.

A2: Main function “optimise” as seen in MATLAB®

```
function optimise()

closeall
clearall
clc

% Initialisestructs
global imp

% Paramters within square brackets ( '[]' ) are given a specific
range and
% the main function then selects a random value within this range
to
% calculate the compressor performance and create the geometry.

% Design specifications
imp.design_m_f_r = 0.325;        % test point mass flow rate
imp.imp_speed = 121000;          % test point impeller speed [rpm]
design_surge_margin = 0.1;       % mass flow rate range ratio

% Main parameters
imp.blade_num = 7;               % number of main blades
imp.r_1_hub = 8.138;             % hub radius at inlet
imp.r_1_shroud = [25 27];        % shroud radius at inlet
imp.imp_height = 35;             % impeller height (z-direction)
imp.beta_0_hub = [50 65];        % inlet angle at hub
imp.beta_0_shroud = [25 35];     % inlet angle at shroud
imp.hub_angle = 0*pi/180;        % hub inlet angle relative to z-
axis
imp.shroud_angle = 0*pi/180;     % shroud inlet angle relative to
z-axis
imp.LE_hub = 2;                  % blade thickness @ hub leading
edge
imp.LE_shroud = 0.6;             % blade thickness @ shroud leading
edge

imp.s_CL = 0.27;                 % tip clearance gap
imp.fillet_radius = 0;           % blade root fillet radius

imp.r_2 = 75/2;                  % radius at outlet
imp.b_2 = 6;                     % blade tip height
imp.beta_3_hub = [60 90];        % outlet angle at hub
imp.hub_angle_out = 0*pi/180;    % Hub outlet angle relative to r-
axis
imp.shroud_angle_out = 0*pi/180;% shroud outlet angle relative to
r-axis
imp.mixed_flow = 0;
imp.TE = 0.6;                    % blade thickness @ trailing edge
imp.lean_angle = 90*pi/180;      % lean angle at blade tip
imp.leanExt = 0;                 % 1 for "Yes" and 0 for "No"
```

```
imp.start_split = 0.275;          % splitter blade starting point
along "u"
imp.ell_end = 0.1;                % ellipse end on "u"
imp.par_start = 0.8;              % parabole start on "u"

% Diffuser parameters
imp.diff_height = 6;              % height at diffuser inlet
imp.diff_height_out = 6;          % height at diffuser outlet
imp.endwall_ext = 0.5;            % fraction extension of endwalls
imp.diff_in_rad = imp.r_2.*1.06;% diffuser inlet radius
imp.diff_out_rad = 48;            % diffuser outlet radius
imp.k3 = [1 5];                   % Diffuser camberline constant 1
imp.k4 = [1 5];                   % Diffuser camberline constant 2

% Bezier parameters
imp.bezier_size = 20;             % bezier curve number of points
(uneven spaced)
imp.size = 20;                    % bezier curve number of points
(even spaced)
imp.LE_refinement = 8;            % leading edge point number
refinement
imp.eps = 10;                     % accuracy of shroud trailing edge
angle [degrees]
imp.fin_ref = 10;                 % final geometry refinement

% Optimisation
%*****************************************************************
********%

% Genetic algorithm (GA) parameters
N_parents = 8;                    % # parent chromosomes   8
N_chrom = N_parents*3;            % # chromosomes
imp.mu = 0.2;                     % mutation rate
imp.block = 0.01;                 % parameter block rate
op_steps = 700;                   % optimisation steps

% Parameter limits
setPopulation(N_chrom);
par_names = fieldnames(imp);
N_par = length(imp.chrom_lims(:,1));

% Objective Function (OF) values
pp_imp = 4;                       % imposed pressure ratio
pp_ref = 4;                       % reference pressure ratio
pp_weight = 2;                    % OF term weight
pp_pow = 2;                       % OF term exponent

eff_imp = 0.80;                   % imposed efficiency (0.798
impeller only)
eff_ref = 0.80;                   % reference efficiency
eff_weight = 2;                   % OF term weight
eff_pow = 2;                      % OF term exponent

% Population matrix
```

```
pop = zeros(N_chrom + 1,N_par + 1);

% Randomly generate chromosomes
fortel = 1:N_chrom
pop(tel,1:N_par) = getChromosome(N_par);
pop(tel,N_par+1) = 10000;
end

fortel = 1:N_par
pop(N_chrom + 1,tel) = imp.chrom_lims(tel,3);
end

bestObf = 10000;

% plot OF convergence

% GA optimisation steps
for steps = 1:op_steps
% calculate OF value
fortel = 2:N_chrom
fortels = 1:N_par
ifisempty(strfind (par_names{pop(N_chrom + 1,tels)}, 'beta')) ==
false
                imp.(par_names{pop(N_chrom + 1,tels)}) = (90 -
pop(tel,tels))*pi/180;
elseifisempty(strfind(par_names{pop(N_chrom + 1,tels)}, 'angle'))
== false
                imp.(par_names{pop(N_chrom + 1,tels)}) =
pop(tel,tels)*pi/180;
else
                imp.(par_names{pop(N_chrom + 1,tels)}) =
pop(tel,tels);
end
end

% Generate compressor geometry from main parameters
        opt_3D();

% Calculate impeller throat area
getThroatArea();

massed_perf = zeros(2,1);
imp.mdot = imp.design_m_f_r -
imp.design_m_f_r*design_surge_margin;
perf = getPerf();   %Q_impPRatioQ_ref    k        W
obFunc = getPenalty(pp_imp, real(perf(1,1)), pp_ref, pp_pow,
pp_weight) + getPenalty(eff_imp, real(perf(2,1)), eff_ref,
eff_pow, eff_weight);
massed_perf(1) = obFunc;    %W*(((Q_imp - Q)/Q_ref)^k); as in
getPenalty
imp.mdot = imp.design_m_f_r;
perf = getPerf();   %Q_impPRatioQ_ref    k        W
```

```
obFunc = getPenalty(pp_imp, real(perf(1,1)), pp_ref, pp_pow,
pp_weight) + getPenalty(eff_imp, real(perf(2,1)), eff_ref,
eff_pow, eff_weight);
massed_perf(2) = obFunc;    %W*(((Q_imp - Q)/Q_ref)^k); as in
getPenalty

obFunc = [1 2]*massed_perf; % mass flow rate weighting

pop(tel,N_par + 1) = obFunc;

ifobFunc<bestObf

            imp.bestk3 = imp.k3;
            imp.bestk4 = imp.k4;

tau_u = [];
tau_l = [];

            [tau_urad_u] = cart2pol(imp.x_u, imp.y_u);
            [tau_lrad_l] = cart2pol(imp.x_l, imp.y_l);

tau_u = [tau_u*180/pi];
tau_l = [tau_l*180/pi];

            z = 360/imp.ZZ;
            k = 1;

fori = z:z:360

tau_u = [tau_utau_u(:,k)+z];
tau_l = [tau_ltau_l(:,k)+z];
rad_u = [rad_urad_u(:,k)];
rad_l = [rad_lrad_l(:,k)];
                k = k+1;

end

diff_X_u = [];
diff_Y_u = [];
diff_X_l = [];
diff_Y_l = [];

fortel = 1:k

                [diff_x_udiff_y_u] =
pol2cart(tau_u(:,tel).*pi./180, rad_u(:,tel));
                [diff_x_ldiff_y_l] =
pol2cart(tau_l(:,tel).*pi./180, rad_l(:,tel));
diff_X_u = [diff_X_udiff_x_u];
diff_Y_u = [diff_Y_udiff_y_u];
diff_X_l = [diff_X_ldiff_x_l];
diff_Y_l = [diff_Y_ldiff_y_l];
```

```
end

imp.bestPerf = perf;
bestObf = obFunc;
bestImp = imp;

figure(4)
gridon
holdon
xlabel ('Optimisation step');
ylabel ('Objective function value');
axis([0 steps 0 0.2]);
            plot(steps,bestObf,'--
rs','LineWidth',2,'MarkerEdgeColor','k','MarkerFaceColor','g','Mar
kerSize',7)%
holdoff

end

end

pop = sorteer(pop, N_par + 1);  % sort chromosomes from fittest to
weakest

pop = mate(pop);                % mate fittest chromosomes

pop = mutate(pop);              % mutate chromosomes (not fittest)
to explore design space

pop = refine(pop);              % refine 2nd fittest chromosome

clc
fprintf('The best value of the objective function is:\t\t%g\n',
bestObf);
fprintf('Design point pressure ratio:\t%g\n', imp.bestPerf(1,1));
fprintf('Design point efficiency:\t\t%g\n\n', imp.bestPerf(2,1));
fprintf('Optimisation step:\t%1.0f\n\n',steps);

for teller = 1:N_par

fprintf(par_names{pop(N_chrom + 1,teller)});
fprintf('\t');

end

fprintf('\t\tOF\n');

forchroms = 1:N_chrom
for pars = 1:N_par
fprintf('%2.3f\t\t', pop(chroms,pars));
end
fprintf('\t%2.3f', pop(chroms,N_par + 1));
fprintf('\n');
```

```
end

end
holdoff

% Create compressor chart
imp = bestImp;
clc
fprintf('Plotting Compressor Chart...\n\n');
displayChart();
[Z_vec none] = size(diff_X_u);
L_mat = zeros(Z_vec);
L_plane = L_mat(:,1);
U_mat = ones(Z_vec);
lin_inc = (imp.diff_height_out - imp.diff_height)/Z_vec;
U_plane = [];
z_h = imp.diff_height;
fori = 1:Z_vec

U_plane = [U_planez_h + lin_inc];
z_h = z_h + lin_inc;

end

U_plane = U_plane';

% Create compressor geometry

L_plane = single(L_plane);
U_plane = single(U_plane);
Diffuser_Coor = [diff_X_udiff_Y_udiff_X_ldiff_Y_lL_planeU_plane];
[diff_rdiff_c] = size(diff_X_u);
diff_text(diff_X_u, diff_Y_u, diff_X_l, diff_Y_l, L_plane,
U_plane);

figure(3)
holdon
plot3(diff_X_u,diff_Y_u,U_plane,'r')
plot3(diff_X_l,diff_Y_l,U_plane)
plot3(diff_X_u,diff_Y_u,L_plane,'r')
plot3(diff_X_l,diff_Y_l,L_plane)
opt_Geom();
holdoff

%Display compressor main parameters and performance
clc
fprintf('The value of the objective function is:\t\t%g\n',
bestObf);
fprintf('Design point pressure ratio:\t%g\n', imp.bestPerf(1,1));
fprintf('Design point efficiency:\t\t%g\n\n', imp.bestPerf(2,1));
fprintf('The impeller free parameter values are as follows:\n\n');

for teller = 1:N_par
fprintf(par_names{pop(N_chrom + 1,teller)});
```

```
fprintf('\t');
end

fprintf('\n');

for pars = 1:N_par
fprintf('%2.3f\t\t', pop(1,pars));
end
fprintf('\n\n');
fprintf('Throat angle:\t\t%gdeg\n', 90-imp.beta_th*180/pi);
fprintf('Throat area:\t\t%g m^2\n\n\n', imp.A_th*7);
clear
```

Appendix B: Impeller & Diffuser theory

B1: Basic Impeller Theory

Air enters the compressor at the eye in an axial direction denoted by absolute velocity vector C_1 (figure 50). The gas then moves into the inducer section where the air is then transferred onto the blades and gradually forced into the radial direction. While the gas moves through the inducer section energy is imparted into it which, as mentioned, increases the absolute and static temperatures and pressures (Dixon, 1998: 200 - 204).

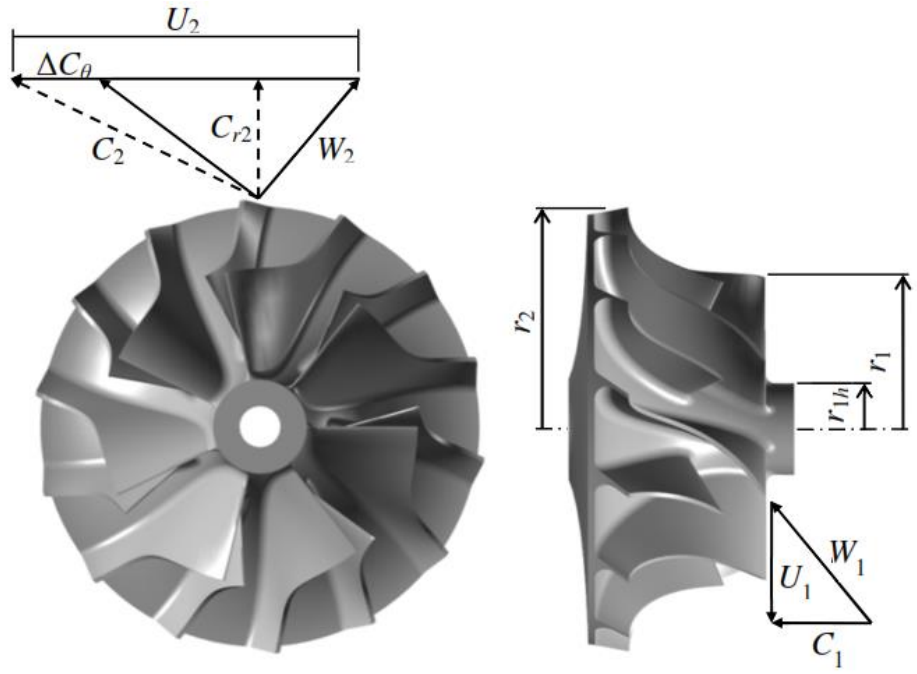

Figure 50: Velocity diagram for centrifugal compressor impeller (Van der Merwe, 2012: 4).

The gas then exits the impeller in a direction denoted by the absolute exit velocity C_2 whilst the blades tangential velocity is denoted by U_2. C_{r2} indicates the radial velocity component of the gas. As shown in figure 50 the absolute velocity has an ideal value (dotted line) or a real value (solid line). This difference between the real and ideal absolute velocity is due to the occurrence of slip.

As mentioned the impeller imparts energy E_i into and increases the enthalpy of the air moving through the inducer. An increase in enthalpy also denotes an increase in temperature and an increase in pressure. Another thermodynamic condition of the gas that experiences an increase is entropy (S). Entropy is, in laymen's terms, the measure of irreversibility and the change of which is defined as

$$\Delta S_{sys} = S_2 - S_1 \tag{B1.1}$$

A large change in entropy will result in an inefficient compressor stage and as such it is imperative that the designer ensure that the entropy rise is as small as possible.

B2: Vaned diffuser performance calculation

The iterative process of determining the performance of a radial diffuser according to Aungier (2000: 88 - 95) is as follows.

The choke within the diffuser throat is calculated by making use of the definition provided by Whitfield *et al* (1990: 58) and the means of calculating the choke provided by the iterative process of Dixon (1998).

Vaned diffuser stall is based on the parameter

$$K = -r\frac{\partial \cos\alpha}{\partial r} \tag{B2.2}$$

evaluated between the diffuser inlet and the throat. An average value between the inlet and the throat is employed, approximated by

$$K = \frac{r_3}{h_{th}}\left[\frac{\cos\alpha_3}{\cos\alpha_{th}} - 1\right] \tag{B2.3}$$

were

$$\sin\alpha_{th} = \frac{A_{th}}{A_3} \tag{B2.4}$$

Mach numbers and inlet blade angles have a significant effect on vaned diffuser stall and as such this "unguided" value of K can be expressed as

$$K + K_0 = 0.39 \tag{B2.5}$$

were

$$K_0 = \frac{M_3^2 (\sin \beta_3)^2 \cos \beta_3}{1 - M_3^2 (\sin \beta_3)^2} \quad \text{(B2.6)}$$

The loss models used are similar to impeller loss models. A skin friction loss coefficient is given by

$$\overline{\omega_{SF}} = 4c_f \left(\frac{\bar{C}}{C_3}\right)^2 \left(\frac{L_B}{d_H}\right) \left(\frac{2\delta}{d_H}\right)^{0.25} \quad \text{(B2.7)}$$

were the hydraulic diameter (d_H) used is defined as

$$d_H = \frac{4(cross-sectional\ area)}{wetted\ perimeter} \quad \text{(B2.8)}$$

and the term $2\delta/d_H$ is either

$$\frac{2\delta}{d_H} = 5.142 c_f \frac{L_B}{d_H} \quad \text{(B2.9)}$$

or

$$\frac{2\delta}{d_H} \leq 1 \quad \text{required} \quad \text{(B2.10)}$$

The optimum or minimum incidence angle is defined as

$$\sin \alpha_3^* = \frac{C_{m3}}{C_3^*} = \sqrt{\sin \beta_3 \sin \alpha_{th}} \quad \text{(B2.11)}$$

For typical vanes this corresponds to modest negative incidence angles of usually around -1° as discussed in section 2.2. The minimum incidence loss angle for this optimum incidence is given by

$$\overline{\omega_{i0}} = 0.8\left[\frac{C_3^* - C_{th}}{C_3}\right]^2 + \left[\frac{z t_{b3}}{2\pi r_3}\right]^2 \quad \text{(B2.12)}$$

The off-design incidence loss is referenced to the velocities at the optimum incidence, C_3^*, and corresponding to the stall incidence, $C_{3S} = C_{m3}/\sin \alpha_{3S}$, as follows: If $C_3 \leq C_{3S}$, then

$$\overline{\omega_i} = 0.8\left[\left(\left(\frac{C_3}{C_{3S}}\right)^2 - 1\right)\left(\frac{C_{th}^2}{C_3^2}\right) + \frac{(C_{3S} - C_3^*)^2}{C_{3S}^2}\right] \quad \text{(B2.13)}$$

Aungier (2000: 92 - 93) presents a modified discharge area blockage correlation shown to be very effective in estimating the pressure recovery of a wide range of vaned diffusers. This correlation employs two basic parameters:

$$2\theta_C = 2\tan^{-1}\left\{\left(\left[\frac{(w_4 - t_{b4})b_4}{b_3}\right] - w_3 + t_{b3}\right)/2L_B\right\} \quad \text{(B2.14)}$$

$$L = \frac{\Delta C}{C_3 - C_4} \quad \text{(B2.15)}$$

were ΔC is the average blade-to-blade velocity difference; and $w = (2\pi r\sin\beta)/z$. From simple potential flow

$$\Delta C = 2\pi\frac{r_3 C_{U3} - r_4 C_{U4}}{zL_B} \quad \text{(B2.16)}$$

Aungier states that an abrupt deterioration in performance occurs when $L > 1/3$ or when $2\theta_C > 11°$. Therefor correction coefficients are defined by

$1 \leq C_\theta \geq 2\theta_C/11$

$1 \leq C_L \geq 3L$ (B2.17)

The discharge area blockage is defined as

$$B_4 = [K_1 + K_2(\overline{C_R^2} - 1)]L_B/w_4 \quad \text{(B2.18)}$$

where

$$\overline{C_R^2} = \frac{1}{2}\left[\frac{C_{m3}\sin\beta_4}{C_{m4}\sin\beta_3} + 1\right] \quad \text{(B2.19)}$$

$$K_1 = 0.2[1 - 1/(C_L C_\theta)] \quad \text{(B2.20)}$$

$$K_2 = \frac{2\theta_C}{125C_\theta}\left[1 - \frac{2\theta_C}{22C_\theta}\right] \quad \text{(B2.21)}$$

It is not common to have another skin friction loss term in equation B2.18 but since the skin friction is treated separately in this analysis it is not necessary. A wake mixing loss is included to account for excessive streamwise diffusion as well as vane discharge metal thickness. The flow is assumed to separate at a velocity defined by

$$C_{SEP} = C_3/(1 + 2C_\theta) \quad \text{(B2.22)}$$

$C_{SEP} \geq C_4$ required (B2.23)

As in the case of the impeller, only the meridional velocity is involved in the wake mixing process. The meridional velocities before and after mixing are

$$C_{m,\,wake} = \sqrt{C_{SEP}^2 - C_{u4}^2} \quad \text{(B2.24)}$$

$$C_{m,\,mix} = A_4 C_{m4}/(2\pi r_4 b_4) \quad \text{(B2.25)}$$

and the wake mixing loss is given by

$$\overline{\omega_{mix}} = \left[\frac{C_{m,wake} - C_{m,mix}}{C_3}\right]^2 \quad \text{(B2.26)}$$

After the wake mixing loss have been calculated the three losses as mentioned in section 2.3.5 and above can be summated and used to calculate the diffuser discharge total pressure. The outlet total pressure is hence defined by

$$p_{t4} = p_{t3} - (p_{t3} - p_3)\sum_i \overline{\omega_i} \quad \text{(B2.27)}$$

The minimum-loss deviation angle is given by

$$\delta^* = \frac{\theta\left[0.92(a/c)^2 + 0.02\left(90^0 - \beta_4\right)\right]}{\sqrt{\sigma} - 0.02\theta} \quad \text{(B2.28)}$$

where the location of the point of maximum camber, solidity and camber angle are given by

$$a/c = \left[2 - \frac{\bar{\beta} - \beta_3}{\beta_4 - \beta_3}\right]/3 \quad \text{(B2.29)}$$

$$\sigma = z(r_4 - r_3)/(2\pi r_3 \sin\bar{\beta}) \quad \text{(B2.30)}$$

$$\theta = \beta_4 - \beta_3 \quad \text{(B2.31)}$$

The variation of the deviation angle with incidence is modelled by an empirical correlation of graphical data and is given by

$$\frac{\partial\delta}{\partial i} = \exp\left[\left(\left(1.5 - \frac{\beta_3}{60}\right)^2 - 3.3\right)\sigma\right] \quad \text{(B2.32)}$$

and the vaned diffuser discharge is given by

$$\alpha_4 = \beta_4 - \delta^* - \frac{\partial\delta}{\partial i}(\beta_3 - \alpha_3) \quad \text{(B2.33)}$$

After p_{t4} and α_4 have been calculated the other thermodynamic conditions at the diffuser outlet can be calculated. As was mentioned in section 3.2 the above process is iterative and must continue until convergence of C_{m4} has been reached.

The design parameter introduced by Aungier (2000: 178) is defined as

$$E_d = \frac{R^2(A_R^2 - 1)}{A_R^2(R^2 - 1)} \quad \text{(B2.34)}$$

and is used to evaluate the effectiveness of a vaned diffuser compared to a vaneless diffuser. The value of E_d should typically be between 1.5 – 1.7.

Appendix C: Initial compressor geometry

C1: MATLAB® geometry plot of centrifugal compressor

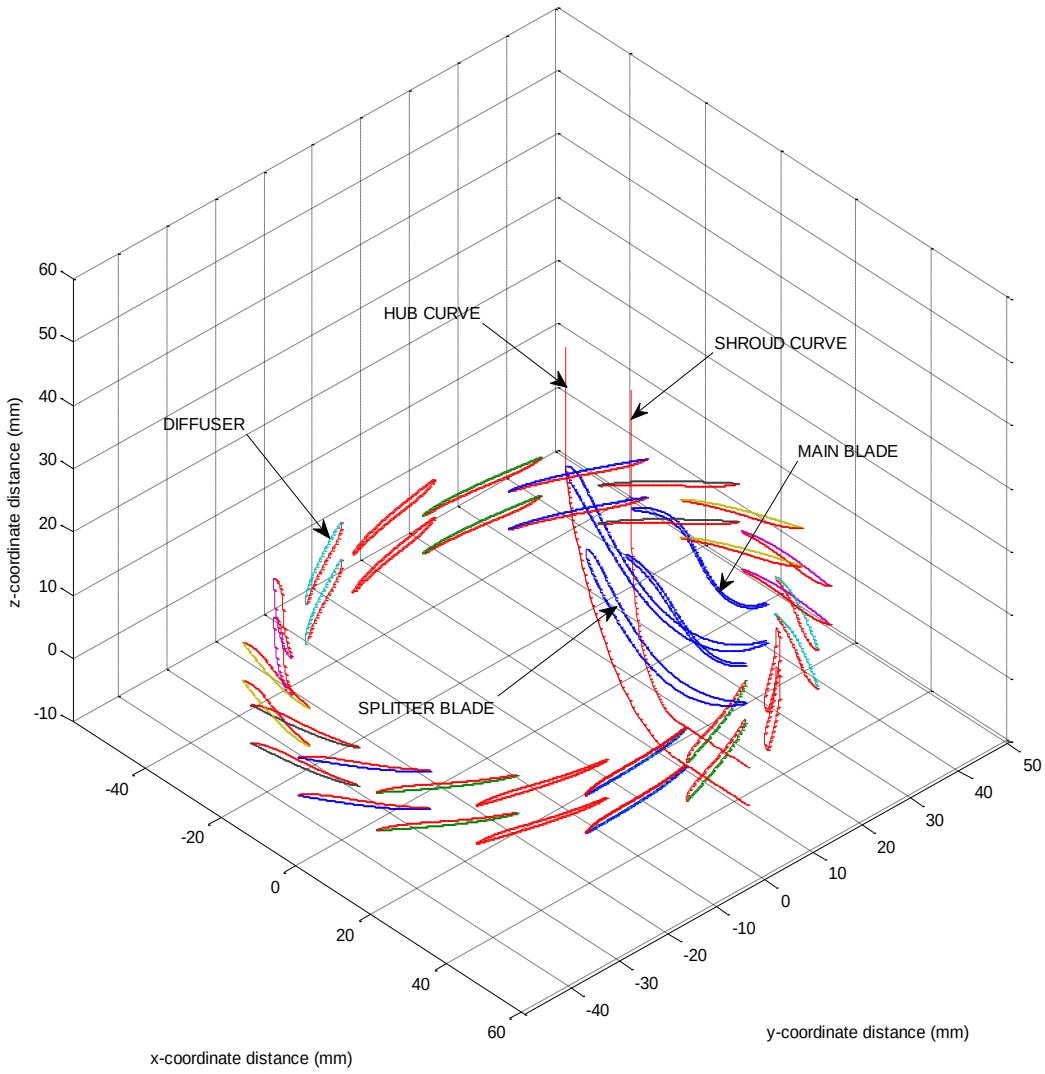

Figure 51: Iso-view of centrifugal compressor (MATLAB® figure).

Appendix D: Graphical User Interfaces (GUI) of various Numeca International modules

D1: Autogrid 5® GUI and mesh enhancing functions.

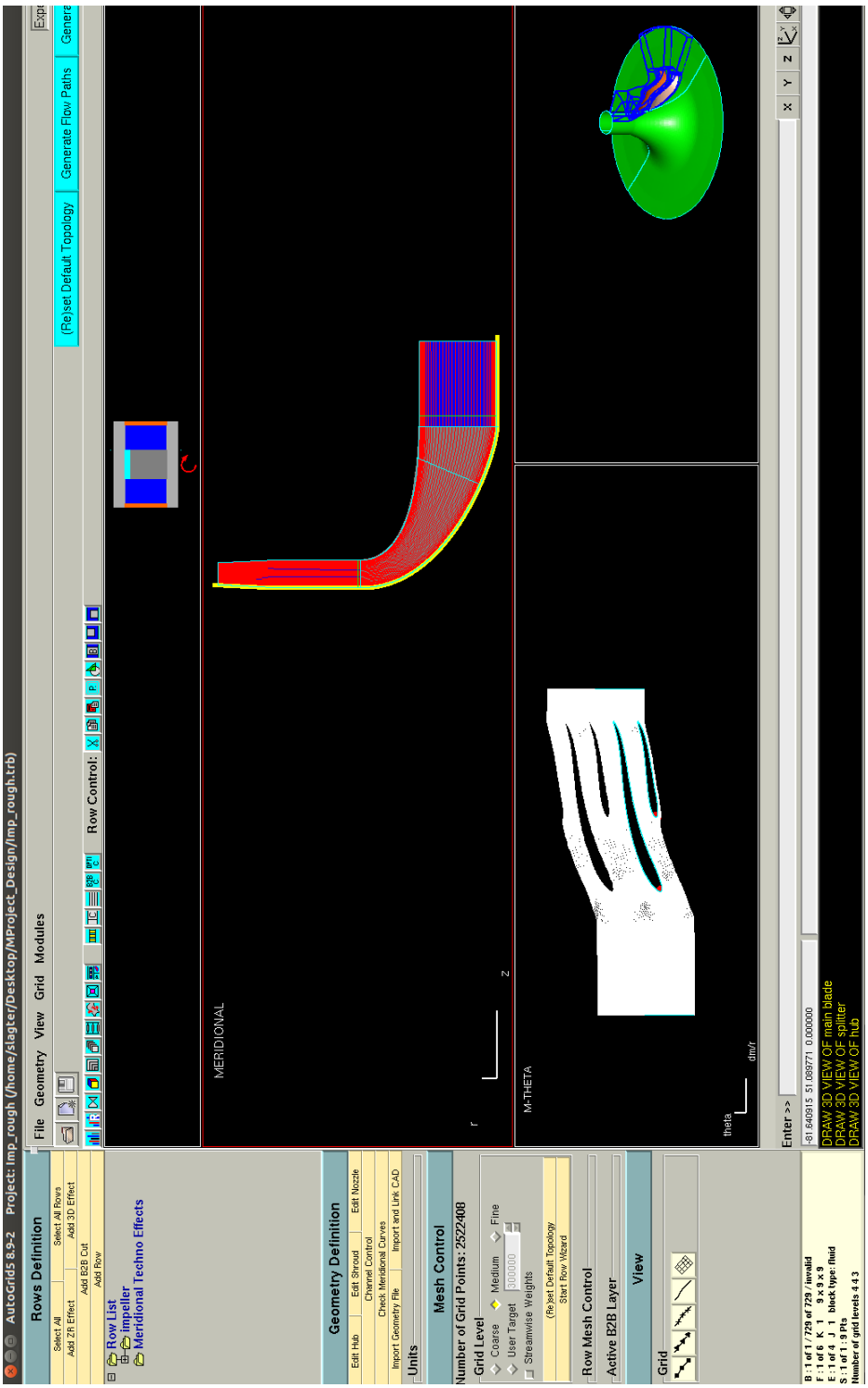

Figure 52: Autogrid 5® GUI.

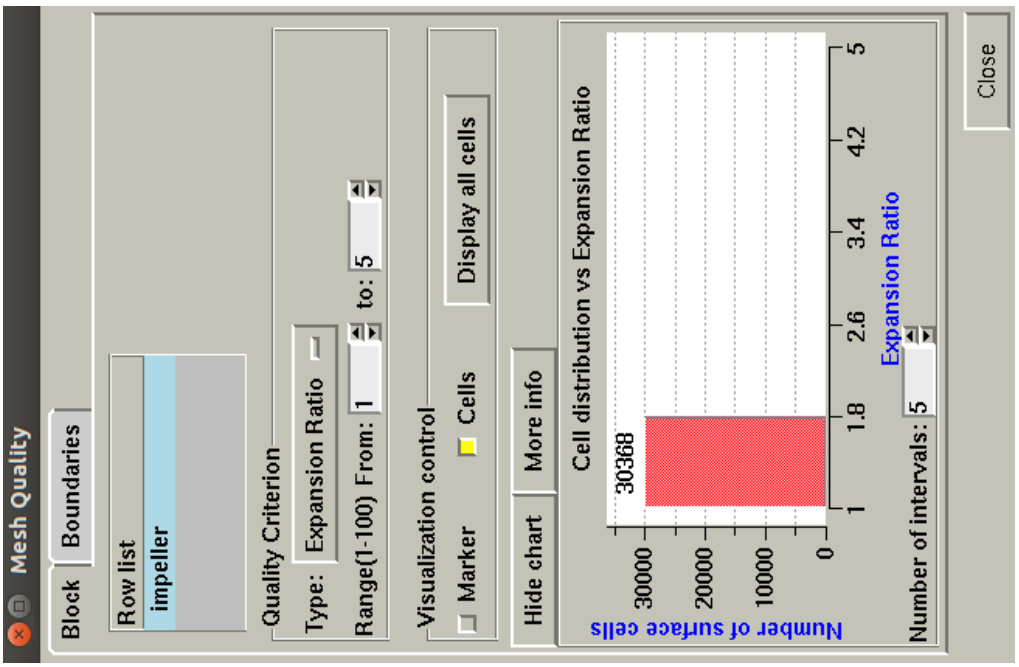

Figure 53: Mesh quality control box

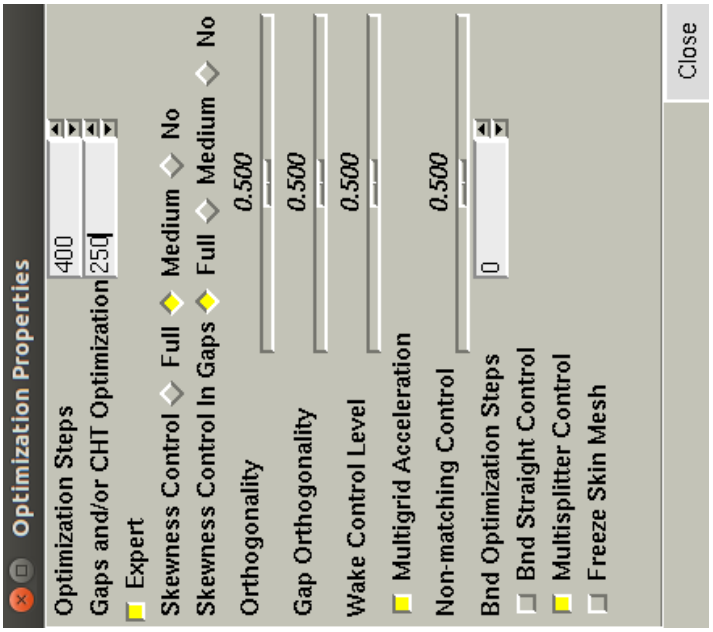

Figure 54: Mesh optimization tool.

D2: FINE™/Turbo GUI

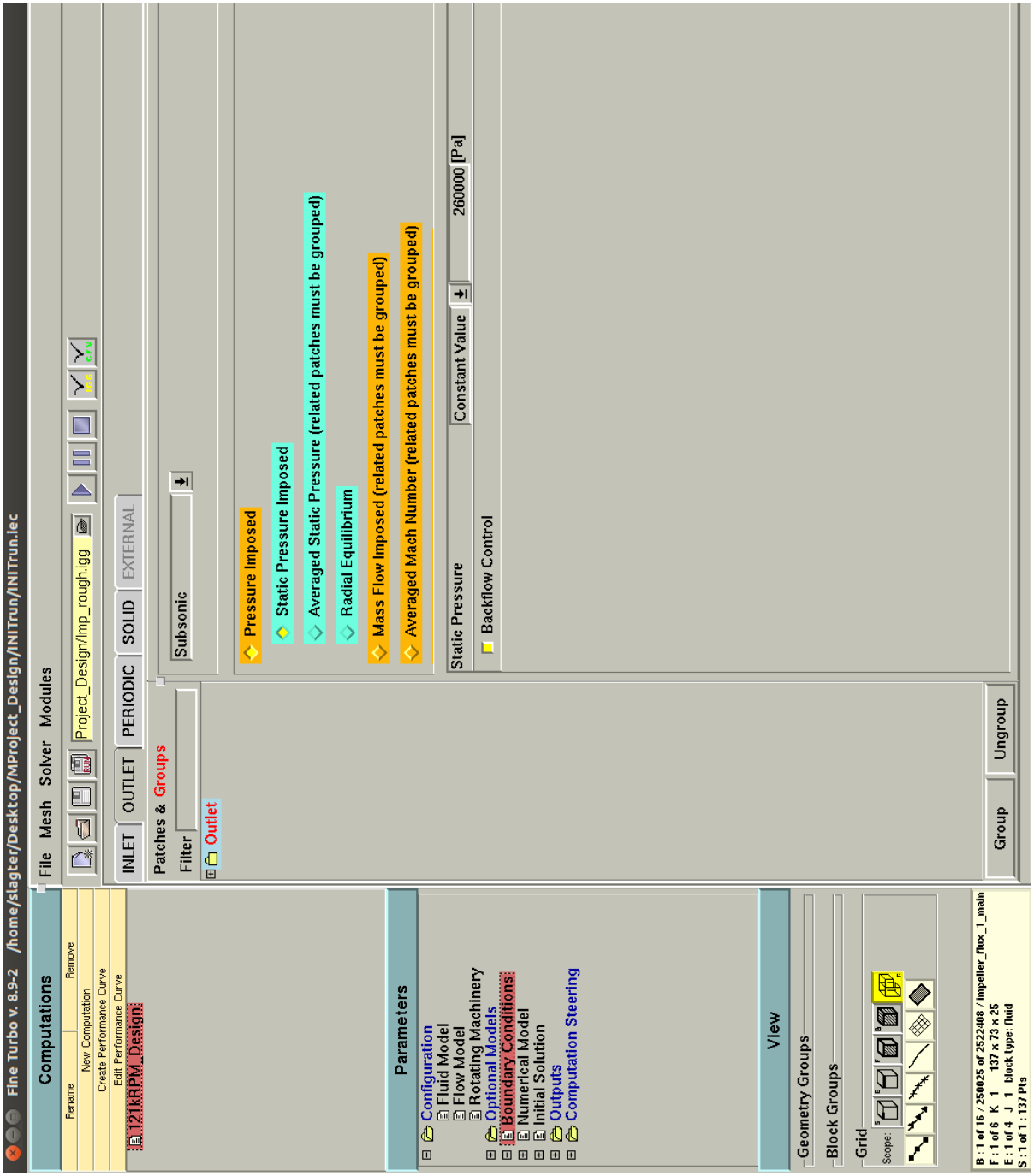

Figure 55: FINE™/Turbo GUI.

D3: Autoblade® GUI

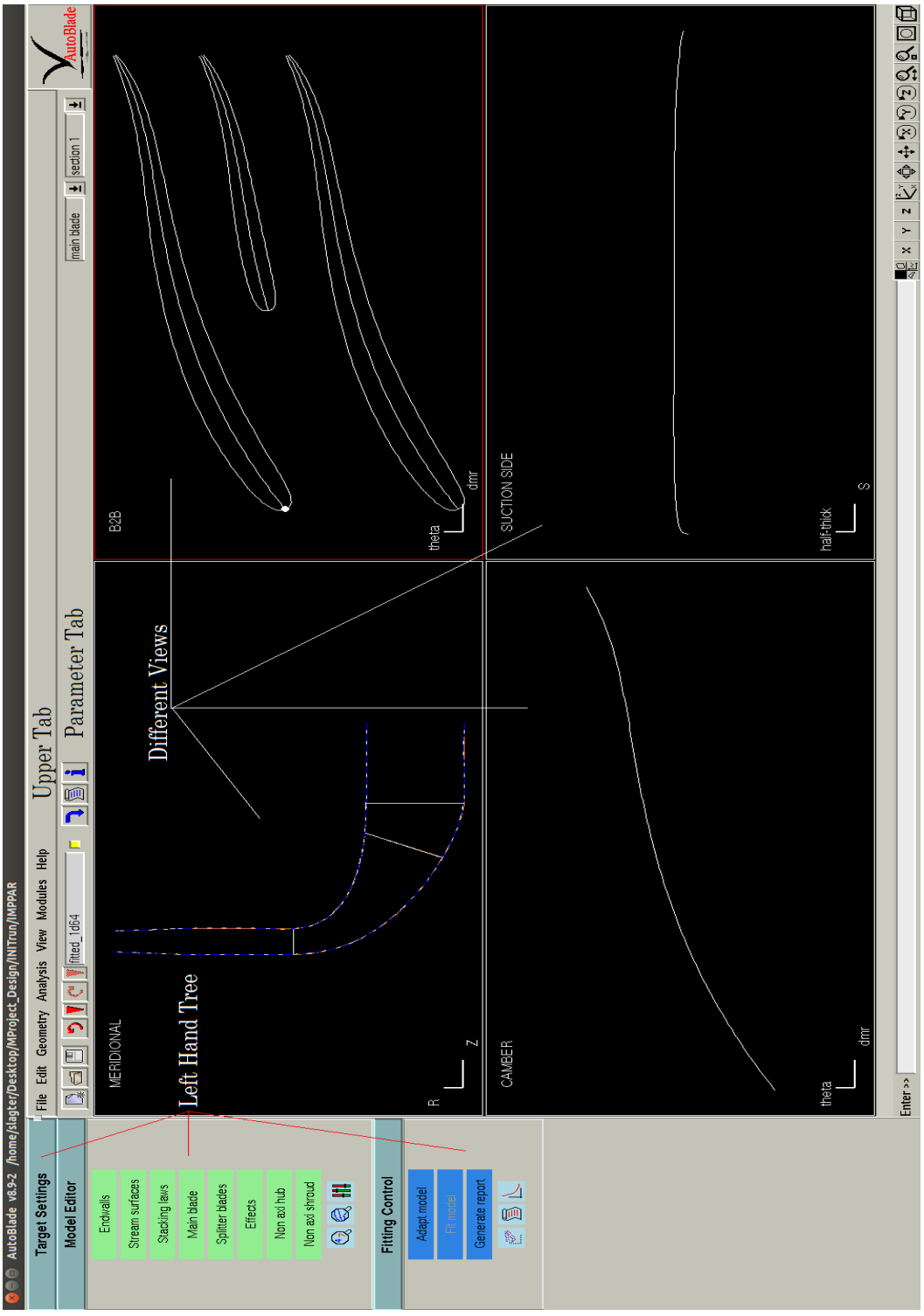

Figure 56: Autoblade® GUI

D4: Design3D GUI

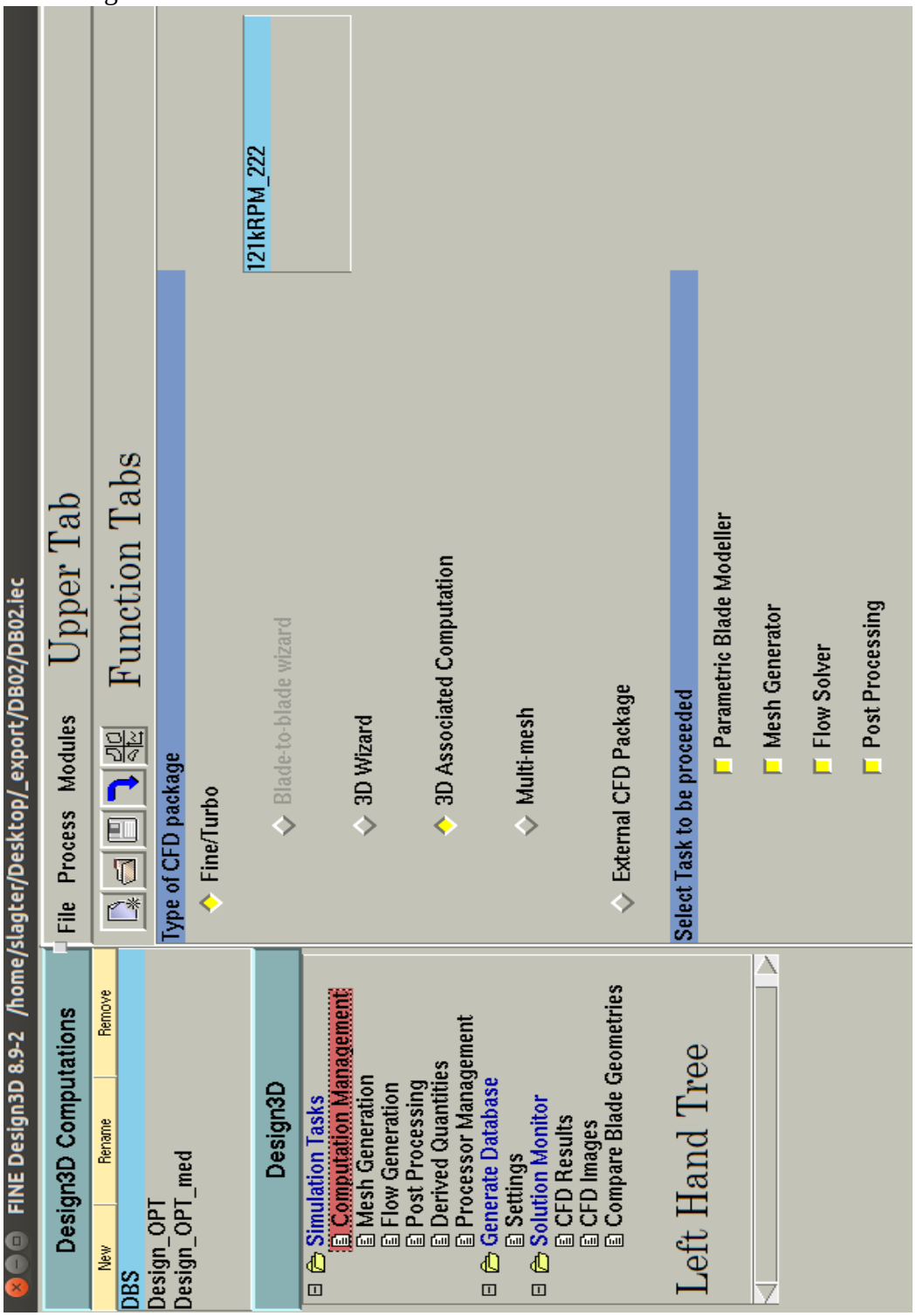

Figure 57: Design3D GUI.

Appendix E: Structure and alterations of database generation and optimization.

E1: Project file directory layout

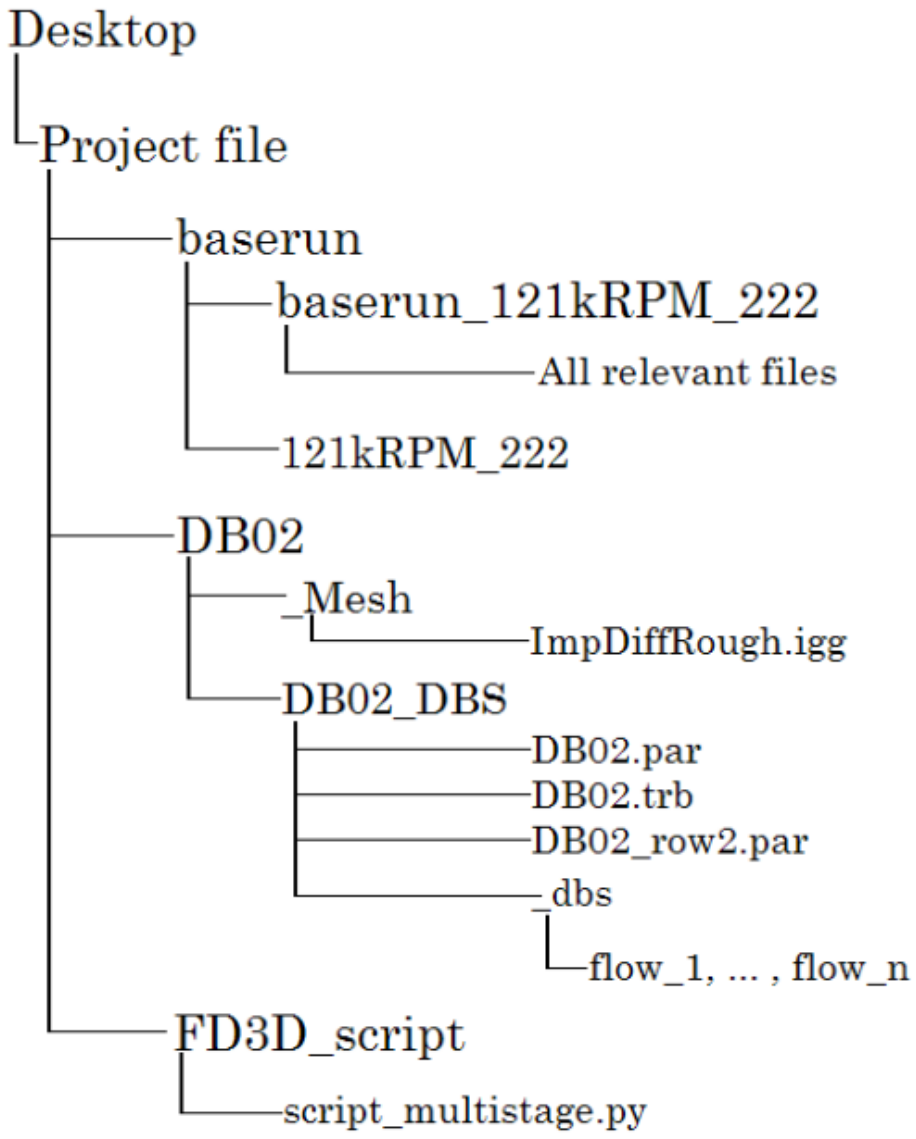

Figure 58: Project directory layout.

E2: User alterations for database generation and optimization.

The first alteration that the user must do manually is changing the "IGG_AUTOGRID_FLAGS" text line of the .iec file within the DB02 directory as follows:

IGG_AUTOGRID_FLAGS "-niversion 89_2 -script /Desktop/ProjectFile//FD3D_script/script_multistage.py"

As can be seen in this text line the designer provides the Autogrid 5® version as well as directory location of the Numeca script file. Since Autobalde cannot handle 2 rows the user must create a parameter list for both of the rows separately and then insert the parameters of the 2nd row into the optional field of the 1st row. Depicted in figure 59 is the parameter list of the 1st row with the addition of the 2nd row free parameters (only) in the optional field.

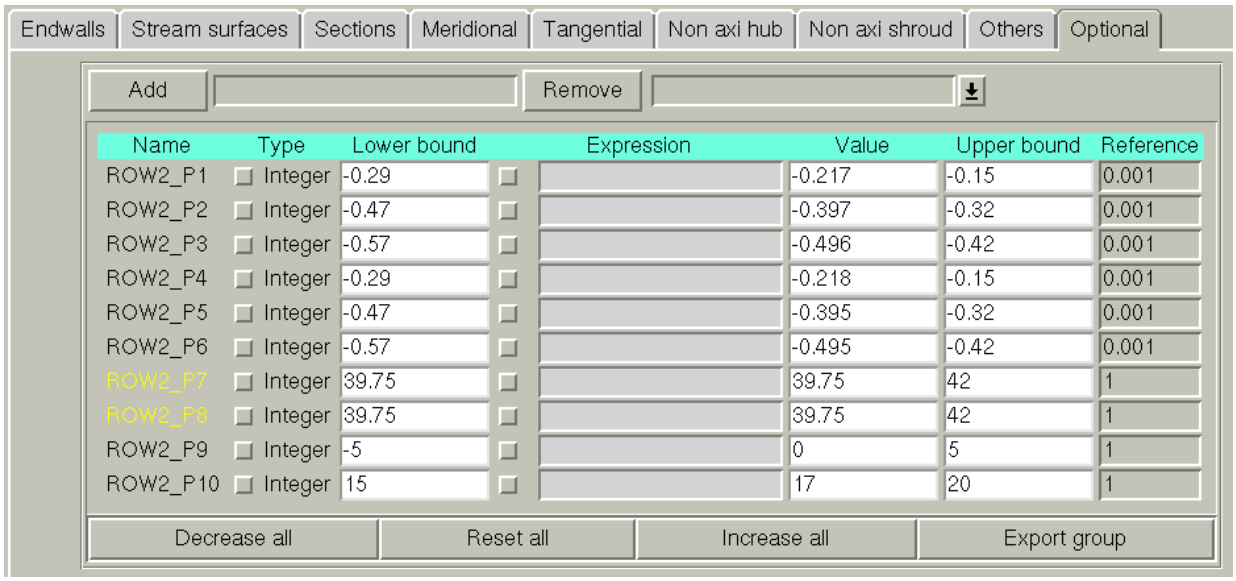

Figure 59: Optional field parameter list.

The 1st row can be left as is with, as mentioned, only as many as required free parameters or else very little valid samples will be created. Under the optional tab in the 1st row parameter list the user adds parameters in the format ROW2_P1, ROW2_P2, …, ROW2_Pn (where n is the amount of free parameters) and should a 3rd row be present the "2" in this sequence is replaced by "3". The lower and upper range limits as well as defining value of every 2nd row free parameter must then be entered manually into the optional parameters field created in the 1st row parameter list. This requires that the designer writes down the values for every parameter to the last decimal place and copy it as is into the optional parameter list. The author found it helpful to reduce not only the upper and lower range limits to a 3rd significant figure but to also have the defining value consist of a number with a number of significant figures that will not create an ill-defined Autoblade geometry. This makes it easier to copy the 2nd row free parameters into the 1st/anchor row free parameter list.

At the top of the script file a vector is defined in which all the 2nd row free parameter names must be defined. The names, with the exact format within the 2nd row parameter file are then entered underneath the vector definition as seen below.

```
row2_parameter_name=[]
row2_parameter_name.append("S1_CAMBER_H1")
row2_parameter_name.append("S1_CAMBER_H2")
row2_parameter_name.append("S1_CAMBER_H3")
row2_parameter_name.append("S2_CAMBER_H1")
row2_parameter_name.append("S2_CAMBER_H2")
row2_parameter_name.append("S2_CAMBER_H3")
row2_parameter_name.append("R_LE_HUB")
row2_parameter_name.append("R_LE_SHROUD")
row2_parameter_name.append("LEAN_BETA")
row2_parameter_name.append("NB")
```

As can be seen from the code above the free parameters of the diffuser are the 3 camber point definitions on both the hub and shroud surfaces, the leading edge radius at the hub and shroud, the lean angle and the number of blades. It was however discovered that the number of blades cannot be changed hence the final free parameter (NB) has no effect whatsoever.

Appendix F: Final design geometry and performance effects

F1: Flow lines over diffuser vanes at spans of 11.25% and 90%

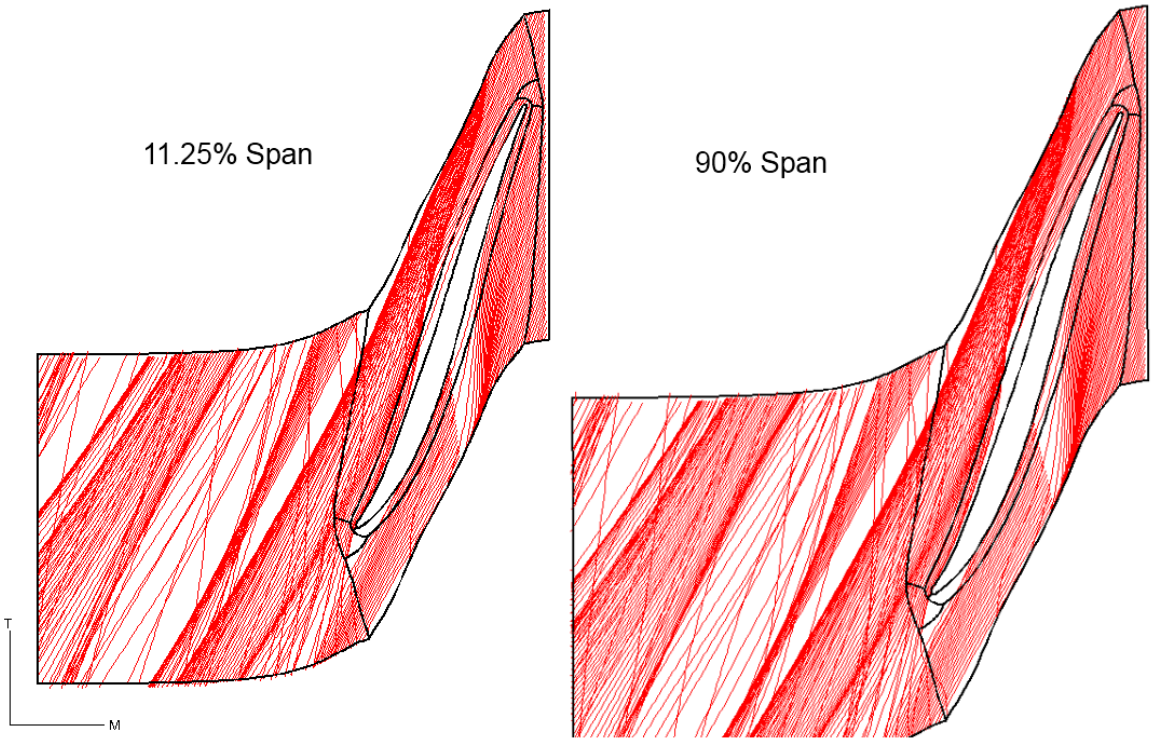

Figure 60: Flow lines over diffuser vanes @ 11.25% span.

It is clear from figure 60 that no stall exists on the diffuser vanes at a span of either 11.25% or 90%. It is also clear that swirl exists at a span of 90% as it does at a span of 11.25%.

F2: Geometry of the newly designed impeller and diffuser.

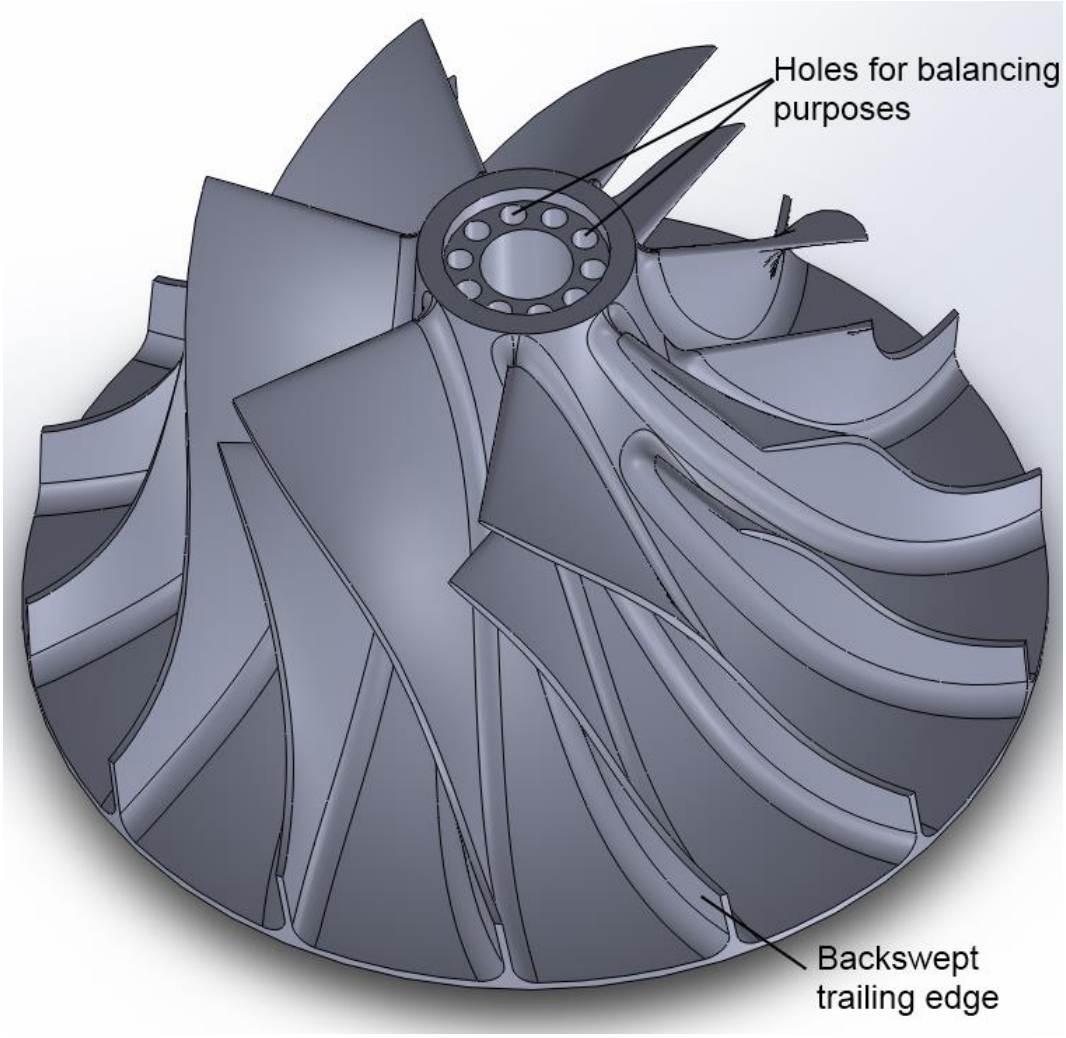

Figure 61: Final design of impeller with holes for balancing purposes.

The geometry of the final design is exported out of Autoblade® in an IGES (.igs) format which provides surfaces only. These surfaces are made solid by making use of SolidWorks. Visible in figure 61 are small holes that are milled into the impeller in the axial direction. These holes will be filled with small amounts of lead in order to balance the impeller when rotating at high speeds. The reason for creating these holes as opposed to grinding material of the top surface of the impeller is purely to create a more aesthetic impeller. The aerodynamic effects are negligible.

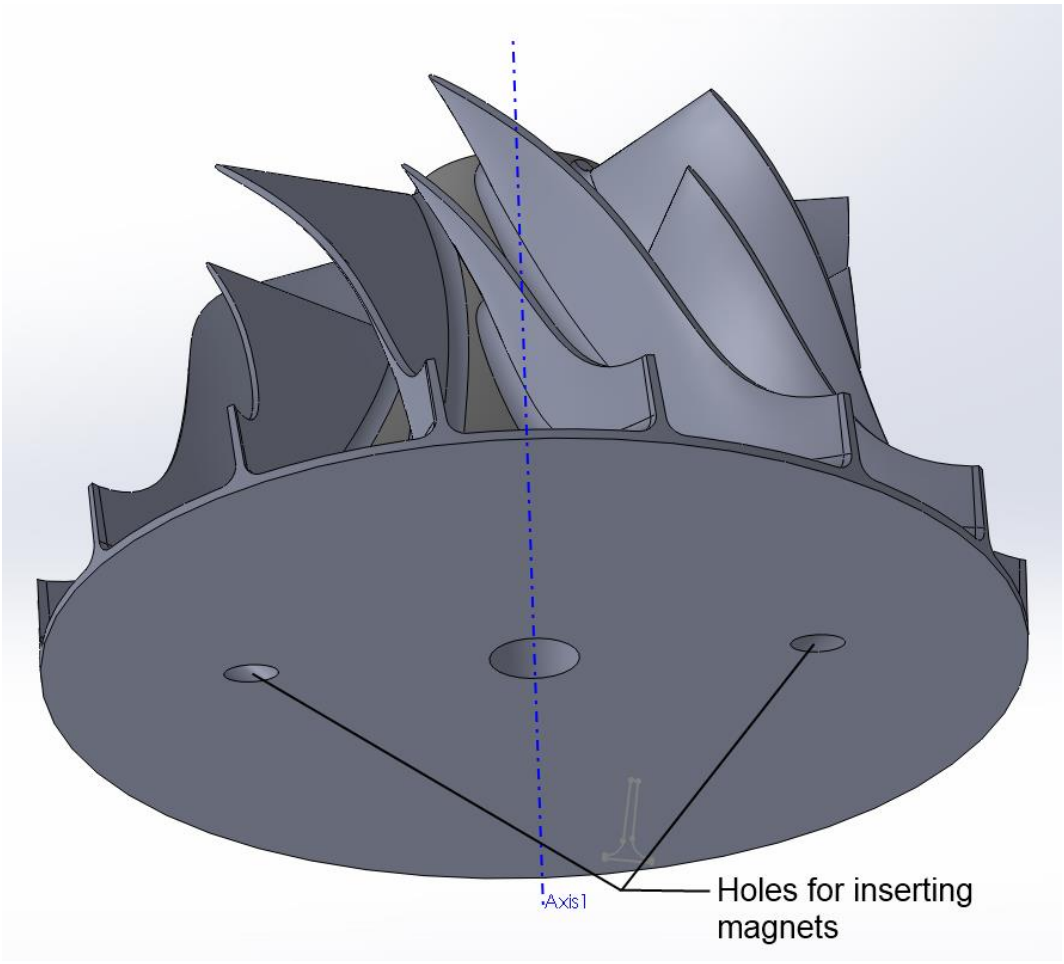

Figure 62: Lower surface of final designed impeller.

The lower surface of the impeller is completely flat. This simplifies the design of the impeller as well as the diffuser in which the impeller turns. It also eases manufacturability. Visible in figure 62 are 2 holes drilled into the back of the impeller in an axial-radial direction. These holes are used to house magnets that will in turn be used to measure the rotational speed of the impeller. The reason that these holes are drilled into the axial-radial direction is so that the centrifugal force be used to push the magnets outward while the impeller is rotating. In doing so it is ensured that the magnets do not fall out whilst the rotor is in operation and hence do not damage the diffuser or damage any other component.

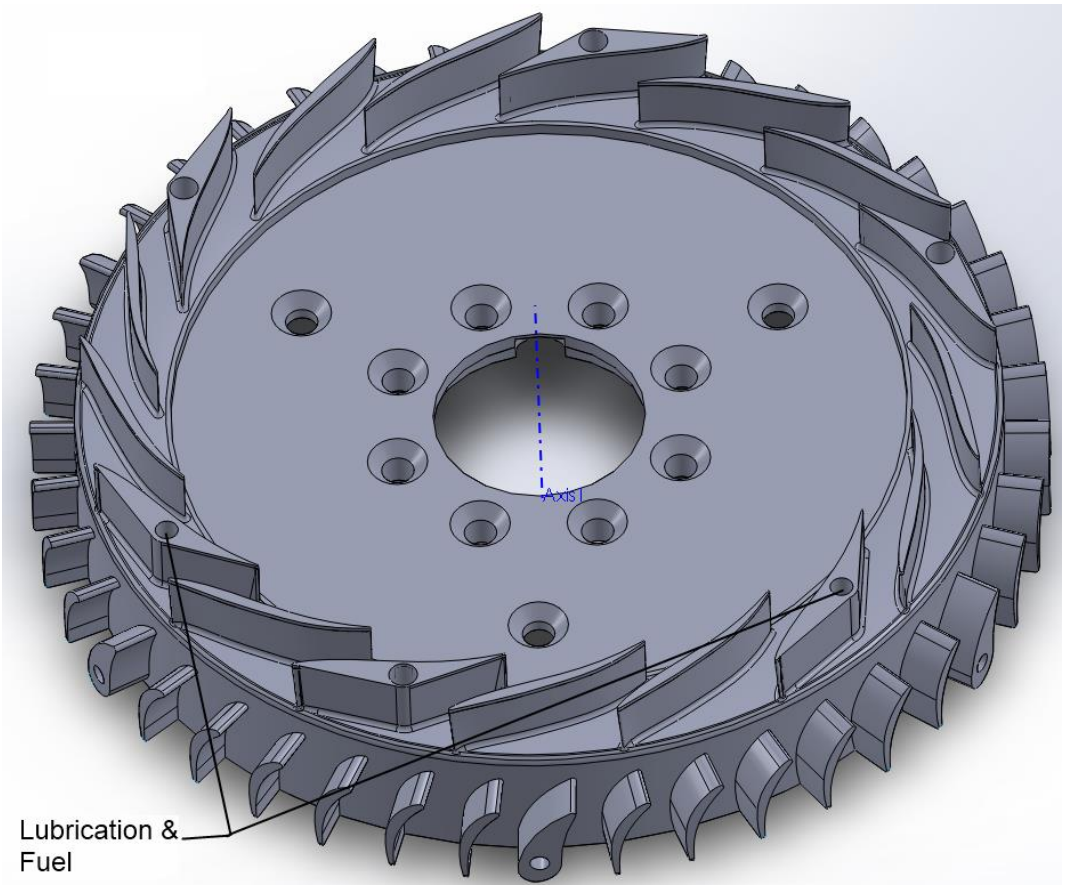

Figure 63: Diffuser final design.

The reference diffuser of Krige (2013) was used and the new blade profiles inserted onto it (figure 63). Due to the means of assembly of the entire MGT the author had to thicken 6 diffuser blades through which holes could be milled. The 2 holes denoted "*Lubrication and Fuel*" will be used to pass tubes through, one of which supplying lubricating oil for the compressor bearing and the other fuel to the combustion chamber. The other thickened diffuser blades will be used to pass threaded holes through in order to fasten the shroud/front cover to the diffuser. The aerodynamic and performance effects that these thickened diffuser vanes will have on the compressor performance are unknown and can only be quantified after the compressor has been tested.

F3: Final manufactured parts

Figure 64: Manufactured rotor for the new compressor design.

Figure 64 shows the lean angle and backswept trailing edge of the rotor blades. Also visible are the holes around the main axis hole in which brass weights have been placed that served to balance the rotor.

Figure 65: Manufactured diffuser for the new compressor design.

Figure 65 shows the 6 diffuser vanes that had to be altered in order for the compressor to be assembled. 4 of the holes are used to fasten the front cover/shroud to the diffuser whereas 2 holes are used to feed lubrication fluid to the bearings and fuel to the combustion chamber.

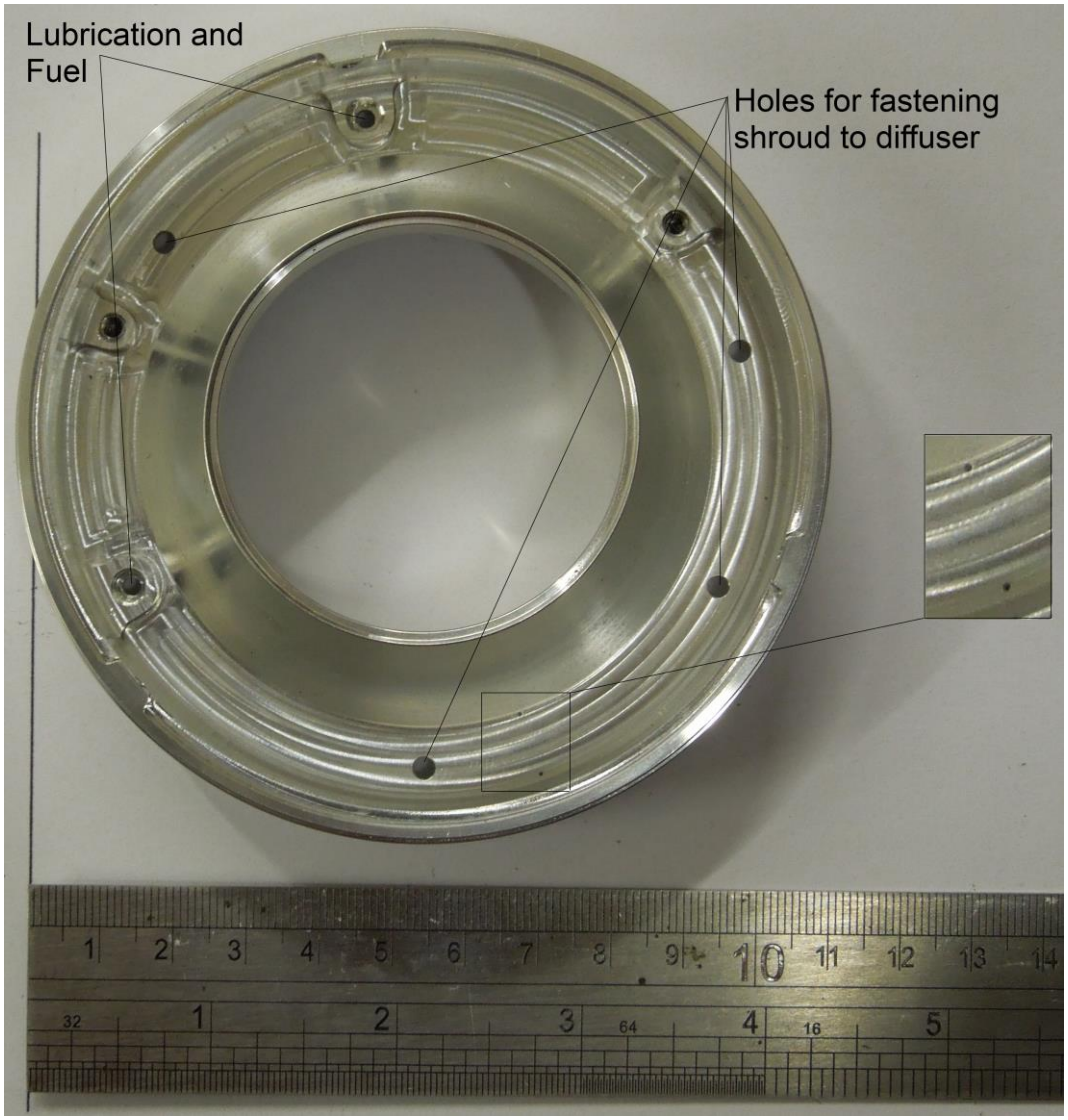

Figure 66: Final front cover/shroud design for the compressor.

Figure 66 shows the details of the final designed front cover. The enlarged inset shows the 0.5 mm diameter holes that were used to measure the static pressure at the inlet and outlet of the diffuser. Also visible are the holes through which the lubrication and fuel must be fed and the 4 holes used to fasten the front cover to the diffuser. It was concluded that the quality of the final manufactured parts were acceptable and that the method of fastening the front cover to the diffuser was acceptable for purposes of tests in order to measure the performance of the newly designed compressor.